2017

Fracture Relative Permeability Estimation by Lattice-Boltzmann Method and its Effect on SAGD Performance in Carbonate Reservoirs

Hu, Yi

UNIVERSITY OF CALGARY

Fracture Relative Permeability Estimation by Lattice-Boltzmann Method and its Effect on SAGD Performance in Carbonate Reservoirs

by

Yi Hu

A THESIS

SUBMITTED TO THE FACULTY OF GRADUATE STUDIES

IN PARTIAL FULFILMENT OF THE REQUIREMENTS FOR THE

DEGREE OF MASTER OF SCIENCE

GRADUATE PROGRAM IN CHEMICAL AND PETROLEUM ENGINEERING

CALGARY, ALBERTA

APRIL, 2017

Abstract

Naturally fractured carbonate reservoirs with huge reserves are becoming more important to the global oil supply. It is of fundamental and practical importance to model naturally fractured reservoirs more accurately. So far, linear fracture relative permeability has been widely used for reservoir simulations. Extensive studies, however, have shown that fracture relative permeability varies with fracture characterizations. In this work, the Lattice Boltzmann Method (LBM) was applied to generate oil-water relative permeability of natural fractures under different fracture characterizations. In addition, the SAGD performance in naturally fractured carbonate reservoirs implemented with new relative permeability was evaluated. Results indicate that relative permeability in fractures presents a nonlinear relationship with saturation, rather than the commonly used X-shape curves. Comparing SAGD performance shows that it is necessary and more practical to utilize nonlinear relative permeability curves in natural fractures, especially for reservoirs with thin thickness, a medium level of matrix porosity and an initial oil saturation.

Acknowledgements

I would like to express my deepest gratitude to my supervisor, Dr. Zhangxing (John) Chen, for his excellent guidance, valuable suggestions and continued support.

I would like to thank my committee members - Dr. Hossein Hejazi and Dr. Shengnan (Nancy) Chen for their efforts and time.

I am thankful to Dr. Yuxuan Liu, Dr. Shawket Ghedan and Mr. Shuhua Wang for their advice and patience in assisting me with my research.

I appreciate the following for their contributions to this study: Flowkit Ltd. for providing open source Palabos; Minitab Inc. for providing software Minitab; and Computer Modeling Group Ltd. for providing the software package CMG.

My gratitude also goes to all members in the Reservoir Simulation Group and all sponsors of this Group.

Last but not the least, I would like to thank my parents for their unconditional love and support throughout my life.

Table of Contents

List of Tables

List of Figures and Illustrations

List of Symbols, Abbreviations and Nomenclature

Symbols

f_o	Oil fractional flow rate
f_w	Water fractional flow rate
g	Constant of gravitational acceleration
I_r	Relative injectivity of JBN method
k	Absolute permeability (D)
k_o	Oil absolute permeability (D)
k_{ro}	Oil relative permeability
$k_{ro}(S_{wir})$	Oil relative permeability at irreducible water saturation
k_{rw}	Water relative permeability
$k_{rw}(S_{or})$	Water relative permeability at residual oil saturation
k_{rg}	Gas relative permeability
k_w	Water absolute permeability (D)
P	Pressure
ΔP	Pressure drop
P_c	Pressure
q_o	Oil flow rate (cm^3/min)
q_t	Total outlet flow rate (cm^3/min)
q_w	Water flow rate (cm^3/min)
Q_w	Water injection volumes at JBN method
S	Distance in direction of flow in Darcy's law
S_{wir}	Irreducible water saturation
S_{or}	Residual oil saturation
v	Fluid velocity
$\overline{v_o}$	Average oil relative permeability decreasing rate
$\overline{v_w}$	Average water relative permeability increasing rate

Subscripts

σ	Phase
i	Lattice direction
nw	Non-wetting phase
w	Wetting phase

Greek Symbols

π	Particle momentum
μ	Fluid viscosity
μ_o	Oil viscosity
$\emptyset_f$	Intrinsic fracture porosity

Abbreviation

CSS	Cyclic steam stimulation
SAGD	Steam assisted gravity drainage
SOR	Steam-to-oil ratio (m^3/m^3)
TAGOGD	Thermally assisted gas/oil gravity drainage

Chapter One: INTRODUCTION

1.1 Overview

Due to the growth of global energy demand, investigations of enhanced oil recovery (EOR) in naturally fractured reservoirs (NFRs) have become popular for their large reserves (Akhondzadeh and Fattahi, 2015). Numerical simulation is an effective method to investigate an efficient way to exploit those reservoirs (Chen et al., 2006). Building an accurate numerical model is important to obtain relatively accurate results. Naturally fractured reservoirs, characterised by high heterogeneity, creates more difficulties in building a reliable numerical model as compared to those built for sandstone reservoirs. At present, dual-porosity and dual-permeability simulators are widely used in naturally fractured reservoirs modelling. Compared to a general single porosity model, the prominent difference is that a dual porosity/dual permeability model needs two input data for the same parameters: one that represents the matrix and the other that represents fractures (Al-Ahmadi and Wattenbarger, 2011). Reliable fracture parameters are essential to reduce the uncertainty of naturally fractured reservoirs models and improve the accuracy of simulation forecasts.

Relative permeability curves, significant for multiphase flow simulation in porous media, are worth investigating. Fracture relative permeability curves can be measured by experiments (Akin, 2001); however, due to limitations of experimental material and apparatus, measurement results are inaccurate and need to be improved. In addition, experiments are time consuming. Considering these disadvantages, an effective, widely used alternative is a computational fluid dynamics (CFD) method (Schembre and Kovscek, 2003).

The Lattice-Boltzmann method (LBM) is one of the CFD methods which can simulate fluid flow in mesoscopic scale. It can solve complex fluid problems by bridging microscopic phenomena with a macroscopic continuum equation (Dou & Zhou, 2013). Owing to its simplicity and high accuracy, it was selected to estimate fracture relative permeability curves in this research.

The purpose of obtaining accurate fracture relative permeability curves is to build an accurate numerical model that can give a relatively accurate forecast both in injection and production performance. Studying the effect of fracture relative permeability on production performance is important. As a huge number of carbonate reservoirs contain heavy oil and used steam assisted gravity drainage (SAGD) as an efficient thermal recovery method in their operations (Sola and Rashidi, 2006), this study investigates influences of different fracture relative permeability curves on SAGD performance.

1.2 Problem Statement

Fracture relative permeability curves are regarded as an important parameter that should be input into dual porosity/dual permeability reservoir models (Boerrigter et al., 1989). The classical linear relative permeability curves (X-type) are most frequently used in fractured reservoir simulation models (Saboorian-Jooybari, 2016). These classical relative permeability curves were provided by Romm in 1966 as shown in Figure 1-1. Fracture relative permeability was correlated with saturation linearly and end-points were 0 and 1, respectively. These linear relative permeability curves can be applied reasonably well under conditions with a large degree of phase segregation (Akin, 2001). In other words, they are not suitable to apply to all reservoir conditions.

As compared to artificial fractures or hydraulic fractures, natural fractures are too complex to simply use the fracture relative permeability curves as shown in Figure 1-1. Previous studies (Wong et al., 2008) showed that X-type curves were only validated in smooth-walled fractures, especially in fractures with small apertures. Therefore, it is necessary to consider fracture characteristics when calculating fracture relative permeability curves. Based on the literature, few attempts have been made to analyze the effects of physical conditions of fractures on the fracture relative permeability, and impacts of fracture relative permeability on reservoir production performance were analyzed alone. Studying such effects on relative permeability can provide important information when building reservoir models by reducing their uncertainty and improving the accuracy of simulation forecasting results.

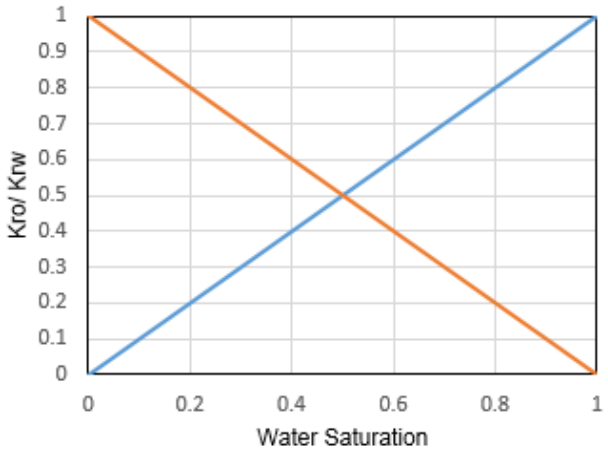

Fig1-1 Romm's fracture relative permeability curves (Romm, 1966)

1.3 Objectives of the Study

The major purpose of this work is to calculate nonlinear fracture relative permeability curves under different fracture porosities using the Lattice-Boltzmann method. Correlation and

regression analyses to investigate fracture porosity impacts on relative permeability curves are presented. Finally, the influence of nonlinear fracture relative permeability curves on SAGD performance is studied. The detailed objectives include:

(1) To study an intrinsic fracture porosity influence on relative permeability curves, 2D LBM models with different intrinsic fracture porosities were established. The intrinsic fracture porosities are each accompanied by a pair of fracture relative permeability curves. Statistics analyses were used to obtain correlations between an intrinsic fracture porosity and fracture relative permeability end points. Reservoir engineers are expected to benefit from such correlations when doing a history match of naturally fractured reservoir models.

(2) To investigate gravity effects on fracture relative permeability, the LBM calculation models were upgraded to 3D to introduce a gravity impact in the model. This study provides a sensitivity analysis of the gravity influence on fracture relative permeability by comparing two curves which were calculated from the LBM models with and without gravity consideration. The necessity of considering gravity effects was proved. A correlation analysis between intrinsic fracture porosity and fracture relative permeability feature points was performed on a 3D LBM model coupled with a gravity effect.

(3) To identify the necessity of applying correlations between intrinsic fracture porosity and fracture relative permeability in SAGD simulation models, SAGD performance was compared. One case used an input fixed linear fracture relative permeability; the other implemented nonlinear fracture relative permeability curves. The production performance under different reservoir conditions (i.e., thickness, porosity and initial oil saturation) between calculated correlations and fixed linear relative permeability curves was

compared. Conclusions provide a practical screen criterion that can be used to decide which reservoirs should or should not consider the effects of correlations between intrinsic fracture porosity and fracture relative permeability curves.

1.4 Outline of the Thesis

The following is a summary of the contents of Chapters 2 to 5:

(1) *Chapter 2* provides a description of various LBM techniques that can simulate multi-phase flow and a review of effects on fracture relative permeability. As this study will investigate the effects of different fracture relative permeability curves on SAGD performance, a literature review of SAGD is included.

(2) *Chapter 3* discusses the successfully developed LBM models to calculate the fracture relative permeability curves. A correlation analysis between fracture relative permeability curves' feature points and intrinsic fracture porosity is derived, based on the newly developed LBM models.

(3) *Chapter 4* displays the effects of nonlinear fracture relative permeability on production performance by comparing the simulation results with those from linear fracture relative permeability curves. The importance of using fracture relative permeability correlations instead of fixed linear curves under different reservoir conditions is presented.

(4) *Chapter 5* provides main conclusions of this work and offers some recommendations for future research.

Chapter Two: LITERATURE REVIEW

2.1 Literature Review of Lattice-Boltzmann Method (LBM)

2.1.1 The Development of LBM method

The LBM, as an effective Computational Fluid Dynamics (CFD) method, has attracted much attention in recent years because of its simplicity and broad applicability. The development of the LBM is based on the lattice gas automata (LGA) method (He et al., 1996). A LGA model is a type of fluid model, where a fluid is composed of a large number of fluid particles. The locations where fluid particles stay are called lattice or nodes. Fluid flow is simulated by moving such fluid particles from lattices to their adjacent lattices. Two major equations that govern a model's process include collision and streaming at each step. This method gained its fame from the paper published by Frish et al. in 1986 (Wolf-Gladrow, 2000). In this paper, the authors displayed that hexagonal lattice gas models obey the Navier-Stokes equations in two dimensions. Even though implementing boundary conditions is easy with the LGA, they also pointed out its limitations (Frish et al., 1986). In the same year, D'humières and Lallemand (1986) applied a LGA model to simulate fluid flow, proving that lattice gas simulations can be a new approach to study fluid mechanics. In 1988, McNamara and Zanetti coupled the Boltzmann equation with a LGA model which made the resulting model more efficient (McNamara & Zanetti, 1988). They opened up a new door for the study of fluid flow mechanisms by using the LBM. From then on, the LBM theory has become more sophisticated and presented fewer limitations. Owing to the LBM theory, more and more complex fluid flow problems can be investigated more easily.

More sophisticated modifications, made by Higuera et al. (1989), consequently enlarge the range of LBM models' application. They first modified a LGA model by enhancing the collision

operator to improve its linear stability. Then their work demonstrated that the LBM can describe the physics of two-dimensional turbulent flows (Benzi & Succi, 1990). In the last series of their work, they proved that a Lattice-Boltzmann equation can solve a broad spectrum of fluid problems from laminar flow to turbulent flow and from two dimensions to three dimensions (Succi et al., 1991).

Drawing from the enhanced collision operator proposed by Higuera et al. (1989), Qian et al. (1992) and Chen et al. (1992) introduced a Bhatnagar-Gross-Krook (BGK) relaxation term into a Lattice-Boltzmann equation (called LBGK) that simplified the collision operator as a single relaxation parameter. After numerical comparisons, they concluded that the LBGK is more efficient, although the original LBE model has more flexibility (Succi et al., 1993). Succi's (1997) review of a Lattice-Boltzmann equation pointed out that the method built a bridge between microscopic and macroscopic worlds. Using the LBM to calculate multiphase flow is easier than any other non-conventional CFD methods. Its amenability to parallel computing offered a new, efficient way to calculate complex flow at industrial levels.

2.1.2 LBM Application in Porous Media

As the LBM can simulate fluid flow for both laminar flow and turbulent flow successfully, it has gained its use for investigating fluid flow in different types of porous media.

Chen et al. (1992) demonstrated that the LBM can simulate three-dimensional fluid flows, generating a proof that simulation results were in agreement with results from a spectral method. For three-dimensional fluid problems with complicated geometries, the LBM can be an

alternative numerical method. Aharonov and Rothman (1993) applied LBM models to simulate non-Newtonian flow thorough complex geometries. The validation of simulation results was performed by matching simulation results with theoretical predictions. In addition, they argued that LBM models might be used to simulate fluid flow in porous media.

Ferréol and Rothman (1995) successfully accomplished simulations for both single phase and two-phase flows through Frontainebleau sandstone by using the LBM. The structure of sandstone is described by using tomographic reconstructions. Permeability was calculated by combining LBM simulations and sandstone 3D reconstruction-tomographic pictures. In addition, their work studied the two-phase flow of an imbibition and drainage process. Martys and Chen (1996) applied multi-components of a LBM model in 3D porous media. Poiseuille flow was reproduced with a constant body force. For two immiscible fluids, their results from the LBM simulation model were consistent with Laplace's law. Simulation results of relative permeability matched experimental data well. Their work demonstrated that it was possible to simulate multi-phase flow in porous media. Hatiboglu and Babadagli (2008) modeled a spontaneous imbibition process in a matrix-fracture system by using a LBM model which was validated with sand pack experiments. They demonstrated that the LBM model can capture physical phenomena during the imbibition process at pore scale. Relative permeability curves, as a most important fluid interaction parameter, can also be calculated in a Lattice-Boltzmann model. By simulating viscous displacement in porous media, Ramstad et al. (2010) computed a capillary pressure and wetting phase relative permeability that showed a highly qualitative agreement with experimental data. In summary, the LBM is an efficient and powerful tool to investigate fluid flow mechanisms in porous media.

2.1.3 Multi-phase Model in LBM

The application of the LBM in studying fluid flow mechanisms in porous media is attractive. In order to investigate fluid interaction problems, a multi-component model of the Lattice-Boltzmann method has been developed. In this section, several mainstream multi-component methods in the LBM, which can simulate immiscible multi-phase fluid flow, will be introduced.

The first multi-component model is the R-K LBM model. This original multi-phase model was built by Rothman and Keller (1988) in a cellular-automaton fluid system and later introduced into a LBM model by Gunstensen et al. (1991) to simulate immiscible fluid flow. In this model, two kinds of fluids are described by two colours (generally Red and Blue). Two distribution functions were formulated separately to simulate the dynamics of each fluid. At each time step, a colour gradient was calculated at every lattice to simulate one phase displaced by the other phase because different phases are characterised by different colors. For a specific lattice, a change in colour stands for the original phase displaced by the other one. The interface position of two fluids can be determined by calculating a colour gradient. To direct fluid particles into their respective bulk fluids at the interface, additional cohesive forces found between two fluids are added into a collision step. As compared to the model proposed by Rothman and Keller, Gunstensen et al. (1991) added a recolouring step into their model. A recolouring step aims to prevent diffusion between the two fluids by maintaining a thin interface. Programing this model is simple; the major disadvantage is that the model needs large computational requirements. A coloured model, at this stage, cannot deal with fluids with different viscosity due to a thin fluid interface. This two-colour model was improved by Tölke et al. (2002) who modified the original recolouring step. Even though their model can simulate two-phase flow in porous media and the

simulation results can match analytical solutions well, it still cannot solve viscosity problems very well. In 2005, Latva-Kokko and Rothman improved the model further by introducing a free parameter which is influenced by the thickness of an interface; this model can simulate fluids with a viscosity up to 10 cp (Latva-Kokko & Rothman, 2005). In their model, a perturbation term was added into the force balance at a fluid-solid surface, which enabled the model to handle two-phase flow, including the effect of capillary pressure and wettability.

The most widely used multi-component multi-phase LBE model is the S-C model proposed by Shan and Chen (1993). In this model, a non-local interaction between particles at neighboring sites was introduced. The interaction between two different kinds of fluids was described by introducing interaction potentials for each component. In the R-K model, a colour gradient was used to determine the interface positions of two fluids; in the S-C model, interaction potentials were used to determine them. Compared to the R-K model, the most important difference is that an extra momentum transfer flux was introduced in the S-C model because of interaction potentials (Hou et al., 1997). The S-C model's additional advantages over the R-K model include: the capacity to simulate more than two phases, a decrease in computational requirements and an ability to simulate two fluids with different viscosity.

The free energy approach in the LBM is also a means to simulate immiscible two-phase flow. It was first proposed by Swift et al. (1995) to simulate a liquid-vapour interface in an isothermal system with a non-ideal pressure tensor introduced. Specifically, two particle velocity distribution functions exist. One tracks the interface positions by calculating an order parameter while the other calculates a velocity without a pressure gradient (Yan & Zu, 2007). This

approach, however, could not ensure Galilean invariance. Nadiga and Zaleski solved this problem by constructing Galilean invariant momentum and mass conservation equations for macroscopic variables (Inamuro et al., 2000). This new approach enables the capability to simulate fluids with a high viscosity ratio.

Considering the computational requirements, applicability of each model, and its numerical stability, the S-C multi-component multiphase model was applied in this work to investigate the oil-water relative permeability curves in fractures.

2.2 Literature Review of Relative Permeability

2.2.1 The Concept of Relative Permeability

Relative permeability is an important parameter used to simulate multi-phase flow in porous media. It is calculated from an extension of Darcy's law. Darcy's law illustrates a relationship between a fluid flow rate and a vertical sand pack height difference where the fluid flows through it:

$$q = KA\frac{h_i - h_o}{L} \tag{2-1}$$

where K is constant; q is rate of water flow, m^3/s; A is column cross sectional area, m^2; L is the length of the column, m; and h_i and h_o are the hydrostatic heads of the sand pack at inlet and outlet. Based on this equation, Darcy's law broadcasts into a reservoir engineering area with some modifications. First, $\frac{k}{\mu}$ replaces K with more physical meaning, k is the permeability of porous media (D) and μ is the fluid viscosity (cp). Then a more widely used single phase Darcy's law is produced which describes incompressible laminar fluid flow:

$$v = -\frac{k\rho}{\mu}\frac{d\Phi}{dx} \tag{2-2}$$

where $\Phi = \frac{P}{\rho} + gZ$ is the fluid potential, P is pressure, Pa; ρ is density, kg/m^3; g is gravitational acceleration, m/s^2; Z is vertical depth, m.

When two immiscible fluids flow in a same porous medium, they will interact and the fractional loss of hydraulic conductivity for each fluid is the definition of relative permeability. As a result, it is calculated by the ratio of effective permeability for each phase to a base value. The existence of a base value makes relative permeability a dimensionless parameter. Formulations of relative permeability for oil, water, and gas can be derived from Darcy's law as shown below (Chen et al., 2006; Chen, 2007; Modaresghazani, 2015):

$$v_o = \frac{kk_{ro}}{\mu_o}\left(\rho_o g\frac{dZ}{ds} - \frac{dP_o}{ds}\right) \tag{2-3}$$

$$v_w = \frac{kk_{rw}}{\mu_w}\left(\rho_w g\frac{dZ}{ds} - \frac{dP_w}{ds}\right) \tag{2-4}$$

$$v_g = \frac{kk_{rg}}{\mu_g}\left(\rho_g g\frac{dZ}{ds} - \frac{dP_g}{ds}\right) \tag{2-5}$$

where o, w and g represent oil, water and gas, respectively. When interference occurs between different phases, the summary of relative permeabilities for all phases should be no larger than 1:

$$\sum k_{ri} \leq 1 \tag{2-6}$$

2.2.2 Development of Fracture Relative Permeability Investigation

A fracture oil-water relative permeability relationship arose from Romm's experiment (1966) using kerosene, water and artificial parallel-plate fractures. Artificial fractures were divided by waxed paper and strips. The result was the well-known and widely used X-type model that described relative permeability as a linear function of saturation:

$$k_{ro} = S_o \tag{2-7}$$

$$k_{rw} = S_w \tag{2-8}$$

This linear relationship exists because the interaction between fluids decreases due to the setting of artificial fractures.

Merrill (1975) conducted experiments using parallel glass plates. Experimental data was obtained from a narrow range of saturation; as a result, the study did not find any correlation between relative permeability and saturation. The study did, however, provide that the sum of relative permeabilities for each saturation is less than one (Pan, 1999).

Fourar et al. (1993) also performed experiments to investigate two-phase flow in fractures using both smooth and rough fractures, and the two fluids were changed from oil and water to air and water. The phenomena of flow from both rough and smooth fractures was similar to the flow in a pipe. Thus experimental results agreed with Lockhart and Martinelli's equation which was derived from two-phase flow in a pipe. An analysis of experimental data came to a conclusion that relative permeability curves were dependent on saturation but the relationship between them was not linear. Relative permeability curves were also dependent on fluid flow rates. As depicted in a sequence of papers, Nowamooz et al. (2009) used a transparent replica of a rock fracture

with a roughed wall and applied the same theories introduced by Lockhart and Matinelli. Only the sandstone's fracture surface made deviations from a cubic ratio. They concluded that interference was presented between two fluids (liquid and gas) which, in turn, led to a sum of the relative permeabilities at a specific saturation that was less than one.

Persoff and Pruess (1995) used a transparent apparatus to visualize flow structure in fractures with roughness. During their experiment, persistent instabilities appeared in two-phase flow under cyclic pressure. Such instabilities can be explained by an interaction between a pressure drop, caused by viscous flow, and a capillary force. The experimental phenomena indicated that the fluid pattern obeyed the capillary theory: The non-wetting phase flowed through pores with a large radius while the wetting phase flowed into small pores continuously. The result of the fracture relative permeability measurements disagreed with the X-type model which showed that relative permeability was equal to its saturation. Their study concluded that an interaction occurred between two phases because, for each phase, their relative permeability reduced sharply at intermediate saturations.

Pyrak-Nolte et al. (1992) conducted experiments to investigate trapping influence on immiscible flow in fractures. Their experiments showed that the non-wetting phase was trapped by the wetting phase. The degree of trapping was related to intrinsic fracture porosity. Residual saturation generated by the non-wetting phase was trapped which led to reducing the wetting phase relative permeability.

Chen et al. (2004, 2006 & 2007) conducted a series of experiments to investigate fracture air-water relative permeability with channel tortuosity. The first experiment was conducted in a smooth-walled fracture to study the flow structure effect on relative permeability. To quantify this effect, a physical tortuous channel was used and the process of measurement was the same as what Fourar et al. (1993) did earlier. Their experiments demonstrated that two-phase relative permeability was not only influenced by fracture geometry, but also by the structure of the two-phase flow. After that, their experiments were improved by using fractures with rough surfaces. In addition to the qualitative conclusion that channel tortuosity had an impact on relative permeability, an empirical equation was also derived. Their study proved that calculated relative permeabilities, using the flow structure approach, were feasible. Chen et al. (2007) further studied the effect of a phase change on steam-water relative permeability in both smooth and rough fractures. Comparing the experiments' results, phase transformation made a flow structure different. Relative permeabilities with phase transformation effects presented the relationship of the Brooks-Corey equation.

Wong et al. (2008) measured oil-water relative permeability for both smooth and rough fractures using the same experimental apparatus and method as mentioned previously. They noted that channel flow led to X-type oil-water relative permeability curves only in a smooth-walled fracture with a separate injection method. Otherwise, the function of relative permeability and saturation was not linear. They agreed with previous conclusions that a flow pattern can be influenced by surface roughness; however, the impact was not significant when a fracture aperture was large.

In addition to those experimental methods to study two-phase flow in fractures, several studies were also completed by numerical methods. Pruess and Tsang (1989) simulated two-phase flow in fractures where aperture distribution obeyed a correlated log-normal distribution by applying a percolation theory. The primary assumptions in this model were that fracture permeability and a capillary force can be estimated by using a parallel-plate model. In this model, the wetting phase occupied in the fractures whose aperture was smaller than a cut off aperture. The value of the cut off aperture was determined by a capillary pressure. For a specific capillary pressure, the effective permeability can be determined using Darcy's law with boundary conditions and a flow rate. The relationship between relative permeability and saturation can be obtained by repeating such steps. Their numerical studies also found interference between two phases. In their numerical work, they concluded that when the two phases flew through a medium which had small capillary numbers, the non-wetting phase was blocked by the wetting phase. The irreducible wetting phase saturation was smaller than the irreducible non-wetting phase saturation; namely, the wetting phase had superiority when flowing into smaller apertures. Similar to Pruess and Tsang' work, Mendoza (1993) built a numerical model based on a percolation theory to calculate capillary pressure and relative permeability in fractures which were generated by the geostatistical method. In his study, relative permeability depended on fracture apertures, as concluded by Monte Carlo simulations. The relationship of relative permeability and saturation can be described by a power-law function (Pan, 1999). Murphy and Thomson (1993) also used numerical methods to calculate relative permeability by implementing a finite volume of mass conservation and a cubic law, rather than using a percolation theory. Their study simulated flow in a single variable aperture fracture and obtained some

phenomenological conclusions. They did not provide any quantitative results related to fractional flow.

Rossen and Kumar (1992) investigated the effect of gravity and fracture aperture distribution on relative permeability curves using the Effective Medium Approximation (EMA). In their study, straight line relative permeability curves can be obtained when gravity segregation dominated flow. On the other hand, if two phases flowed without a gravity effect, the relative permeability curves' cross point approached zero when the fracture aperture became broader. In addition, viscous effects could make relative permeability curves linear to saturation.

Except for the numerical method to calculate relative permeability curves in fractures, analytical methods were also used to derive relative permeability functions. Chima et al. (2010) derived oil-water relative permeability by using shell momentum balance, Newton's law and Darcy's law. The derived equation should meet the assumptions that the two fluids are Newtonian and incompressible and have laminar flow with constant temperature and gravitational segregation. Following this paper, Chima and Geiger (2012) derived a water-gas relative permeability equation under the same assumptions used in the oil-water system. Based on Chima's work, Lei et al. (2014) derived a new gas-water relative permeability equation encompassing the coupled fracture aperture and the influence of tortuosity. The model was further improved by Li et al. (2014) who took the irreducible water saturation effect into consideration in the original Chima's model. All these models were validated by experiment results.

In summary, the results from mathematical and experimental studies showed that it is not reasonable to describe two-phase flow in fractures by using X-type curves. Interference between two phases led the relative permeability curves to being nonlinear and their sum to be less than one.

2.2.3 Measurement of Relative Permeability

Steady-state and unsteady-state methods are most commonly used to measure relative permeability (Modaresghazani, 2015). In some articles, the capillary and centrifuge methods are also mentioned (Honarpour and Mahmood, 1988). In a steady-state method, a fluid is injected into a core sample at a fixed ratio; relative data is measured when a steady pressure drop and uniform saturation are reached. An unsteady-state method injects a fluid in a certain sequence; relative data is recorded at the outlet of a core sample. Equations are used to calculate relative permeability. The measurement of the capillary pressure method will be used if the purpose is to obtain drainage relative permeability curves or if the core is displaced by gas in the non-wetting phase while the wetting phase is a liquid. Relative permeability curves are calculated using equations, whereas capillary pressure curves should be known as prerequisites. The centrifuge method is to put a core sample, which was saturated with two phases, into a centrifuge. Fluids produced from the core during the entire process are measured (Honarpour, 1986). The centrifuge method will avoid viscous fingering effects and shorten experiment time, as compared to the steady-state methods; both methods, however, are widely used. Details of the steady and unsteady methods are discussed in the following section.

2.2.3.1 Steady-state Method

In the steady-state method, a uniform ratio of fluids is injected through a core sample, which leads to a uniform saturation of the sample when the steady state of pressure drops and fluid flow rates at the outlet of the core sample is reached (Honarpour et al., 1986). To obtain relative permeability curves, several rounds of experiments should be done to cover a full range of saturations. Capillary end effects at the outlet of the core sample will influence experiment results; eliminating these effects becomes challenging during steady state experiments. The widely used Penn-State method sees a core sample divided into three segments (Dana and Skoczylas, 2002). Relative permeabilities are measured primarily from the middle segment. The function of the front segment is to mix two phases completely to ensure that fluid distributions are stable before they enter the middle segment. The end segment of the core sample is to reduce the effect of the capillary end. Experiments start with a sample saturated with a single phase fluid, usually water. Fluids are injected simultaneously at constant rates or pressure and given time to reach equilibrium. By measuring saturations, flow rates and pressure gradients, the effective relative permeability for each phase at this specific saturation can be calculated by using Darcy's law. The steps are repeated to calculate the effective permeability at different saturations by changing the ratio of injection rates (Honarpour and Mahood, 1988). Methods to measure saturation vary. The simplest method is to weight a core sample before and after experiments (Modaresghazani, 2015). Measuring electric resistivity of a core sample is another method to determine saturation (Wyllie and Spangler, 1952). Nuclear magnetic resonance, X-ray absorption and gamma-ray are also used by some investigators (Saraf and Fatt, 1967; Vinedar and Wellington, 1987). The steady-state method can measure relative permeability with a long range of saturations, leading to more accurate results. This method, however, is time consuming.

2.2.3.2 Unsteady-state Method

Compared to the time consuming steady-state method, the unsteady state method is more efficient for measuring relative permeability (Maini et al., 1990). This method, however, is more difficult to process experimental data to achieve relative permeability relationships. The core of this theory, as developed by Buckely and Leverett (1942), is to calculate fractional water flow at the outlet of a core sample by combining Darcy's law and capillary pressure definition:

$$f_w = \frac{1 + \frac{k_o}{q_t \mu_o}\left(\frac{\partial P_c}{\partial x} - \mathrm{g}\Delta\rho \sin\theta\right)}{1 + \frac{k_o}{k_w} \cdot \frac{\mu_w}{\mu_o}} \tag{2-9}$$

where q_t is the total flow rate at the outlet of the core sample, $\Delta\rho$ is the difference of two fluids' densities, and θ is the direction between the horizontal and core central axis. The simplification of this equation was first derived by Welge (1952) under the condition that a core was placed horizontally and capillary pressure was negligible:

$$S_{w.avg} - S_w = f_o Q_w \tag{2-10}$$

where $S_{w.avg}$is the average water saturation and Q_w is the cumulative volume of water injection. They all can be calculated by using mass balance with experimental injection data. f_o is the fractional flow of oil at the outlet of the core sample, which can be determined by plotting $S_{w.avg}$ versus Q_w. The equation is shown as:

$$f_o = \frac{q_o}{q_o + q_w} \tag{2-11}$$

By combining Darcy's law, this equation can be further derived:

$$f_o = \frac{1}{1 + \frac{\mu_o / k_{ro}}{\mu_w / k_{rw}}} \tag{2-12}$$

From equation (2-12), the ratio of relative permeabilities of oil and water can be calculated. The calculation of gas-oil or gas-water relative permeability ratio is the same with oil-water. In order to calculate the relative permeability for each phase separately, the model is further developed, in the form of the Johnson-Bossler-Naumann (JBN) method. For this JBN method, an injectivity parameter, I_r, was added into the equation. Equations for oil and water relative permeability calculations are shown as:

$$k_{ro} = \frac{f_o}{d\left(\frac{1}{I_r Q_w}\right) \Big/ d\left(\frac{1}{Q_w}\right)} \tag{2-13}$$

$$k_{rw} = \frac{f_w}{f_o} \cdot \frac{\mu_w}{\mu_o} k_{ro} \tag{2-14}$$

To reach a stable displacement, the flow rate should be high enough to ensure that the pressure drop across the core sample is high. Two fluids should be immiscible and incompressible in order to maintain a constant velocity in all cross-sectional areas during experiments.

2.3 Literature Review of SAGD

2.3.1 The concept of SAGD

Steam assisted gravity drainage (SAGD), an efficient thermal recovery method, is widely used in heavy oil reservoirs (Abdel-Halim and Subramanian, 2002). This method relies on a gravity force by utilizing a pair of parallel horizontal wells perforated near the bottom of a reservoir (Figure 2-1). The bottom well is the producer while the upper one is the injector which is several meters above the producer. Because of the difference in density, steam rises to the upper layer of the formation, creating a steam chamber. Oil in the reservoir is then heated and its viscosity is reduced through several orders of magnitude. With the help of gravity, the oil flows to the

producer along the steam chamber border. The steam chamber grows vertically and laterally, with continuous steam injection leading to heating more oil surrounding the chamber.

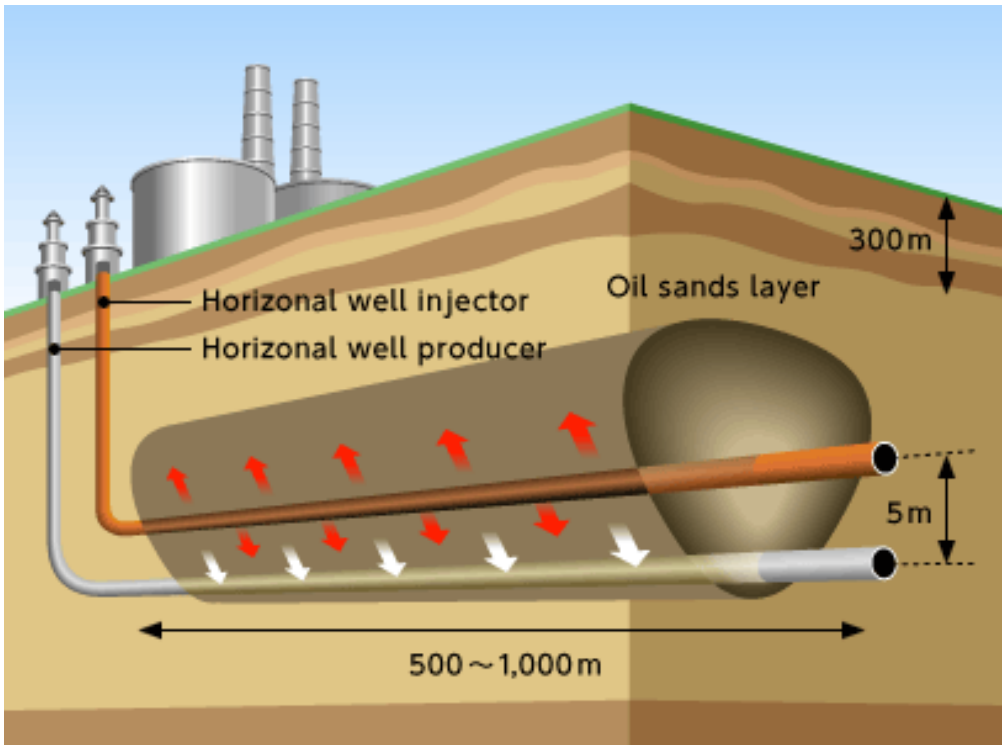

Figure 2-1 SAGD process
(http://www.japex.co.jp/english/business/ep_o/oilsands_sagd.html)

2.3.2 The Start-up Stage of SAGD Process

The success of a SAGD operation is highly dependent on a strong start-up process. During the start-up process, heat communication is built between a producer and an injector by steam circulation in both wells. The purpose is to maintain the temperature and quality of the steam. Vincent et al. (2004) proposed three stages to the start-up process. In the first stage, circulating steam is injected into both the injector and production wells at the same pressure which aims to heat wellbores evenly. The second stage is to apply a pressure gradient between the two wells. The objective is to speed-up the process by adding convective heating in the region near the

wellbores. Finally, when the mobility of the heavy oil or bitumen is high enough, the operation constraints of the well pair convert into the fully SAGD mode. Start-up process heat efficiency can be directly evaluated by circulation time. Several researchers provided optimal scenarios of different start-up processes based on reservoir characteristics. Shin and Polikar (2007) pointed out that start-up time increased as well spacing increased. An optimal circulation rate corresponded to a maximum conductive heat transfer (Vanegas et al., 2005).

2.3.3 The Operation Process of SAGD

The SAGD process starts when the heat communication is reached. SAGD can be subdivided into two stages in this period. The first stage is a production period: A steam chamber has not reached the top of a formation and an oil rate increases with the growth of the steam chamber. The latent heat of steam is consumed to heat the oil; heat efficiency is high. As a result, the larger the steam chamber, the higher the oil rate. When the steam chamber contacts the top of the formation, the second stage of SAGD begins. A large amount of heat loss runs into overburden (Khaleeq, 2014), and hence the steam-oil ratio (SOR) increases in this stage.

2.3.4 Steam-trap Control

For typical SAGD production, a steam trap control is necessary to maintain the stability and longevity of its operation. To avoid injected steam directly produced from a production well, the liquid level should be controlled above the producer. In industry, $10℃/m$ of a liquid level is an acceptable value. A minimum value is needed with wellbore drawdown consideration; the liquid level should be increased as the wellbore drawdown is decreased (Yuan & Nugent, 2013).

2.3.5 Impact Factors of SAGD Production

Llaguno et al. (2002) provided reservoir screening methods for SAGD operations and concluded that, for optimal oil production, the most sensitive parameters were thickness, porosity and oil saturation. Nguyen et al. (2012) ranked reservoir parameters that affected SAGD performance. Porosity was the most important one as compared to others. Kiasari et al. (2010) displayed that a steam-oil ratio decreased when reservoir porosity increased. For reservoir thickness, the higher the pay thickness, the greater the oil produced. The screen criterion of reservoir thickness in which SAGD can be applied should not be less than 15 m. The reason for this limitation is that when a reservoir is too thin, a steam chamber will reach the overburden within a short time, leading to much waste of enthalpy (Edmunds & Chhina, 2001). Because low permeability negatively impacts water drainage, oil flow and steam chamber growth, the ratio of vertical permeability and horizontal permeability should be higher than 0.6 to ensure that the SAGD operation is economical (Mukherjee et al., 1994). Oil viscosity will also influence SAGD performance. With a reduction in oil viscosity, injectivity and oil production will be improved in carbonate reservoirs (Das & S.K., 2007). Several investigators have studied the selection of optimal operating parameters in SAGD. Singhal et al. (1998) demonstrated that the optimal length of horizontal wells is 500m and optimal well spacing is 100 m. For the optimal distance between an injector and a producer, the conclusion is not determined. Sasaki et al. (2001) declared that a larger distance contributed to a larger steam chamber, a higher rising rate, and a higher oil production rate. Canbolat et al. (2002) showed that it was possible to increase recovery efficiency in this way.

2.3.6 The Feasibility of SAGD Application in Naturally Fractured Reservoirs

SAGD is an efficient way to produce heavy oil and bitumen in sandstone heavy oil reservoirs. The feasibility of a SAGD application in naturally fractured reservoirs, especially for carbonate reservoirs, warrants discussion. Sadaee et al. (2006) used a field-scale carbonate reservoir model to show that SAGD can be applied as a better EOR method when compared to other thermal methods for Iranian heavy oil carbonate reservoir development. Bagci (2006) displayed, through both experimental studies and simulations, that it is feasible to apply SAGD in fractured reservoirs. In their studies, SAGD performance can be improved by vertical fractures that can enhance a steam chamber expansion rate. Das (2007) showed that commercial production rates can be achieved by using SAGD in fractured carbonate reservoirs. Considering economic factors, reservoirs with high viscosity oil and high pay thickness are more suitable for the SAGD process.

Chapter Three: FRACTURE RELATIVE PERMEABILITY CALCULATIONS IN LBM

3.1 Calculation Theory

The Lattice-Boltzmann method is a bridge which brings microscopic particle dynamics and macroscopic continuum equations together. Specifically, fluids are simulated as particles located in lattices which interact with other lattices through streaming and collision steps. At each lattice, a particle distribution function is described, denoted as $f_i(\mathbf{X}, t)$, where i represents each direction, **X** describes each lattice, and *t* denotes time. For a 2D model, the D2Q9 lattice structure is widely used (Sun et al., 2009); for a 3D model, D3Q19 is most widely used (Hecht and Harting, 2010). The particle distribution function of the Lattice-Boltzmann equation is shown as (Mahabadian et al., 2015):

$$f_i^{\sigma}(\mathbf{X}, t) - f_i^{\sigma}(\mathbf{X} + \boldsymbol{e}_i \Delta t, t + \Delta t) = \frac{\Delta t}{\tau_{\sigma}}\left[f_i^{\sigma}(\mathbf{X}, t) - f_i^{\sigma,eq}(\mathbf{X}, t)\right] \tag{3-1}$$

where the distribution function of component σ is described as $f_i^{\sigma}(\mathbf{X}, t)$, $f_i^{\sigma,eq}(\mathbf{X}, t)$ is the equilibrium particle distribution function and Δt is the time step which equals 1 for one time iteration. The streaming step, which simulates particle movement to its neighbouring lattices, is described by the left-hand side of the equation, while the right-hand side of the equation stands for the collision step. The Bhatnar-Gross-Krook (BGK) dynamics was selected in this study. In BGK dynamics, the relaxation parameter, $\tau_{\sigma,}$ which is related to kinematic viscosity, is a single value for the entire simulation process. The equilibrium particle distribution function for one component is shown as:

$$f_i^{\sigma,eq}(\mathbf{X}, t) = \omega_i \rho_{\sigma}\left[\frac{\boldsymbol{e}_i \cdot \boldsymbol{u}_{\sigma}^{eq}}{c_s^2} + \frac{(\boldsymbol{e}_i \cdot \boldsymbol{u}_{\sigma}^{eq})^2}{2c_s^4} - \frac{(\boldsymbol{u}_{\sigma}^{eq})^2}{2c_s^2}\right] \tag{3-2}$$

$$c_s = c/\sqrt{3} \tag{3-3}$$

where c is the ratio of lattice spacing which is equal to the lattice length unit divided by the time step, ω_i is the weight of velocity in each direction, and $\boldsymbol{e}_i$ is the discrete unit velocity in each direction. In the D2Q9 structure (displayed in Figure 3-1), the values of ω_i and $\boldsymbol{e}_i$ are shown in equations (3-4) and (3-5).

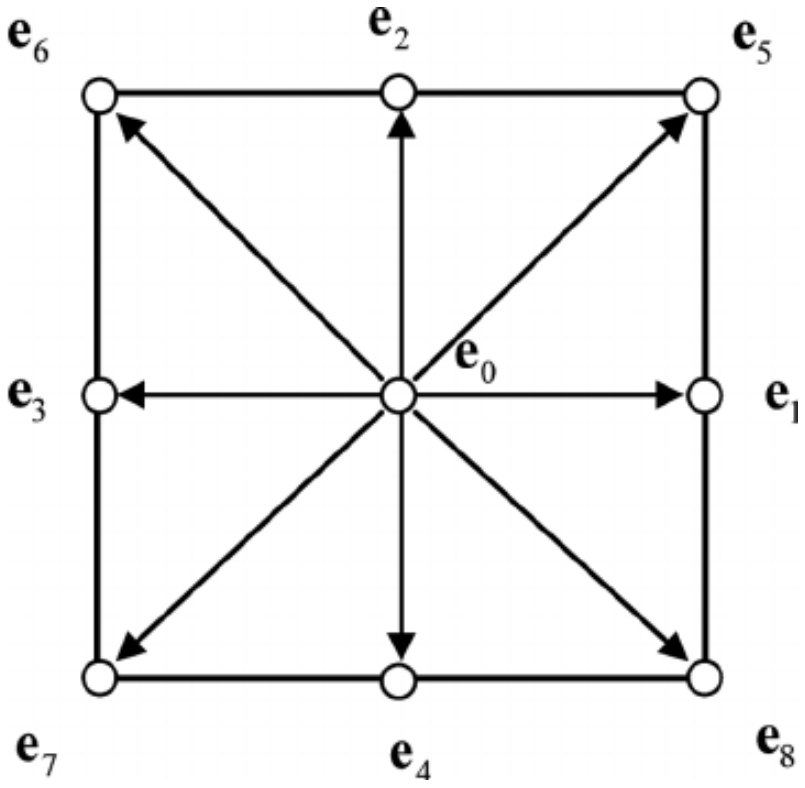

Figure 3-1 D2Q9 Structure (Imani et al., 2012)

$$\omega_i = \begin{cases} \frac{4}{9} & i = 0 \\ \frac{1}{9} & i = 1,2,3,4 \\ \frac{1}{36} & i = 5,6,7,8 \end{cases} \tag{3-4}$$

$$\boldsymbol{e}_i = \begin{cases} (0,0) & i = 0 \\ (\cos\theta_i, \sin\theta_i)c, \theta_i = \dfrac{(i-1)\pi}{2}, & i = 1,2,3,4 \\ \sqrt{2}(\cos\theta_i, \sin\theta_i)c, \theta_i = \dfrac{(i-5)\pi}{2} + \dfrac{\pi}{4}, & i = 5,6,7,8 \end{cases} \tag{3-5}$$

For macroscopic parameters, the density and velocity for each component are calculated by the equations:

$$\rho_\sigma = \sum_i f_i^\sigma \tag{3-6}$$

$$\boldsymbol{u}_\sigma = \left(\sum_i f_i^\sigma \boldsymbol{e}_i\right)/\rho_\sigma \tag{3-7}$$

$$\boldsymbol{u}_\sigma^{eq} = \boldsymbol{u}'_\sigma + \frac{\boldsymbol{F}_{ext}\tau_\sigma}{\rho_\sigma} \tag{3-8}$$

where $\boldsymbol{u}'_\sigma$ is the velocity calculated before the collision step.

In this study, the Shan-Chen multi-component LBM model was used and the program proceeded in three parts at each iteration. First, the program was initialized with velocity and density distribution. Then particles executed the collision step and the related parameters, such as velocity and equilibrium functions, were calculated from the equations, as previously mentioned. Finally, the program executed the stream step and new particle distributions were obtained. The algorithm of this program is illustrated in Figure 3-2. Fluid lattices, solid lattices and bounce back lattices were used in this program. Fluid lattices simulated fluid particles which flowed from one lattice to the other; bounce back lattices represented the surface of the solids. No fluids existed in the solid lattice.

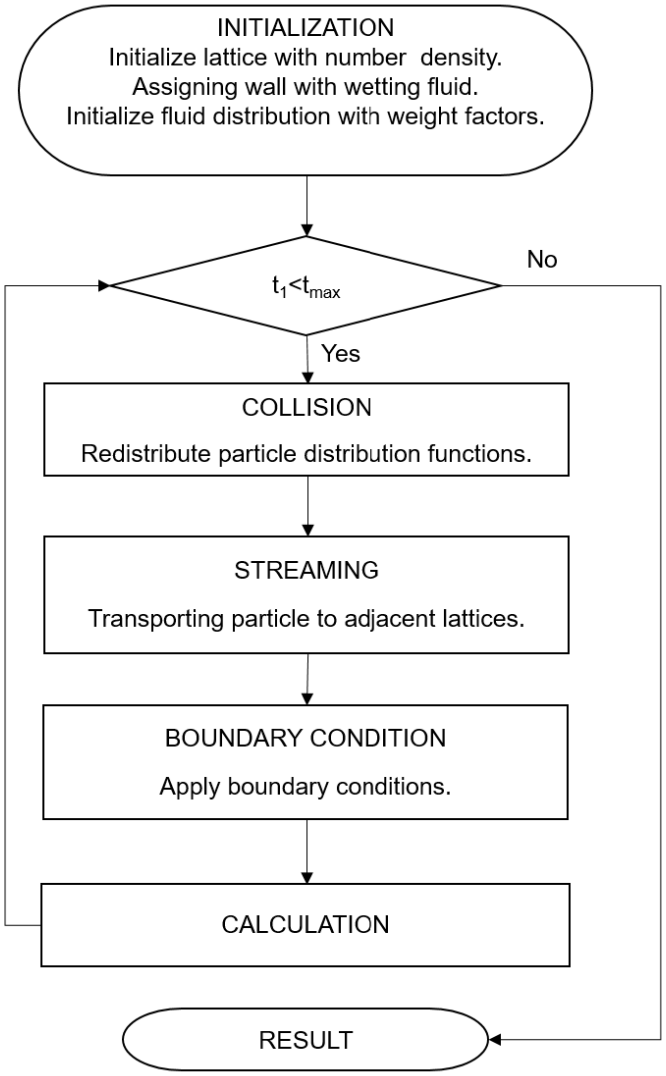

Figure 3-2 LBM Algorithm

In the Shan-Chen multi-component model, the interactions between different kinds of fluids, described by a function of pseudo-potential inter-particle forces, are defined (Landry, 2013):

$$\boldsymbol{F}_{p,\sigma}(\boldsymbol{X},t) = -G_c\rho_\sigma(\boldsymbol{X},t)\sum_i \omega_i\rho_{\bar{\sigma}}(\boldsymbol{X}+\boldsymbol{e}_i\Delta t,t)\,\boldsymbol{e}_i \tag{3-9}$$

where G_c is the parameter which describes the strength of an inert-particle force. The calculation of this force only executes in the nearest neighboring lattices. The adhesive force between the

solid surface and fluid lattices is formulated by introducing fictitious densities for each component on the bounce back lattices:

$$\boldsymbol{F}_{ads,\sigma}(\boldsymbol{X},t) = -G_{ads,\sigma}\rho_{\sigma}(\boldsymbol{X},t)\sum_{i}\omega_i s(\boldsymbol{X}+\boldsymbol{e}_i\Delta t,t)\,\boldsymbol{e}_i \tag{3-10}$$

where s indicates the existence of a bounce back node. In other words, when $\boldsymbol{X}+\boldsymbol{e}_i\Delta t$ fluid moves to a bounce back lattice, then $s(\boldsymbol{X}+\boldsymbol{e}_i\Delta t,t)$ equals 1. In general, the wetting fluid's fictitious density's value is negative while the non-wetting fluid's is positive. Their absolute values are the same. The definition of this fictitious density is different from a fluid density, indicating the strength of the adhesive force between the solid surface and fluids. After including these forces in the Lattice-Boltzmann equation, the velocity equilibrium equation was modified to:

$$\boldsymbol{u}_{\sigma}^{eq} = \boldsymbol{u}'_{\sigma} + \frac{(\boldsymbol{F}_{ext,\sigma}+\boldsymbol{F}_{ads,\sigma}+\boldsymbol{F}_{p,\sigma})\tau_{\sigma}}{\rho_{\sigma}} \tag{3-11}$$

All LBM simulations presented above were executed using 'Palabos' which is an open source written by C++.

To calculate two-phase relative permeability, a steady-state method of relative permeability measurement was simulated. In the initialization step, the wetting phase fluid distributes along a fracture surface wall while the non-wetting phase fluid is in the center of the fracture channel and is sandwiched with the wetting-phase fluid at desired saturation. Fracture walls are assumed to be strongly water wet in the study. To calculate relative permeability curves, the total momentum of each phase at the target wetting phase saturation is calculated first (Ramstad et al., 2010):

$$\pi_{\sigma}(S_w) = \sum_{x}\rho_{\sigma}\,\boldsymbol{u}_{\sigma} \tag{3-12}$$

Then relative permeability for each phase, defined as a fractional flow, was calculated:

$$k_{r\sigma} = \frac{\pi_\sigma(S_w)}{\pi_\sigma(S_\sigma = 1)} \cdot \frac{\Delta P(S_\sigma = 1)}{\Delta P(S_w)} \tag{3-13}$$

The convergence criterion in the steady state was:

$$\varepsilon > \left| \frac{\pi_\sigma(t - 5000) - \pi_\sigma(t)}{\pi_\sigma(t)} \right| \tag{3-14}$$

where $\varepsilon = 10^{-3}$ (Landry, 2013).

3.2 Validation of LBM Simulation Model

Yiotis et al., (2007) derived an analytical solution of a two-phase relative permeability functions coupled with a viscous effect when fluids flowed through parallel plates. The assumption of this analytical model was that the non-wetting phase was sandwiched by the wetting phase, which is the same with our fluid distribution, as shown in Figure 3-3.

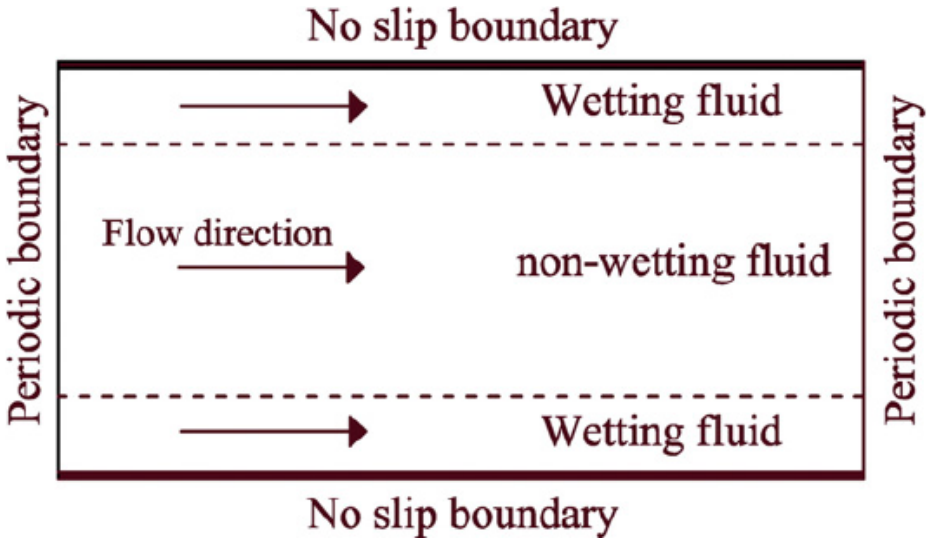

Figure 3-3 Schematic of immiscible two-phase flow between parallel plates (Ghassemi & Pak, 2011)

The definition of each phase saturation is: the width of fluid occupation divided by the whole width of a channel. Relative permeability as a function of saturation and a viscosity ratio is shown as:

$$k_{r,w} = \frac{1}{2} {S_w}^2 (3 - S_w) \tag{3-15}$$

$$k_{r,nw} = S_{nw} \left[\frac{3}{2} M + {S_{nw}}^2 \left(1 - \frac{3}{2} M \right) \right] \tag{3-16}$$

where M is a viscosity ratio defined as $M = \mu_{nw}/\mu_w$.

To validate the accuracy of the LBM simulation model, including settings of boundary conditions, the model was first simplified as a 2D channel, which indicated that the intrinsic fracture porosity is 1. In other words, in the validation case, the model simulated immiscible two-phase fluid flow through parallel plates, as shown in Figure 3-3. A 300×100 lattice domain was built. The bottom and top of this domain are described as solid walls such that a no-slip boundary was implemented. A periodic boundary condition is set at the right and left of the domain to simulate the infinite length of the plates in the direction of flow. A pressure gradient was applied to both fluids along the direction of fluid flow to realize co-current flow in fractures.

The study first validated the solution when M<1; the wetting phase viscosity is larger than that of the non-wetting phase. Figure 3-4 are results from LBM simulations and analytical solutions of the two-phase flow in parallel plates when M=0.1. The figure shows that the non-wetting phase increases faster than the wetting phase under the same pressure gradient because the wetting phase viscosity is larger than that of the non-wetting phase. This figure displays that LBM

simulation results have a sound agreement with analytical solutions. The deviation between the LBM simulation results and analytical solutions is less than 10%, which is tolerable.

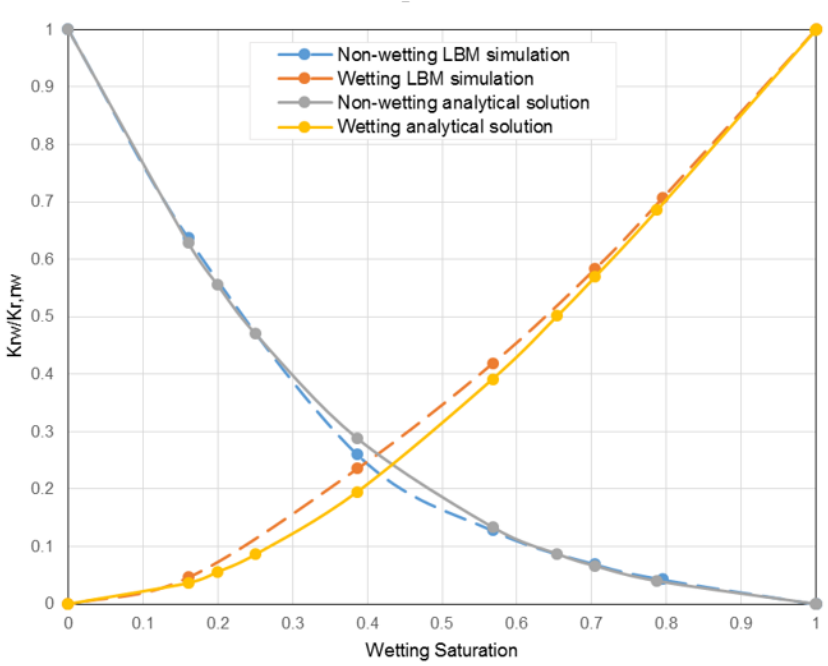

Figure 3-4 Comparison of relative permeability curves between LBM simulation results and analytical solutions when M=0.1.

The LBM simulation model was further validated when M>1. In the study, M=10 was studied. LBM simulation results agreed with analytical solutions, as displayed in Figure 3-5. The picture shows that when M>1, the relative permeability of the non-wetting phase can be larger than 1, caused by the 'lubricating effect' of the wetting phase films covering the solid surface (Yiotis et al., 2007; Ghassemi & Pak, 2011).

The error of LBM simulation results comes from the discrete nature of rendering fractures. The error is less than 10%, which can be practically negligible.

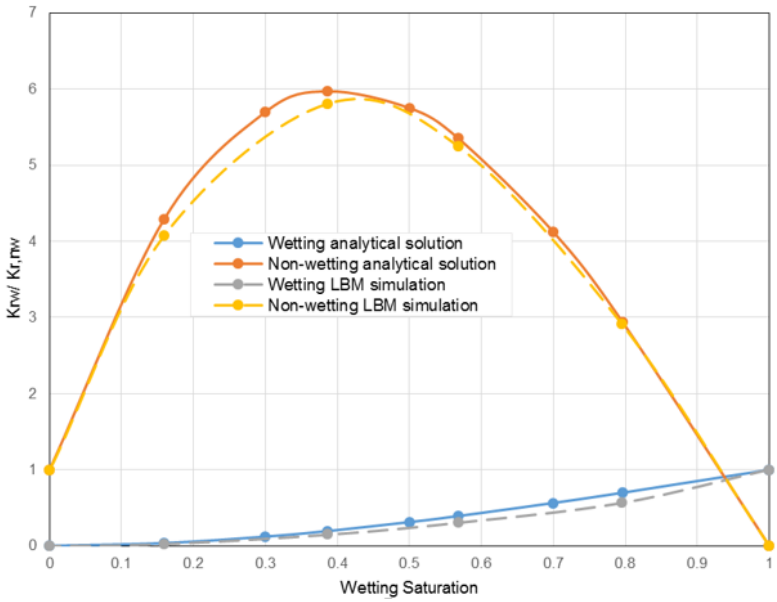

Figure 3-5 Comparison of relative permeability curves between LBM simulation results and analytical solutions when M=10.

3.3 Effect of Intrinsic Fracture Porosity on Oil-water Relative Permeability Curves

After the 2D fracture LBM model was validated with analytical solutions, intrinsic fracture porosity effects on oil-water relative permeability were studied by changing the proportion of the solid lattices. Figure 3-6 illustrates the 2D model in the LBM simulation. The intrinsic fracture porosity, described as the volume fraction of the void volume to the whole volume, varied as the proportion of the solid lattices in the whole fracture lattice system varied. The distribution of fluid particles at the initialization step is the same as the model in the validation part: The wetting fluid (water) flowed along the rock surface, while the non-wetting fluid (oil) flowed in the middle of the fracture. A 300×100 lattice domain was built. Boundary conditions applied in the model were almost the same with the validation case. The bounce-back boundary condition was applied to the surface of solid walls and the periodic boundary conditions were

implemented into the inlet and outlet of the fracture. The only difference was that the new model existed with an additional no-fluid domain located inside the solid walls.

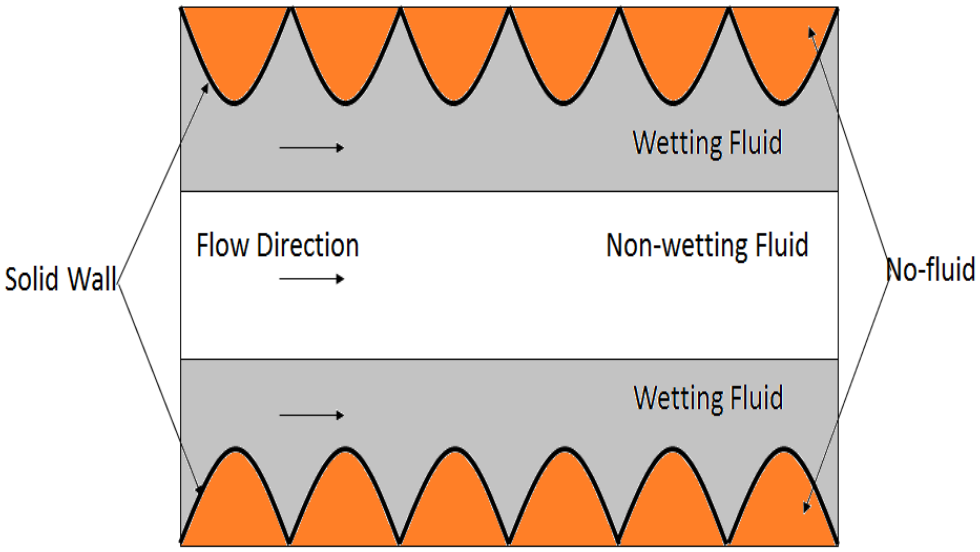

Figure 3-6 Schematic of LBM model with various intrinsic fracture porosity

Figure 3-7 displays one of fluid distribution when intrinsic porosity is 80.4% at steady-state as an example. The fluctuant interface between two phases illustrates the interaction between oil and water.

The values of relative permeability curves' feature points, including the end points and relative permeability curves average increase or decrease rate corresponding to each fracture porosity, are listed in Table 3.1. The study of the intrinsic fracture porosity impact on relative permeability curves was accomplished by a correlation and regression analysis of the data using the statistical software, Minitab (Version 17) [Computer software]. (2017). Retrieved from https://www.minitab.com/en-us/products/minitab/.

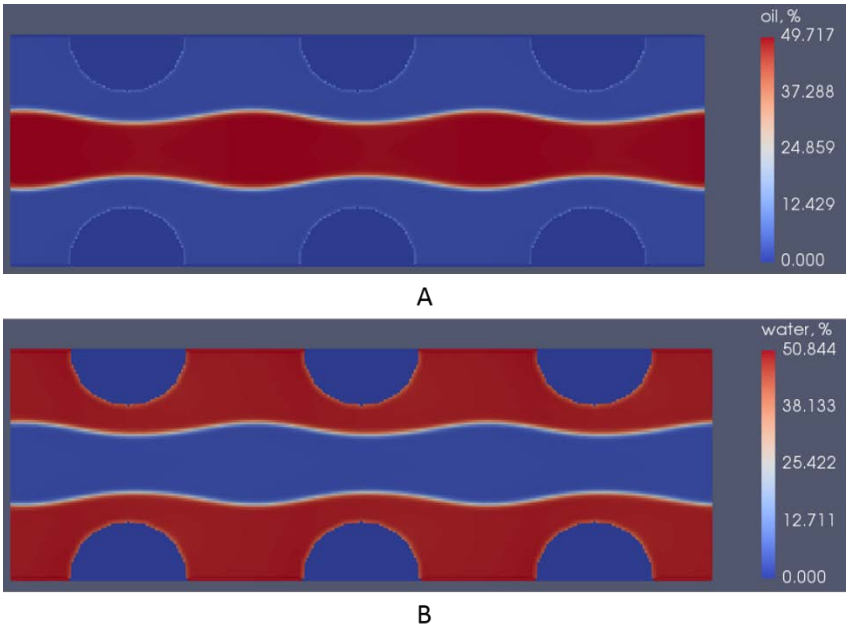

Figure 3-7 Fluid distribution when intrinsic fracture porosity is 80.4% (A: oil distribution; B: water distribution)

From Table 3-1, irreducible water saturation increased with a reduction in intrinsic fracture porosity. Table 3-2 shows the result of the regression analysis between irreducible water saturation and intrinsic fracture porosity as an example.

Table 3-1 Relative permeability curves' end points and changing rate at different intrinsic fracture porosity

$\emptyset_f$	S_{wir}	S_{or}	$k_{rw}(S_{or})$	$k_{ro}(S_{wir})$	$\overline{v_w}$	$\overline{v_o}$
0.392	0.395	0.153	0.591	0.617	1.307522	1.365044
0.497	0.339	0.126	0.663	0.684	1.239252	1.278505
0.593	0.255	0.068	0.717	0.740	1.059084	1.093058
0.717	0.244	0.039	0.761	0.895	1.061367	1.248257
0.804	0.194	0.034	0.859	0.910	1.112694	1.178756
0.898	0.125	0.019	0.881	0.934	1.029206	1.091121

Table 3-2 Regression analysis: S_{wir} versus intrinsic fracture porosity

Analysis of variance					
Source	DF	Adj SS	Adj MS	F-Value	P-Value
Regression	1	0.045614	0.045614	107.12	0.000
Fracture porosity	1	0.045614	0.045614	107.12	0.000
Error	4	0.001703	0.000426		
Total	5	0.047317			
Model summary					
S	R-sq	R-sq (adj)	R-sq (pred)		
0.0206355	96.40%	95.50%	93.51%		
Coefficients					
Term	Coef	SE Coef	T-Value	P-Value	VIF
Constant	0.5833	0.0325	17.96	0.000	
Fracture porosity	-0.4994	0.0482	-10.35	0.000	1.00
Regression equation					
$S_{wir} = 0.5833 - 0.4994 \times \emptyset_f$					

The rest of the regression analysis table is listed in Appendix A. Hypothesis testing in Minitab uses a P-value approach. As a result, the P-value in the regression analysis for the significant test, which reported less than 0.05, can be a strong evidence that the dependent variable is linearly related to the independent variable (Montogomery et al., 2015). Meanwhile, the value of R-sq in Table 3-2, which shows that the percentage of the response variable variation is larger than 95% and close to 100%, can prove the confidence of the regression equation. The residual plot for irreducible water saturation regression was also analysed in Figure 3-8. In a normal

probability plot, most points distribute along the straight line; for a fitting plot, the dots display a strong unusual pattern. The regression model has no inadequacies. Through regression and its residual plot analysis, the irreducible water saturation has a linear relationship with the intrinsic fracture porosity.

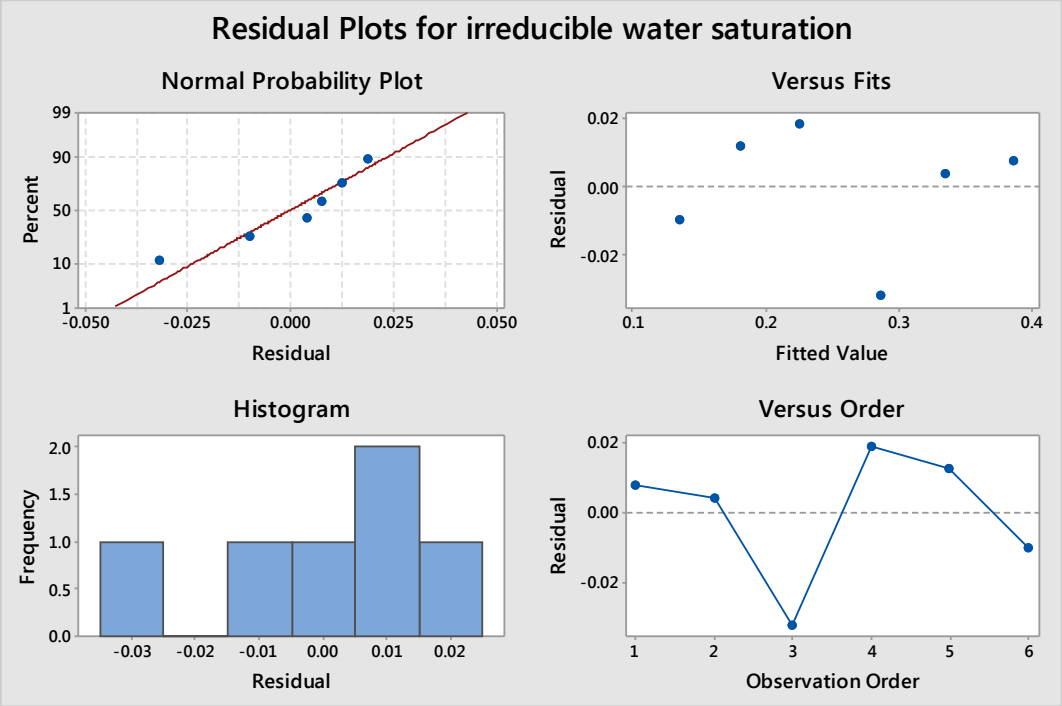

Figure 3-8 Residual plots for irreducible water saturation regression

A regression analysis of intrinsic fracture porosity and residual oil saturation, final water relative permeability, initial oil relative permeability, and oil and water relative permeability changing rates were completed in the same manner. Except for the oil relative permeability's average decreasing rate, others were all correlated linearly to intrinsic fracture porosity. Figure 3-9 displayed the linear relationship between fracture porosity and critical saturations (irreducible water and residual oil saturation). Both saturations will be reduced as the intrinsic fracture

porosity increased. Irreducible water saturation's decreasing rate was larger than the residual oil saturation rate which implied that irreducible water saturation is more sensitive to intrinsic fracture porosity than residual water saturation. The reason for this phenomenon is that water, as the wetting phase in the LBM simulation, contacts the rock surface directly which was influenced by rock deeper. By contrast, oil, as the non-wetting phase fluid, sandwiched by water initially, was not in contact with rock and was influenced more by water.

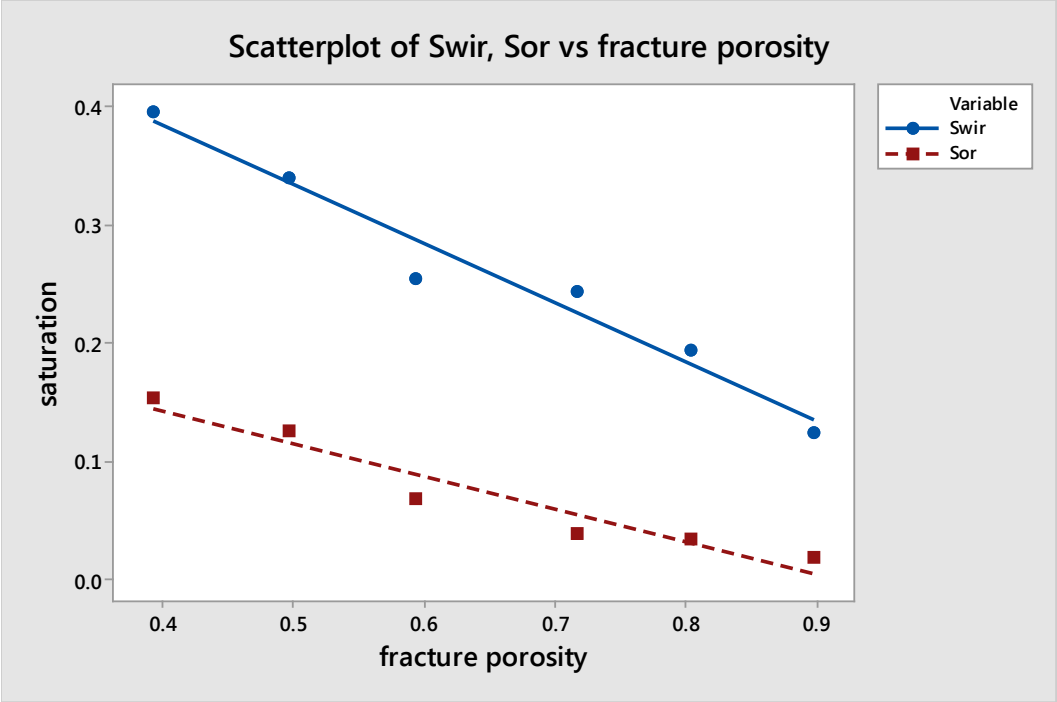

Figure 3-9 Regression relationship between fracture porosity and critical saturations

The impact of intrinsic fracture porosity on relative permeability curves' end points at critical saturations (initial oil relative permeability and final water relative permeability) is all increased with intrinsic fracture porosity increasing linearly, as shown in Figure 3-10. These results were the same with the phenomena Morgan and Gordon found in 1970. The explanation is that the radius of a pore is decreased and the surface of rock increased with a reduction in fracture

porosity. The thickness of water becomes more significant, leaving less space for fluid flow (Morgan & Gordon, 1970). For each fracture porosity, the end point of oil relative permeability is larger than water relative permeability. The reason for this phenomena is that oil, as the non-wetting phase fluid, flows through large spaces which have a better ability of flow as compared to small spaces in which water flows.

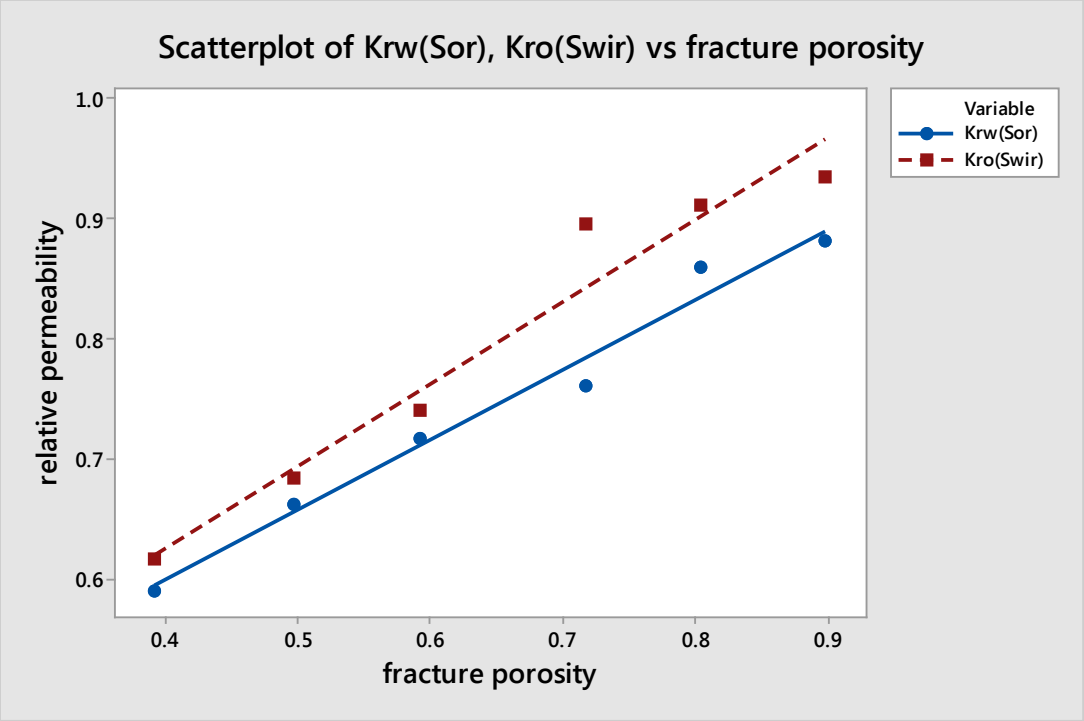

Figure 3-10 Regression relationship between fracture porosity and oil, water relative permeability end points at critical saturations

In addition to a correlation analysis of intrinsic fracture porosity and relative permeability feature points, relationships between intrinsic fracture porosity and relative permeability curves' changing rate were also studied. As oil-water relative permeability curves were not linear, a derivative of their function was not a constant number. In this study, the average changing rate

was calculated. Table 3-1 demonstrates the oil and water's average relative permeability increasing or decreasing rate for each intrinsic fracture porosity. At specific fracture porosity, the decreasing rate of oil relative permeability is larger than the increasing rate of water relative permeability. For these two variables, a correlation and regression analysis was also completed. A linear relationship between intrinsic fracture porosity and water relative permeability increasing rate was exhibited. The decreasing rate of oil relative permeability, however, is not linearly related to intrinsic fracture porosity but is correlated to it. As intrinsic fracture porosity increased, the average changing rate of relative permeability decreased. The reason is that when intrinsic fracture porosity increased, the space of fluid flow decreased. This enhanced the interaction between the two fluids, reducing the changing rate.

3.4 Gravity Effect on Oil-water Relative Permeability at Different Intrinsic Fracture Porosity

After studying the intrinsic fracture porosity effect on relative permeability curves, the LBM simulation model was upgraded to a 3D model to study gravity effects on oil-water relative permeability curves. The typical D3Q19 structure was used in the LBM model (shown in Figure 3-11). The core theory of the relative permeability calculation in the LBM model was not changed. Differences were the weight of velocity in each direction, $\omega_{i,}$ and the parameter, $\boldsymbol{e}_i$ which depends on the direction of the structure. Equations 3-17 and 3-18 display new ω_i and $\boldsymbol{e}_i$.

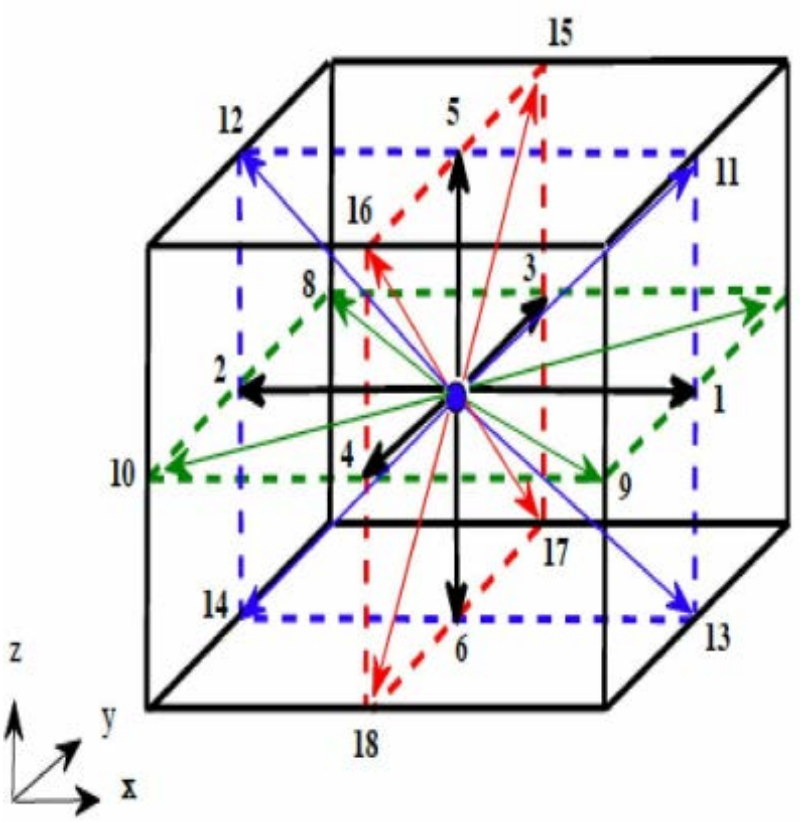

Figure 3-11 Illustration of D3Q19 structure (Benioug et al., 2015)

$$\omega_i = \begin{cases} \frac{1}{3} & i = 0 \\ \frac{1}{18} & i = 1, \dots, 6 \\ \frac{1}{36} & i = 7, \dots, 18 \end{cases} \tag{3-17}$$

$$\boldsymbol{e}_i = \begin{cases} (0,0,0) & i = 0 \\ c(\pm 1,0,0), c(0,\pm 1,0), c(0,0,\pm 1), & i = 1, \dots, 6 \\ c(\pm 1,\pm 1,0), c(\pm 1,0,\pm 1), c(0,\pm 1,\pm 1), & i = 7, \dots, 18 \end{cases} \tag{3-18}$$

where c is the lattice speed, whose equation is written below:

$$c = \Delta x / \Delta t \tag{3-19}$$

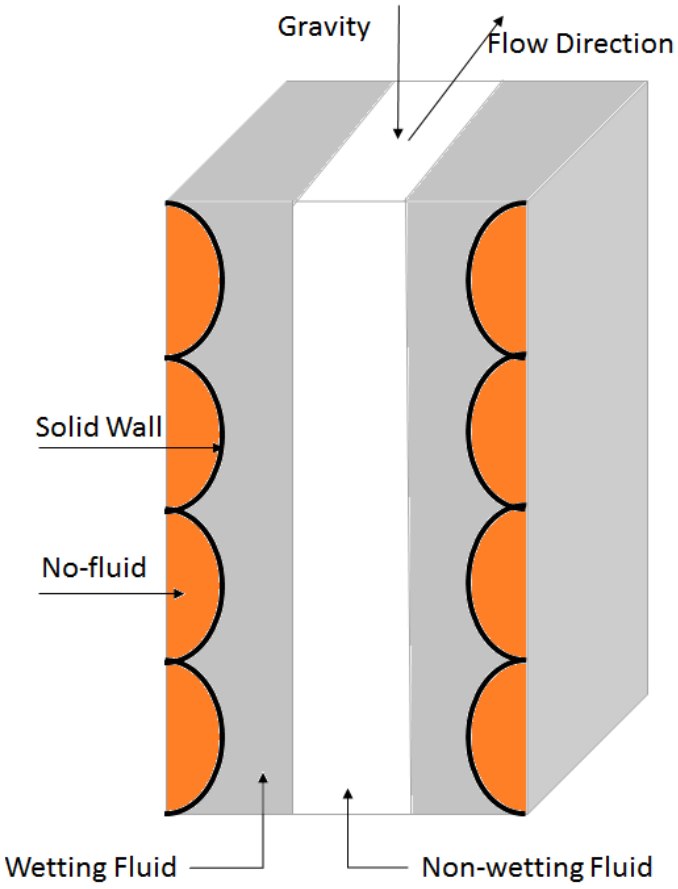

Figure 3-12 Schematic of immiscible two-phase flow in 3D LBM model

Figure 3-12 illustrates the 3D model for the LBM simulation. The wetting fluid (water) runs along the rock surface, while the non-wetting fluid (oil) flows in the middle of the fracture. The intrinsic fracture porosity is described as the volume fraction of the void volume to the whole volume. A $80 \times 80 \times 100$ lattice domain was built. Boundary conditions applied in the model were the same as with the 2D model. In the *Z*-axis direction, gravity forces were applied to both the wetting and non-wetting fluids. Values of gravity forces were different due to their different density. The measurement method and calculation equation were the same as in the 2D LBM model. To investigate gravity effects on relative permeability curves at different intrinsic fracture

porosity, two series of experimental groups were set. The first series was a test group where gravity was introduced into the LBM model for different intrinsic fracture porosity. The other series was a control group where gravity was removed for different intrinsic fracture porosity.

Figure 3-13 shows the comparison of the oil-water relative permeability curves where the intrinsic fracture porosity is 1. In this case, there was no rock in the fracture; the two fluids flow regime was the same as the flow in the channel. Thus, relative permeability curves reflected the interaction between two fluids rather than a solid-fluid interaction at different intrinsic fracture porosity. For the same water saturation, both water and oil relative permeabilities, with the gravity effect, were larger than those without gravity consideration. The presence of gravity in the simulation model promotes phase segregation which impairs interaction between two fluids.

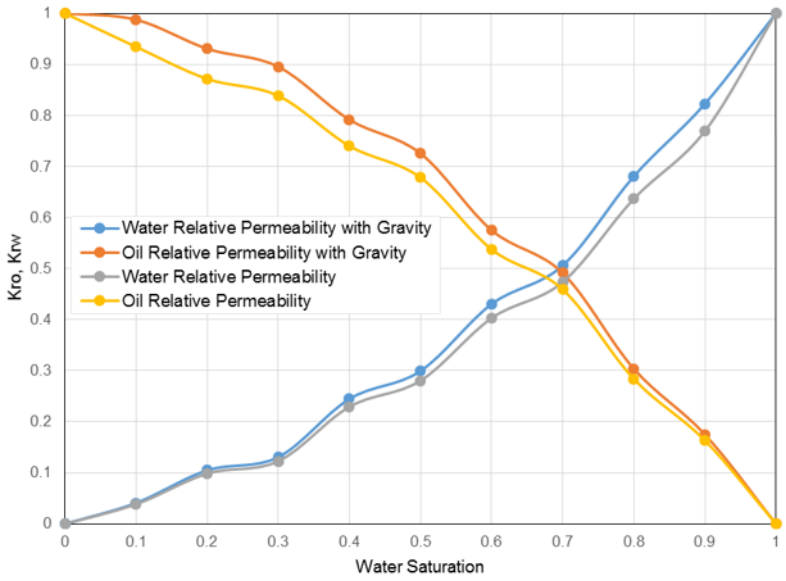

Figure 3-13 Comparison of oil-water relative permeability curves for fracture porosity equal to 1

The study compared two groups of relative permeability when intrinsic fracture porosity was 1. For all intrinsic fracture porosity from 50% to 100%, comparisons were accomplished individually. Figures 3-14 to 3-18 show the differences between two groups of relative permeability curves at different intrinsic fracture porosity. For each figure, the area of two-phase flow is larger in the group where the gravity impact factor was added. The figures show that oil and water relative permeability points, calculated from the model including the gravity effect, are higher than points calculated without gravity consideration at the same water saturation. In addition, irreducible water saturation is larger than residual oil saturation at all levels of intrinsic fracture porosity with and without gravity effects.

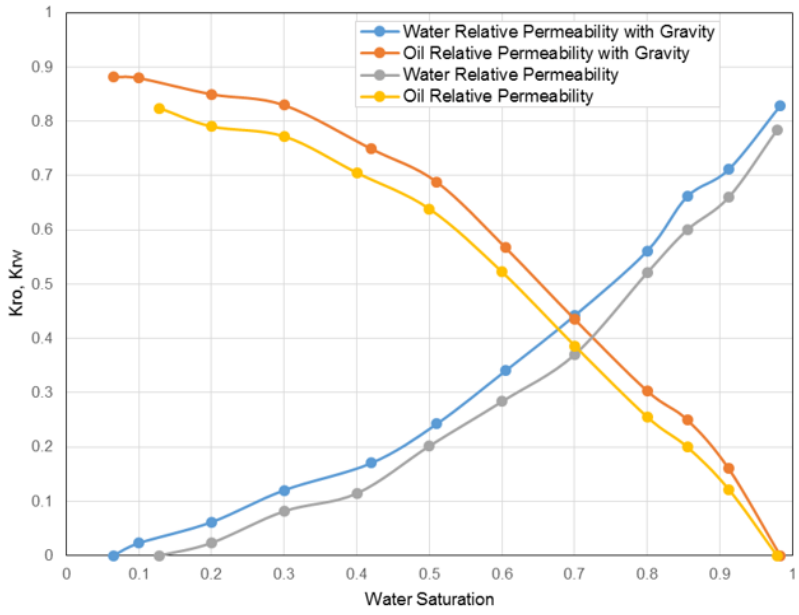

Figure 3-14 Comparison of oil-water relative permeability curves for intrinsic fracture porosity equal to 89.8%

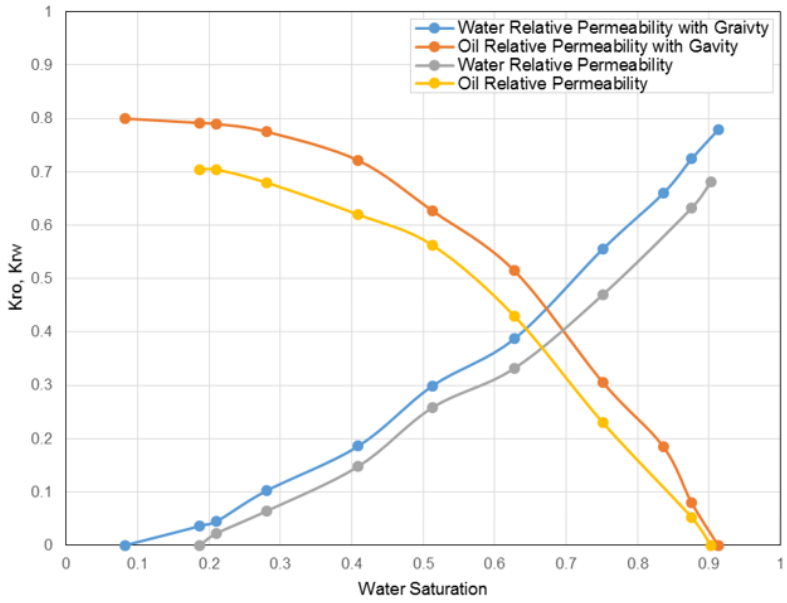

Figure 3-15 Comparison of oil-water relative permeability curves intrinsic fracture porosity equal to 80.4%

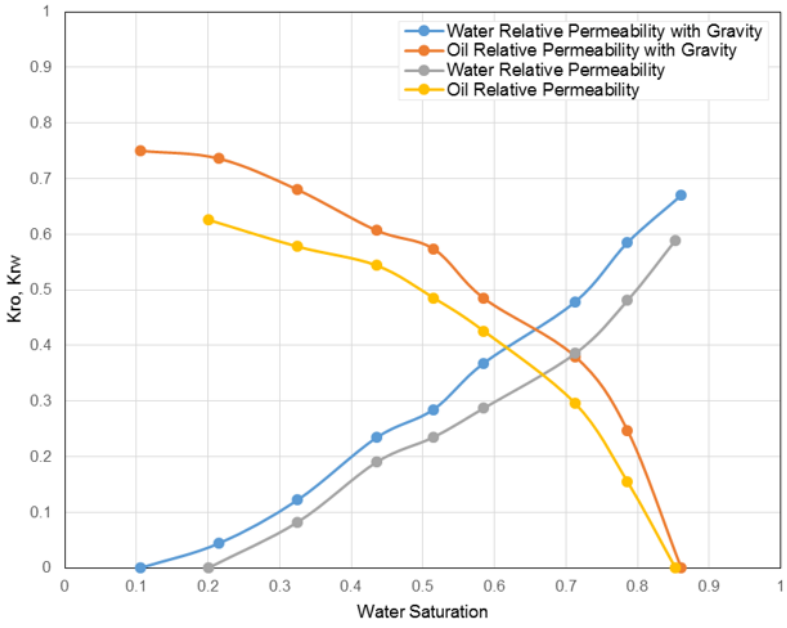

Figure 3-16 Comparison of oil-water relative permeability curves for intrinsic fracture porosity equal to 71.8%

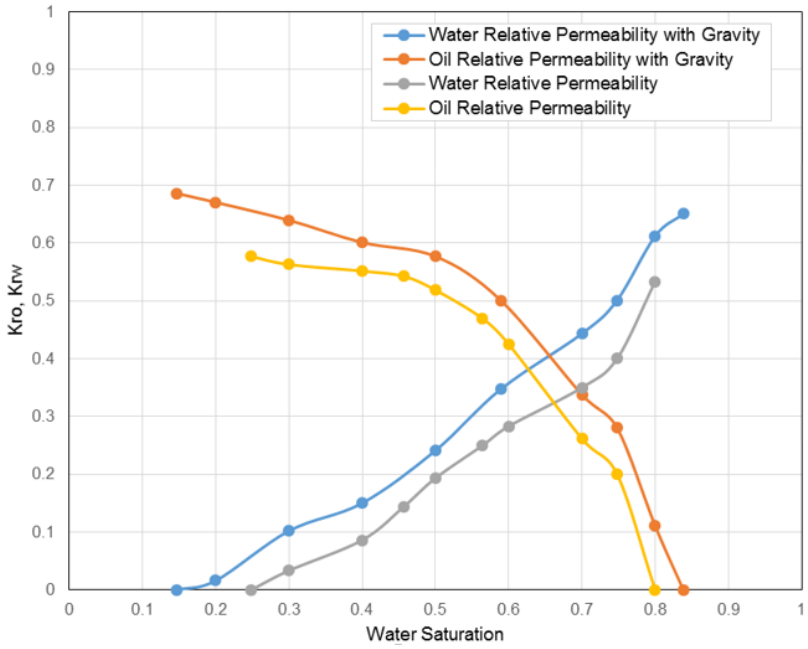

Figure 3-17 Comparison of oil-water relative permeability curves for intrinsic fracture porosity equal to 59.2%

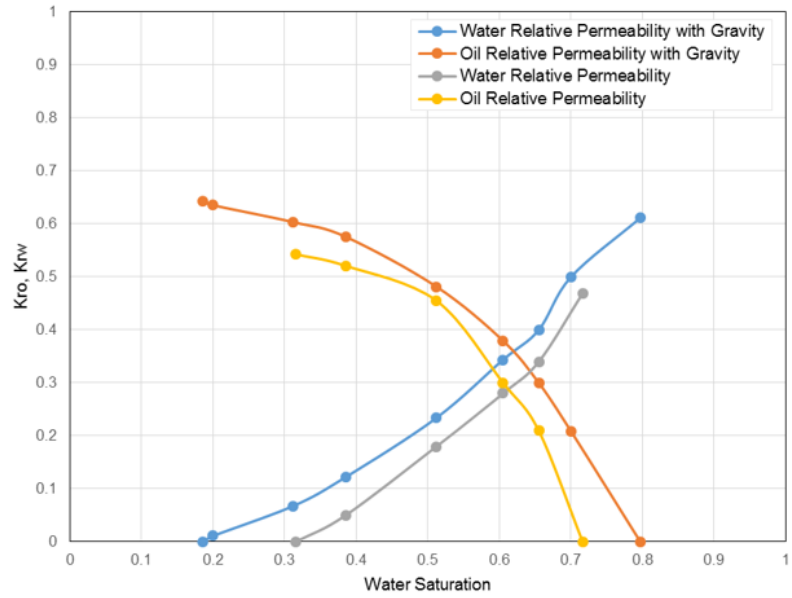

Figure 3-18 Comparison of oil-water relative permeability curves for intrinsic fracture porosity equal to 49.7%

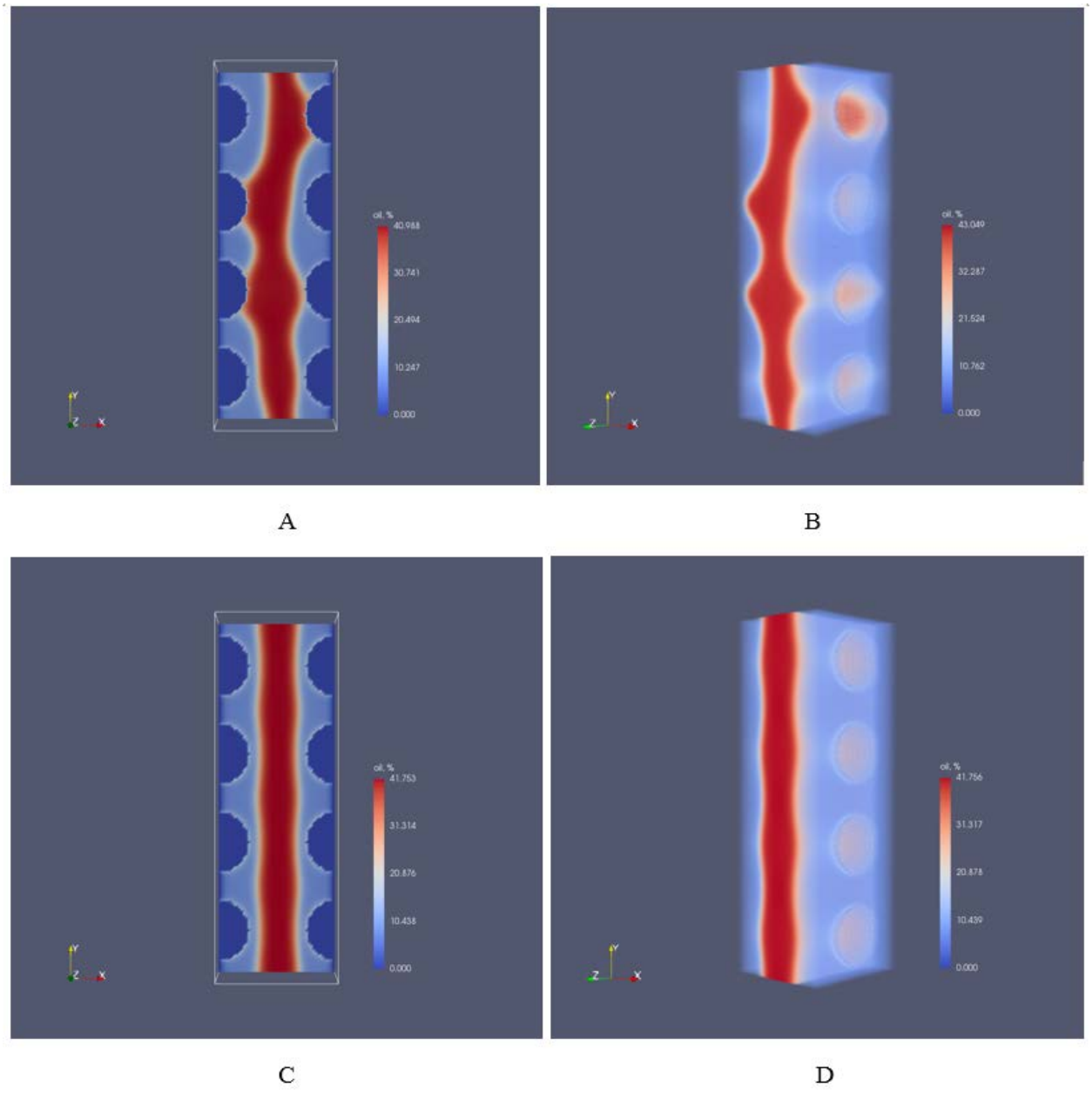

Figure 3-19 Oil distribution comparison between two calculation models (A: cross section of oil distribution in the model with gravity effect; B: 3D view of oil distribution in the model with gravity effect; C: cross section of oil distribution in the model without gravity effect; D: 3D view of oil distribution in the model without gravity effect)

Figures 3-14 to 3-16 reveal that the influence of gravity on residual oil saturation is small; its impact on residual oil saturation becomes larger when fracture porosity is smaller than 60%

(Figure 3-17). The five figures, in common, show that the effect of gravity on irreducible water saturation is large. Thus, we can conclude that gravity has a more significant influence on irreducible water saturation, and when the intrinsic fracture porosity becomes small enough, its effects on residual oil saturation becomes prominent. A comparison of these five figures reveals that both irreducible water and residual oil saturation increased with a reduction in intrinsic fracture porosity; this has a good agreement with conclusions from the 2D LBM simulation model. In terms of the curvatures of these curves, the larger the intrinsic fracture porosity, the more linear both the oil and water relative permeability curves. For the same intrinsic fracture porosity, the curvatures do not change obviously with the gravity impact factor introduced into the calculation model. Figure 3-19 displays oil distribution comparison when intrinsic porosity is 89.8% at steady-state as an example.

For determining the impacts of gravity on relative permeability curves feature points, the study completed both qualitative and quantitative analyses using Minitab. Table 3-3 lists values of those feature points at desired intrinsic fracture porosity. An analysis of data is divided into crosswise and longitudinal comparisons.

In the crosswise comparison for the LBM model, a correlation and regression analysis of intrinsic fracture porosity and relative permeability curves' feature points considers with and without gravity consideration. Gravity effects on the correlation analysis results of relative permeability curves' feature points are studied in the longitudinal comparison.

Table 3-3 Relative permeability curves' end points and average changing rate at different intrinsic fracture porosity with or without gravity impact

$\emptyset_f$		0.497	0.592	0.718	0.804	0.898	1
S_{wir}	Gravity	0.186	0.147	0.106	0.083	0.065	0
	No-Gravity	0.315	0.248	0.200	0.187	0.129	0
S_{or}	Gravity	0.203	0.162	0.139	0.087	0.017	0
	No-Gravity	0.284	0.200	0.147	0.098	0.022	0
$k_{rw}(S_{or})$	Gravity	0.437	0.520	0.582	0.677	0.828	1
	No-Gravity	0.268	0.34	0.471	0.592	0.784	1
$k_{ro}(S_{wir})$	Gravity	0.642	0.686	0.751	0.805	0.882	1
	No-Gravity	0.488	0.577	0.625	0.704	0.824	1
$\overline{v_w}$	Gravity	0.715	0.753	0.771	0.816	0.902	1
	No-Gravity	0.668	0.615	0.721	0.828	0.923	1
$\overline{v_o}$	Gravity	1.051	0.993	0.995	0.970	0.961	1
	No-Gravity	1.217	1.045	0.957	0.985	0.971	1

The correlation analysis demonstrated that irreducible water saturation, residual oil saturation, initial oil relative permeability and final water relative permeability are all linearly correlated to intrinsic fracture porosity. The average changing rate of water relative permeability curves in both groups is all linearly correlated to intrinsic fracture porosity. The average changing rate of oil does not have a linear relationship with intrinsic fracture porosity. Correlation equations for linear relationships with intrinsic fracture porosity in the LBM simulation model without gravity effect are:

$$S_{wir} = 0.5940 - 0.5511 \cdot \emptyset_f \tag{3-20}$$

$$S_{or} = 0.5521 - 0.5681 \cdot \emptyset_f \tag{3-21}$$

$$k_{rw}(S_{or}) = -0.510 + 1.445 \cdot \emptyset_f \tag{3-22}$$

$$k_{ro}(S_{wir}) = -0.0134 + 0.953 \cdot \emptyset_f \quad (3\text{-}23)$$

$$\overline{v_w} = 0.2206 + 0.761 \cdot \emptyset_f \quad (3\text{-}24)$$

Linear regression equations for relative permeability feature points and intrinsic fracture porosity in the LBM model including gravity consideration are:

$$S_{G,wir} = 0.3541 - 0.3410 \cdot \emptyset_f \quad (3\text{-}25)$$

$$S_{G,or} = 0.4196 - 0.4236 \cdot \emptyset_f \quad (3\text{-}26)$$

$$k_{G,rw}(S_{or}) = -0.1545 + 1.098 \cdot \emptyset_f \quad (3\text{-}27)$$

$$k_{G,ro}(S_{wir}) = 0.2718 + 0.6878 \cdot \emptyset_f \quad (3\text{-}28)$$

$$\overline{v_{G,w}} = 0.4199 + 0.5402 \cdot \emptyset_f \quad (3\text{-}29)$$

Regression relationships of irreducible water saturation and intrinsic fracture porosity were plotted in Figure 3-20:

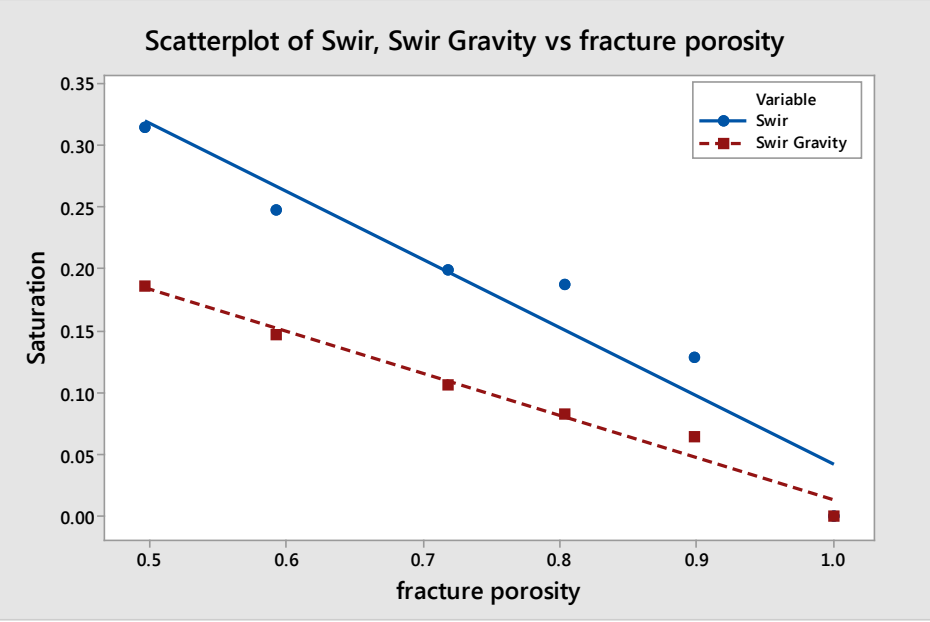

Figure 3-20 Regression relationship between fracture porosity and irreducible water saturation with and without gravity effect

The plot clearly displays gravity effects on irreducible water saturation. For each fracture porosity, irreducible water saturation will be augmented if gravity is ruled out. In addition, the slope of a regression line that considers gravity in the model is less than the slope of the blue line. This explains that the occurrence of gravity weakened intrinsic fracture porosity effects on irreducible water saturation.

A gravity effect on residual oil saturation is similar, yet different, in its influence on irreducible water saturation. The similar effect is that gravity can contribute to reducing residual oil saturation. Comparing Figures 3-20 to 3-21 shows that the difference of the straight line slope between the blue one and the red one is smaller in Figure 3-21. The interpretation of this difference between the two figures is that the degree of gravity contribution in reducing residual oil saturation is lower than in irreducible water saturation.

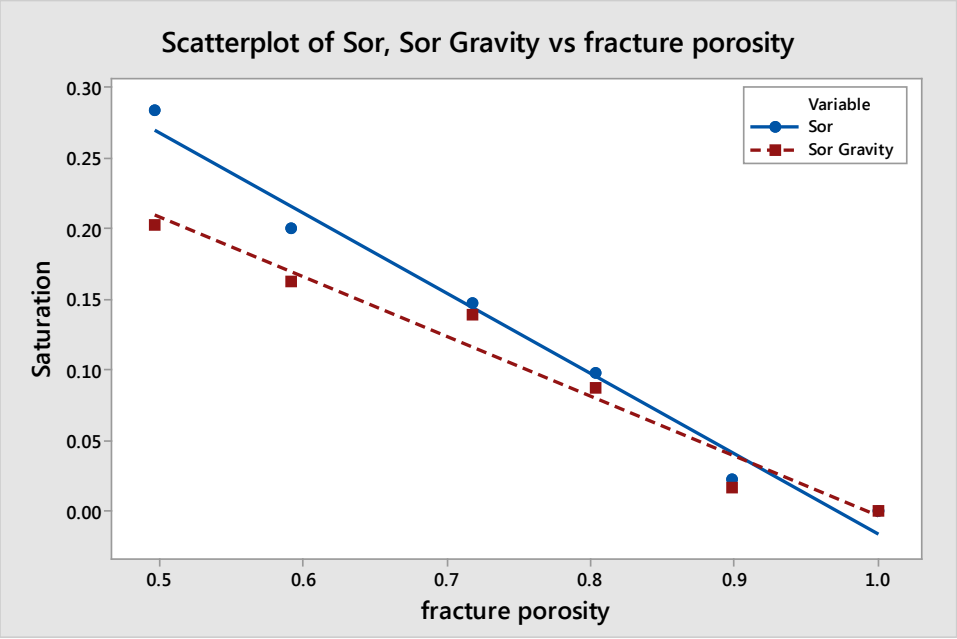

Figure 3-21 Regression relationship between fracture porosity and residual oil saturation with and without gravity effect

The influence of gravity on initial oil relative permeability and final water relative permeability was plotted in Figures 3-22 and 3-23. Intrinsic fracture porosity has a positive effect on these relative permeability curves' end points. They all increased when intrinsic fracture porosity increased; the addition of gravity in the model promoted these end points. By comparing the slopes of the blue and red lines, gravity occurrence reduced the endpoints increasing rate. The degree of a gravity impact is described as the difference of the correlation coefficient between the model which considered gravity and the model which was gravity free. The difference of the coefficient in the final water relative permeability groups is 0.347; for initial oil relative permeability, the difference is 0.2652. The similarity of the two difference values demonstrated that gravity effects on oil relative permeability and water relative permeability are also similar.

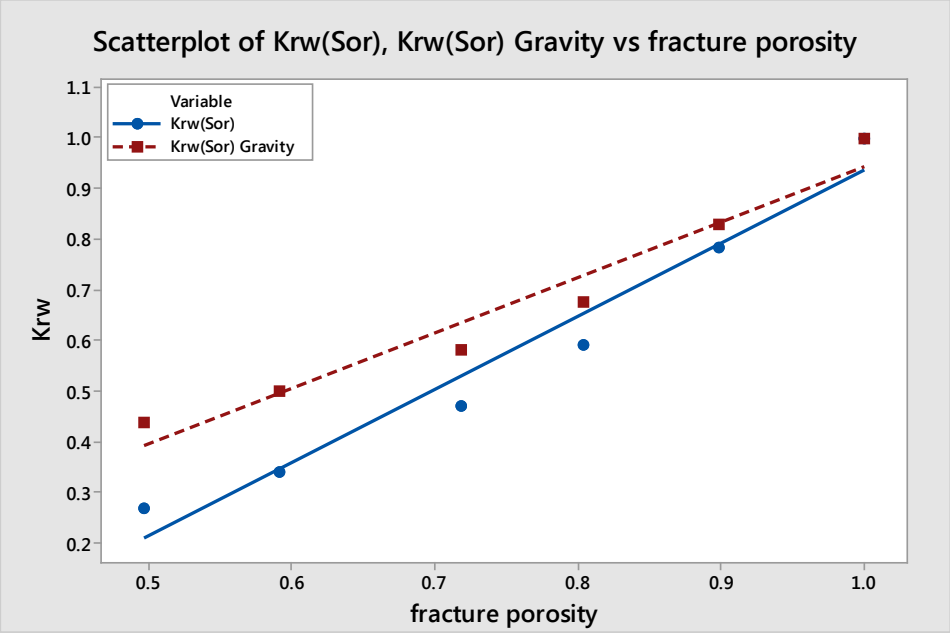

Figure 3-22 Regression relationship between fracture porosity and final water relative permeability at residual oil saturation with and without gravity effect

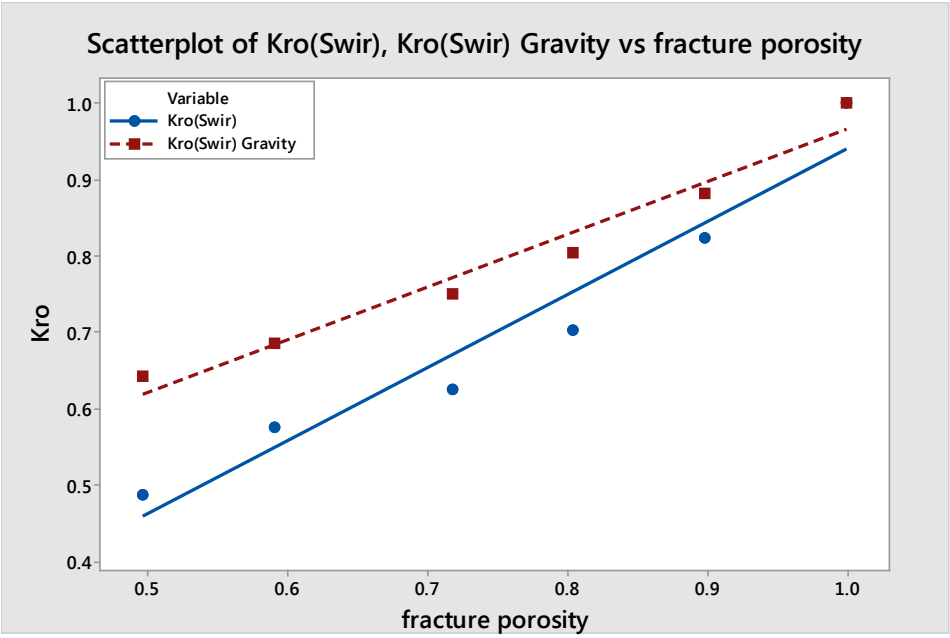

Figure 3-23 Regression relationship between fracture porosity and initial oil relative permeability at irreducible water saturation with and without gravity effect

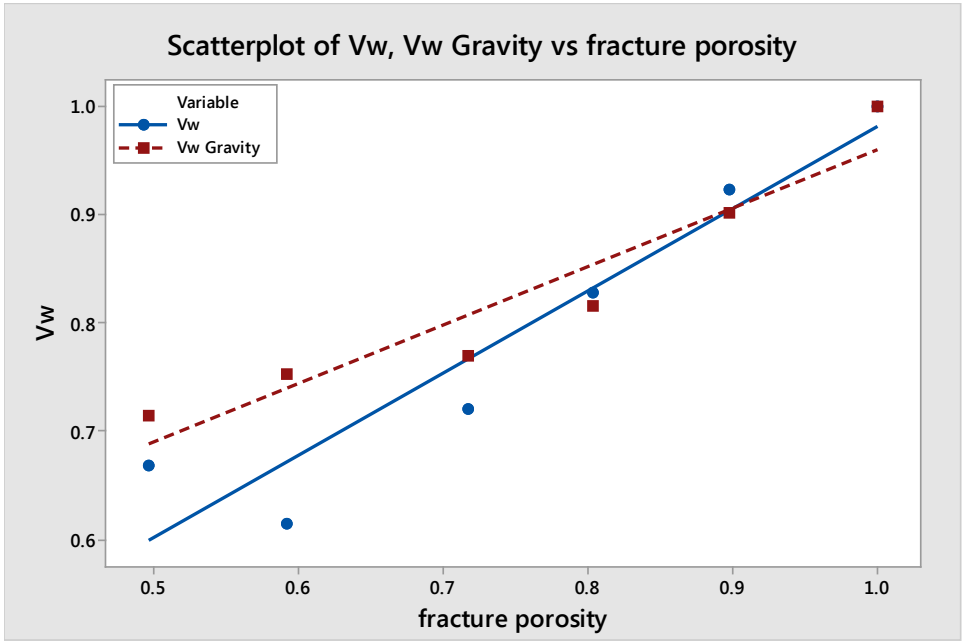

Figure 3-24 Regression relationship between fracture porosity and average changing rate of water relative permeability with and without gravity effect

Figure 3-24 shows the regression relationship of water relative permeability average changing rate with intrinsic fracture porosity. The red points are all larger than the blue points for the entire range of intrinsic fracture porosity; the slope of the red line is lower than that of the blue line. As a result, the water relative permeability changing rate is larger in the model with the gravity effect consideration than in the case without gravity influence. The degree of intrinsic fracture porosity influence on the water relative permeability changing rate, however, is smaller in the gravity effect case than in the non-gravity effect case.

Chapter Four: INFLUENCE OF FRACTURE RELATIVE PERMEABILITY CORRELATION APPLICATION ON SAGD PERFORMANCE

4.1 Background

The proportion of oil which is formed in carbonates is larger than 40%, much of which is heavy oil, which requires thermal-enhanced oil recovery (Sola et al., 2007). SAGD, as an effective thermal recovery method, was widely used and investigated in heavy oil and bitumen reservoir production. The application of SAGD in sandstone heavy oil reservoirs has been characterized quite well, and research related to this technique, including sensitivity studies, screen criteria, and operation optimization has been developed. However, a SAGD application in carbonate heavy oil reservoirs is still in the early stage due to its heterogeneity. Researchers have used numerical simulation methods to investigate the feasibility of SAGD applications in naturally fractured carbonate reservoirs. Dual porosity and/or dual permeability modeling methods are widely used in naturally fractured reservoir simulation models. In these simulation models, typically X-type relative permeability curves are used in the fracture system (Sola & Rashidi, 2006). No matter how reservoir characteristics change, fracture relative permeability curves are fixed as a linear X type. Chapter 3 in our research demonstrates that oil-water relative permeability curves are not linear only to water saturation in fractures and have correlation relationships with intrinsic fracture porosity. In this chapter, a field scale naturally fractured reservoir model was built to simulate the SAGD process. Both X-type and nonlinear relative permeability curves, calculated from the LBM model and corresponding to different intrinsic fracture porosities, were input in this field scale model. The application of fracture relative permeability curves correlation influence on SAGD performance was investigated. Reservoir porosity, thickness and oil saturation are three sensitive parameters in SAGD performance. This

chapter also investigates the necessity of using a fracture relative permeability correlation in reservoirs with different reservoir properties during the SAGD process.

4.2 Description of Reservoir Model

A dynamic simulation model is built in CMG STARS using the dual permeability method. There are $45 \times 5 \times 26$ (I, J, K) grid blocks in the model, which covers a $90 \times 100 \times 26\ m^3$ reservoir. The direction of the horizontal well is J, the length of which is 800m. In our dynamic model, matrix and fractures distribute alternately with the same properties in each system. The model selects 1/8 of the normal field case model in the J direction (Figure 4-1). As a result, injection and production rates were scaled down due to the shortened length of the horizontal well. Tables 4-1 and 4-2 show reservoir rock, formation and fluid properties in the simulation model. This dynamic model was built analogical to the Grosmont formation, and all data is from reference papers related to the Grosmont reservoir (Hosseininejad et al., 2014; Yang et al., 2014; Song, 2015; Ali et al., 2012; Qi & Yuan, 2013). There are three components in this thermal compositional model - water, oil and methane. For matrix relative permeability curves, end points at three different temperatures were provided to mimic temperature dependence. The relationship between oil viscosity and temperature is shown in Figure 4-2. In the section of well operation settings, two horizontal wells are set in the model with 5 meters well spacing in the vertical direction (K direction). Steam is injected at a maximum pressure of 1,800kPa, while the minimum pressure of the production well is 1,600kPa. In order to prevent steam escaping from the producer, a steam trap is set at 8°C. The warm-up stage in this model is five months. After the warm-up stage, steam will be injected with 0.9 steam quality.

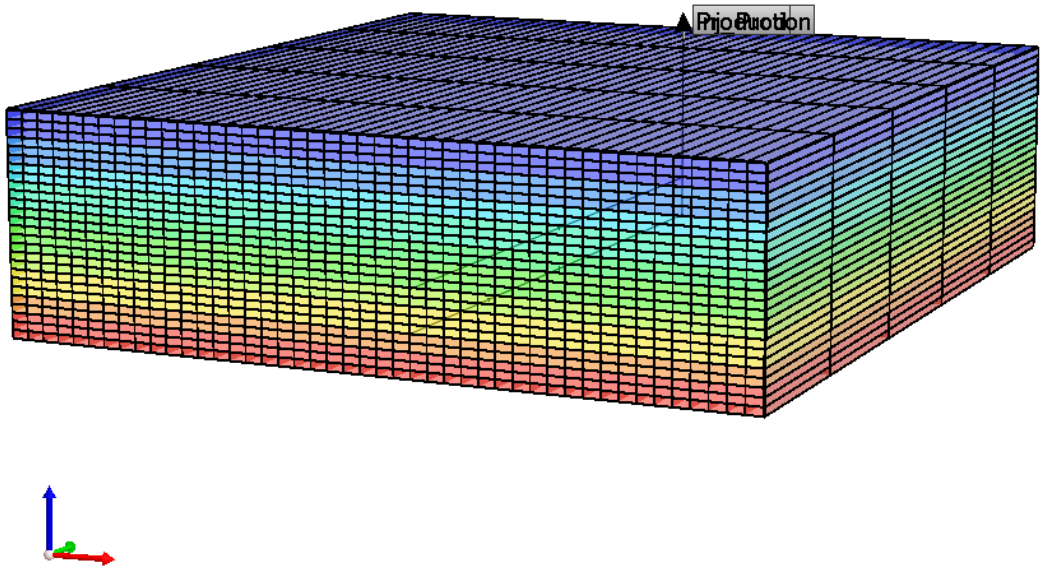

Figure 4-1 Naturally fractured SAGD base case model

Table 4-1 Reservoir formation properties

Thickness (m)	26
Matrix porosity (%)	27
Fracture volume fraction (%)	1
Matrix permeability (mD)	250
Fracture permeability (mD)	10000
Fracture spacing (m), DI	0.3
Fracture spacing (m), DJ	0.5
Fracture spacing (m), DK	3
Initial pressure (kPa)	1600
Initial oil viscosity (cP)	3×10^6 @15°C

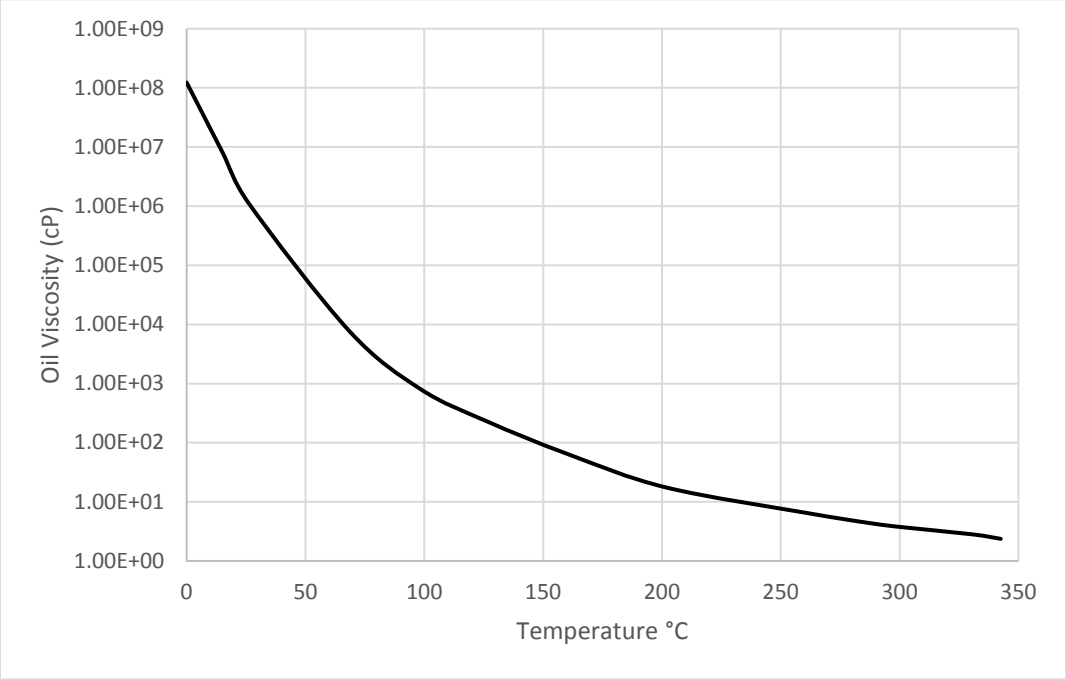

Figure 4-2 Oil viscosity as a function of temperature

Table 4-2 Rock, fluid and thermal properties

Rock compressibility (1/kPa)	2×10^{-5}
Rock heat capacity ($J/m^3 \cdot ℃$)	2.347×10^6
Overburden/underburden heat capacity ($J/m^3 \cdot ℃$)	2.350×10^6
Overburden/underburden heat conductivity ($J/m \cdot day \cdot ℃$)	1.46×10^5
Rock thermal conductivity ($J/m \cdot day \cdot ℃$)	5×10^5
Water thermal conductivity ($J/m \cdot day \cdot ℃$)	1.15×10^4
Oil thermal conductivity ($J/m \cdot day \cdot ℃$)	5.35×10^4
Gas thermal conductivity ($J/m \cdot day \cdot ℃$)	1.4×10^2

4.3 Comparison of SAGD Performance between Application of Fracture Relative Permeability Correlation and Fixed Relative Permeability Curves

There are two series of simulations in this section. In the first instance, fracture relative permeability changed with intrinsic fracture porosity using curves obtained in Chapter 3, called the LBM model. For the control group, fixed X-type linear fracture relative permeability curves are implemented in this field scale SAGD model, called the fixed linear model. The simulation model simulates 10 years of SAGD operation. For an analysis of SAGD performance, cumulative steam injection as an operation cost, cumulative oil production as a profit parameter, and a steam-to-oil ratio (SOR) as a parameter which can quantify the efficiency of oil recovery are used. As steam injection is reported in cold water equivalent (CWE) generally, the study compares water injection plots in future analysis. Cumulative SOR (cSOR) was analysed in this study, which was defined as the ratio of the volume of cumulative steam injected to the volume of cumulative oil produced at a given point of time.

Figures 4-3 and 4-4 show the difference of cumulative oil production and cSOR when intrinsic fracture porosity is 1. Cumulative oil production is higher in the LBM model than in the fixed linear model, while cSOR and cumulative water injection are almost the same in these two models. The reason for the difference in cumulative oil production is that oil relative permeability is higher in the LBM model than in the fixed linear model at the same water saturation when intrinsic fracture porosity is 1. However, there is not a great difference between these two models because when intrinsic fracture porosity is 1, flow in fractures is like a channel flow, the interaction between oil and water is small, and the LBM model applied in this SAGD simulation includes gravity effect and thus phase segregation. As a result, the oil water relative

permeability curves calculated from LBM model are similar to those from the linear fixed model. There is not much difference between the two models in SAGD performance. In addition, relative permeability end points are the same, and the curvatures are slightly different. We can conclude that the curvature of relative permeability curves influences SAGD performance, and if the change of the curvature is small, the impact on SAGD performance will be less.

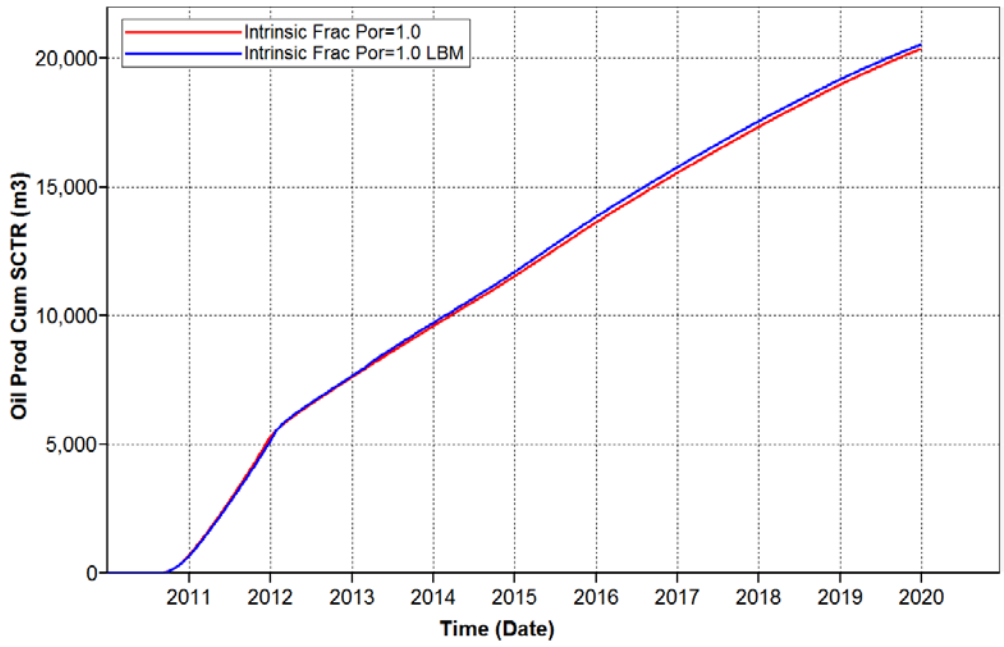

Figure 4-3 Comparison of cumulative oil production between fixed linear model and LBM model when intrinsic fracture porosity is 1

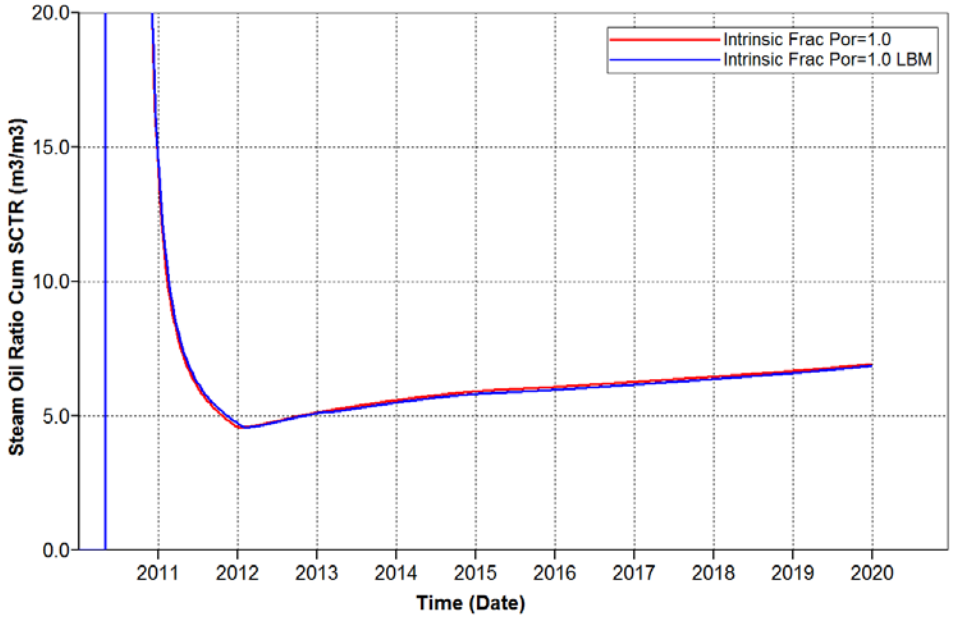

Figure 4-4 Comparison of cSOR between fixed linear model and LBM model when intrinsic fracture porosity is 1

When a large proportion of rock is present in the fractures, intrinsic fracture porosity decreased, and the difference between oil-water relative permeability curves (calculated from the LBM model and the fixed linear model) increased. When intrinsic fracture porosity was not 1, both feature points and the curvature of relative permeability curves were different between the LBM model and the fixed linear model. The difference in SAGD performance becomes prominent when intrinsic fracture porosity is not 1. SAGD simulation run comparison cases used intrinsic fracture porosities ranging from 1 to 0.497. Table 4-3 shows cumulative oil production, steam injection (CWE) and cSOR between two relative permeability models for all simulation runs. The study selected three groups of simulations that represent high (intrinsic fracture porosity is 0.898), middle (intrinsic fracture porosity is 0.718) and low levels (intrinsic fracture porosity is 0.497) of intrinsic fracture porosity to analyse in the plots.

Table 4-3 SAGD performance list at 10th-year

$\emptyset_f$		0.497	0.592	0.718	0.804	0.898	1
Cumulative oil production (m^3)	Fixed linear	19046.8	19363.2	19736.2	19943.3	20216	20377.8
	LBM	18792.2	19294.4	18817.1	19024.4	19411.6	20553.9
Cumulative water injection (m^3)	Fixed linear	141197	141168	141052	141057	141211	141280
	LBM	104555	104538	97982.2	100298	98484.1	141072
cSOR (m^3/m^3)	Fixed linear	7.411	7.291	7.157	7.073	6.985	6.933
	LBM	5.540	5.418	5.379	5.272	5.073	6.873

In order to analyse data from all simulations more effectively, cumulative water injection versus intrinsic fracture porosity for both the fixed linear model and the LBM model are plotted in Figure 4-5. The volume of water injected at the end of simulations is a constant for the fixed linear model at all levels of the intrinsic fracture porosity. For the LBM model, there is a fluctuation in cumulative water injection. When the intrinsic fracture porosity is at the medium level, the difference between the fixed linear model and the LBM model is greatest. For all ranges of intrinsic fracture porosity, the difference between these two models is greater than 25%. The fixed linear model will over-estimate cumulative water injection volume in the SAGD process.

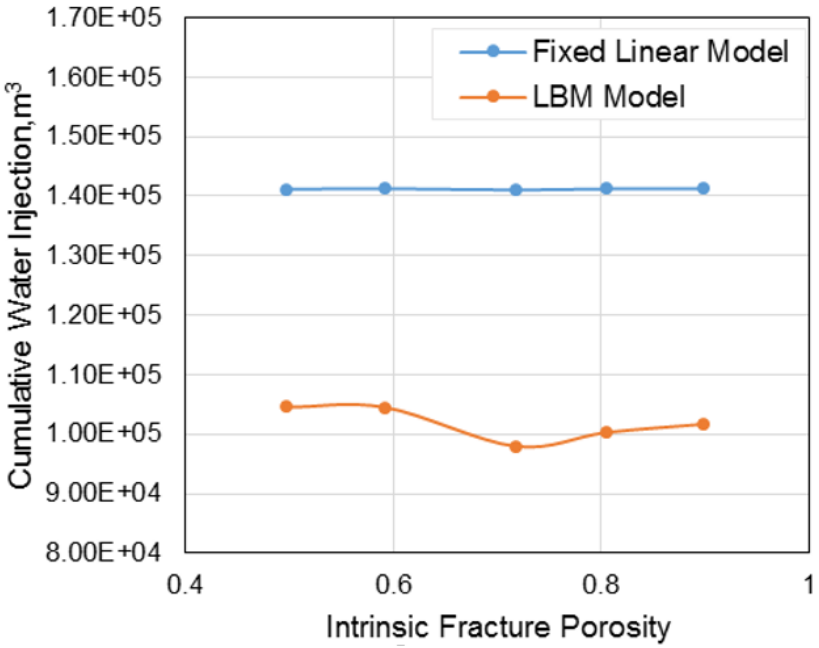

Figure 4-5 Comparison of cumulative water injected between LBM model and fixed linear model at different intrinsic fracture porosity

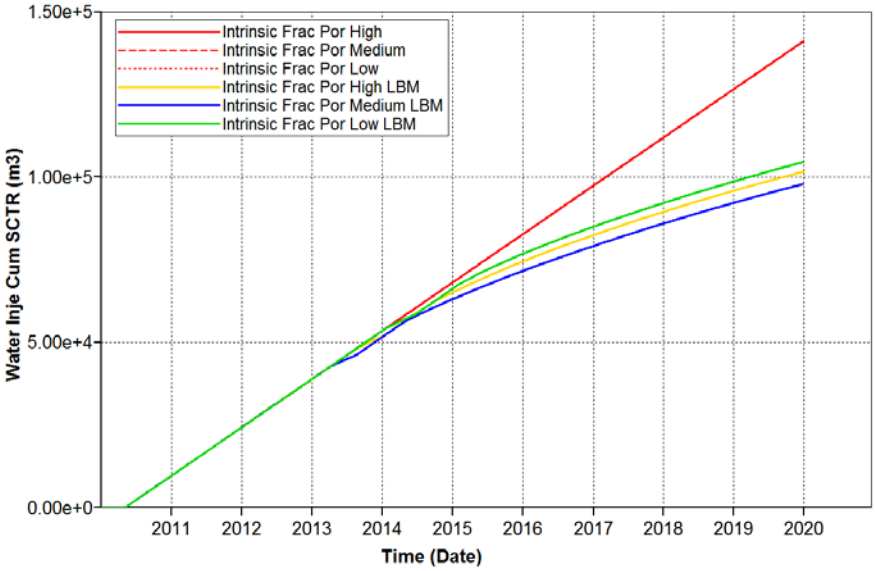

Figure 4-6 Comparison of cumulative water injection between LBM model and fixed linear model for three levels of intrinsic fracture porosity

Figure 4-6 plots cumulative water injection versus time for different simulation runs. Cumulative water injection is the same in the fixed linear model at all times, regardless of how intrinsic fracture porosity changed. For the LBM model, the volume of water injection varies with intrinsic fracture porosity, because water relative permeability changes at the same time. The difference of a water injection volume between the LBM model and the fixed linear model is greatest when the intrinsic fracture porosity is at the medium level. This phenomenon can be described as follows: When intrinsic fracture porosity is large, the difference between two types of relative permeability curves is small, which results in a small difference in water injection performance. For intrinsic fracture porosity at a high level, bottom hole pressure cannot reach maximum pressure at the early stages of production, which requires the injector to inject steam at a constant rate for a long period of time. As a result, cumulative water injection is high in the reservoir, with a low level of intrinsic fracture porosity. In conclusion, water injection will be overestimated if the fixed linear model is used. It is necessary to change water relative permeability curves as fracture characteristics change, especially if intrinsic fracture porosity is at the medium level.

For cumulative oil production, the difference between the two models at a whole range of intrinsic fracture porosity is less than 4.83%. Table 4-3 demonstrates that the cumulative oil production volume will be increased with an increase in intrinsic fracture porosity if the fracture relative permeability curves are fixed as the linear type. However, when the correlation relationship of intrinsic fracture porosity and fracture relative permeability is applied in the SAGD model, the production performance will differ from the fixed linear model. Similar to cumulative water injection, the difference of cumulative oil production between two relative

permeability models is greatest at the medium level of intrinsic fracture porosity. Cumulative oil production for 10 years of operation will be over-estimated in the fixed linear model. However, the difference between these two models is not large. Even at the medium level of fracture porosity, the difference is only 4.83%. Thus, we can conclude that the fracture relative permeability influence on cumulative oil production is small at the whole range of intrinsic fracture porosity during SAGD operation.

Comparison of cumulative oil production between the LBM model and the fixed linear model in three levels of intrinsic fracture porosity, which varied with time, is displayed in Figures 4-7 to 4-9.

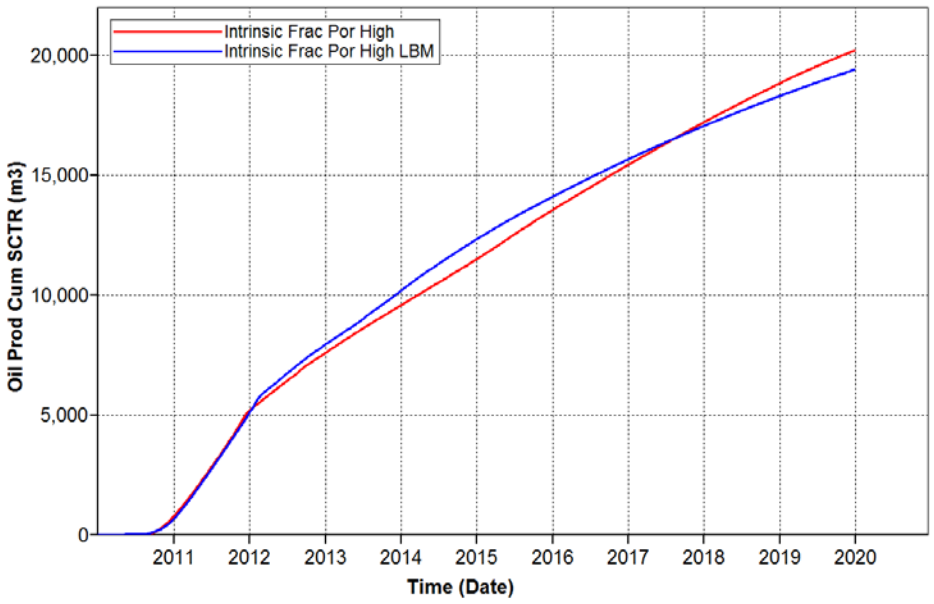

Figure 4-7 Comparison of cumulative oil production between fixed linear model and LBM model when intrinsic fracture porosity is at a high level

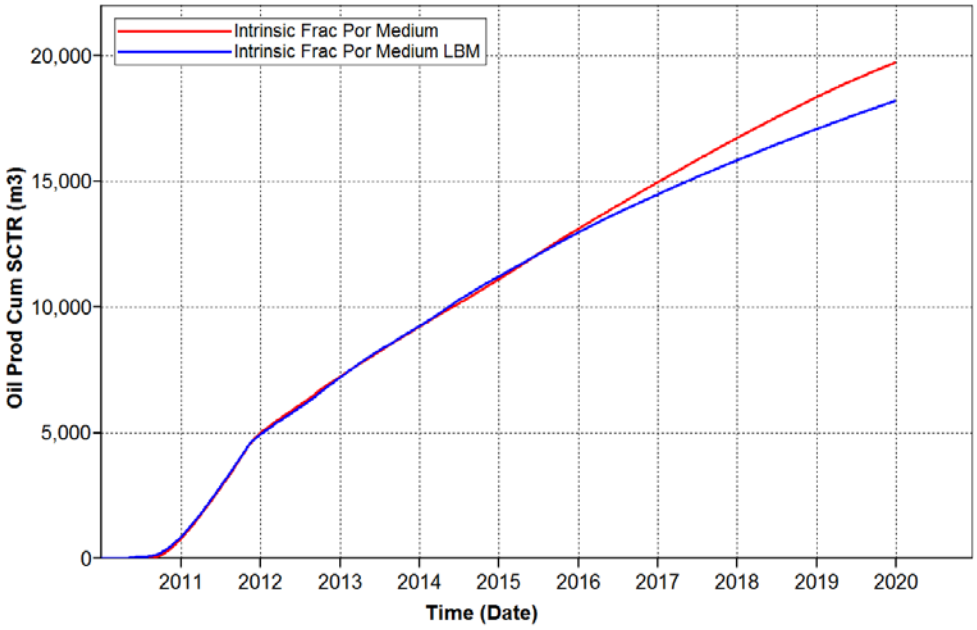

Figure 4-8 Comparison of cumulative oil production between fixed linear model and LBM model when intrinsic fracture porosity is at a medium level

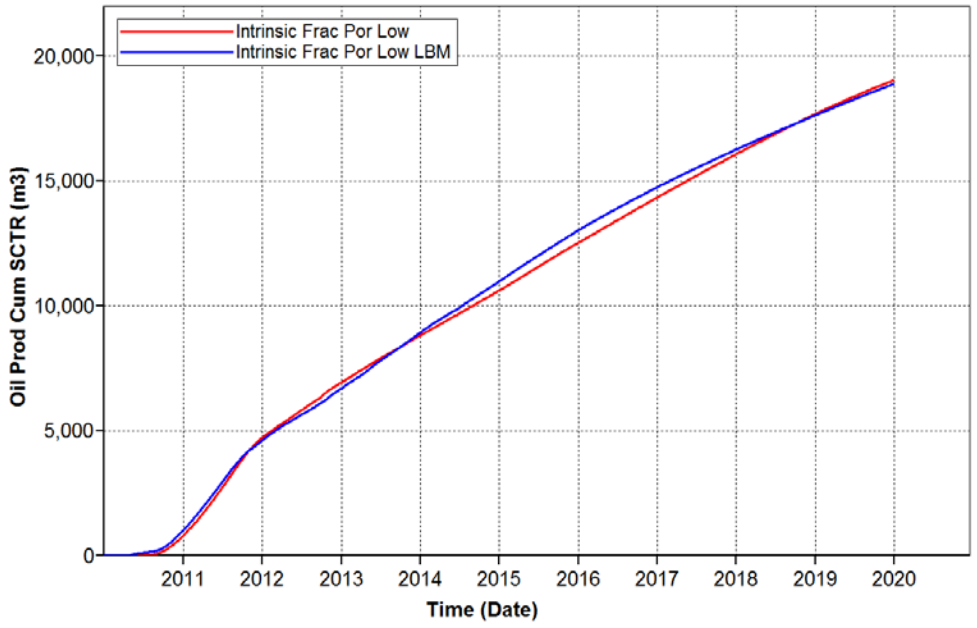

Figure 4-9 Comparison of cumulative oil production between fixed linear model and LBM model when intrinsic fracture porosity is at a low level

When intrinsic fracture porosity is at a high level (Figure 4-7), during the first two years of operation cumulative oil production is almost the same in both models. After two years of operation, cumulative oil production in the fixed linear model is not higher than that in the LBM model until 7.5 years of operation. The fixed linear model will over-estimate or under-estimate an oil production volume depending on the number of years of SAGD operation. The trend of the difference between the two relative permeability models in cumulative oil production is similar in the reservoir, which has low level intrinsic fracture porosity. Oil production in the LBM model will be higher than in the fixed linear model after approximately 3.5 years of operation, and the other cross point occurs in almost nine years of operation. The occurrence of these two cross points is one or two years later than in the reservoir, which has a high level of intrinsic fracture porosity. The performance in a reservoir with a medium level intrinsic fracture porosity is different from the other two reservoirs. In the first five years of operation, oil production is almost the same in both the LBM and the fixed linear model. The difference appears after five years of operation, and the difference will increase with time.

In summary, even the difference in cumulative oil production between two relative permeability models at ten years of operation is small. We cannot confirm that there is no influence of relative permeability curves on SAGD performance. Whether the fixed linear model will over-estimate oil production depends on the length of forecasting and the level of intrinsic fracture porosity.

The definition of cSOR is the ratio of the volume of cumulative steam injected to the volume of cumulative oil produced at a given point in time. Figure 4-10 below shows the cSOR versus intrinsic fracture porosity for the two relative permeability models at the 10th year of operation.

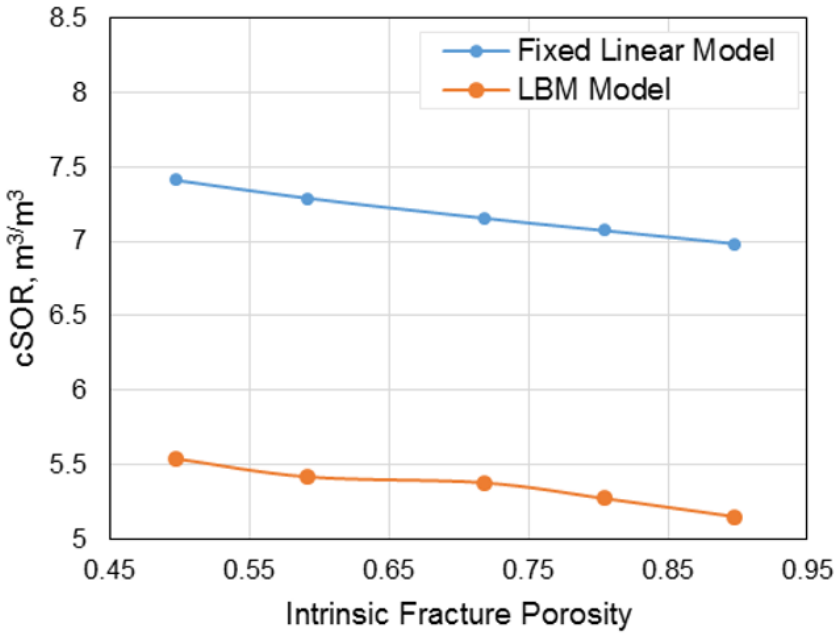

Figure 4-10 Comparison of cumulative SOR between LBM model and fixed linear model at different intrinsic fracture porosity

Cumulative SOR decreased as intrinsic fracture porosity increased in both the fixed linear model and the LBM model. For each intrinsic fracture porosity, the SAGD performance of cSOR in the fixed linear model is higher than in the LBM model. The difference between them can reach 35%, which is too large to be ignored.

Figures 4-11 to describes the comparison of cSOR for two types of relative permeability curves at high, medium and low levels of intrinsic fracture porosity. There are large deviations of cSOR

between the LBM model and the fixed linear model at all intrinsic fracture porosity levels. The lowest points of cSOR are the same between the two relative permeability groups at different intrinsic fracture porosities, which are all around 5 m^3/m^3. The occurrence time of the lowest points is approximately the same as those occurring around two years of SAGD operation. After 10 years of operation, cSOR predicted in the LBM model is 5.15 m^3/m^3, 5.37 m^3/m^3 and 5.53 m^3/m^3, corresponding to high, medium and low levels of intrinsic fracture porosity, respectively. They are predicted as 6.99 m^3/m^3, 7.16 m^3/m^3 and 7.41 m^3/m^3 in the fixed linear model. Lower intrinsic fracture porosity means more rocks in the fractures, which has a negative effect on thermal conductivity. The lower the intrinsic fracture porosity, the higher the cSOR. The shape of cSOR is the same at the whole range of intrinsic fracture porosity, but the shape of cSOR is different between the fixed linear model and the LBM model. After the curve reaches the lowest point of cSOR, it will increase sharply in the model which applied the fixed linear relative permeability curves. In contrast, cSOR changed smoothly in the LBM model. The interpretation of this phenomenon is that a steam injection rate is constant in the fixed linear model, while it is reduced in the LBM model after several years' operation. The difference of cSOR between the two relative permeability curves models are 35.73%, 33.06% and 33.78% in respect to high, medium and low levels of intrinsic fracture porosity, respectively.

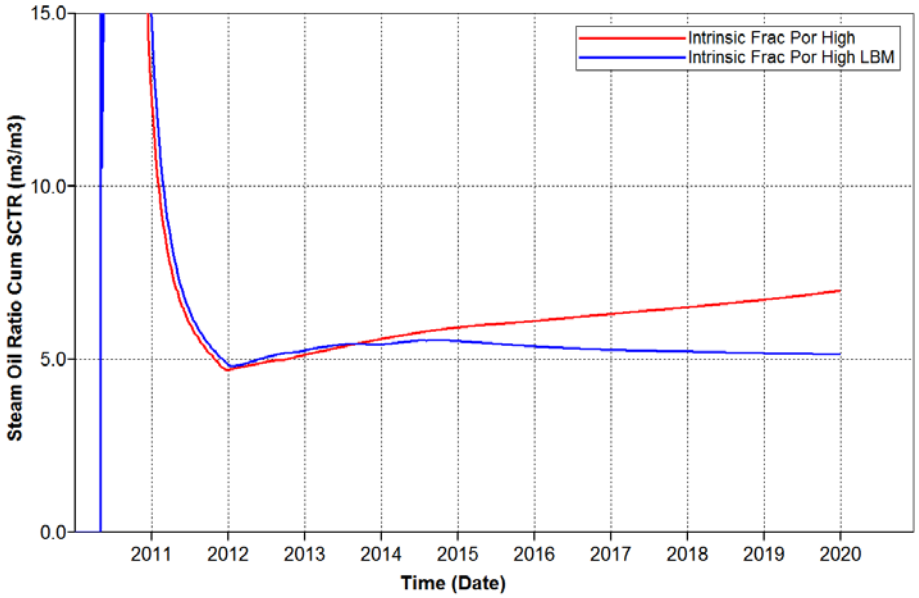

Figure 4-11 Comparison of cumulative steam-to-oil ratio between fixed linear model and LBM model when intrinsic fracture porosity is at a high level

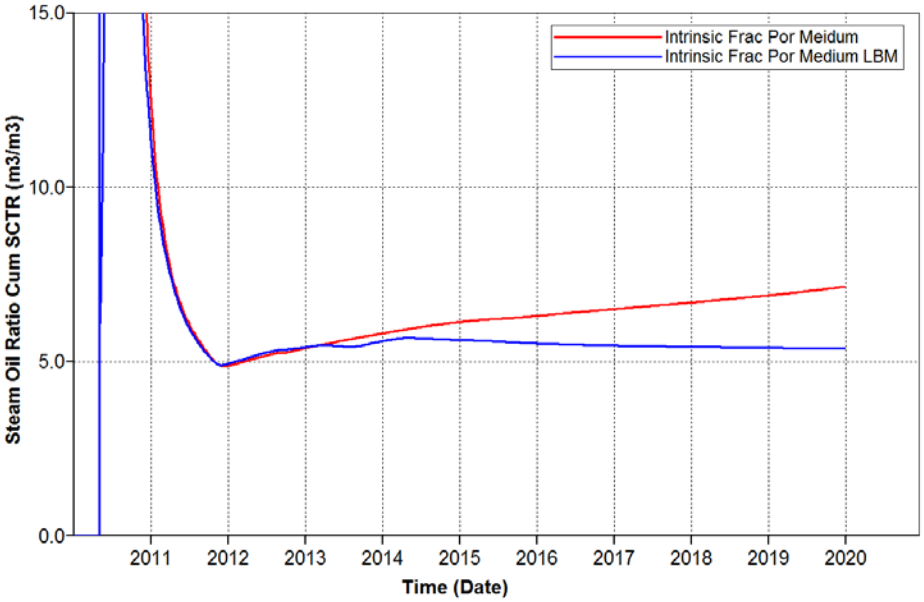

Figure 4-12 Comparison of cumulative steam-to-oil ratio between fixed linear model and LBM model when intrinsic fracture porosity is at a medium level

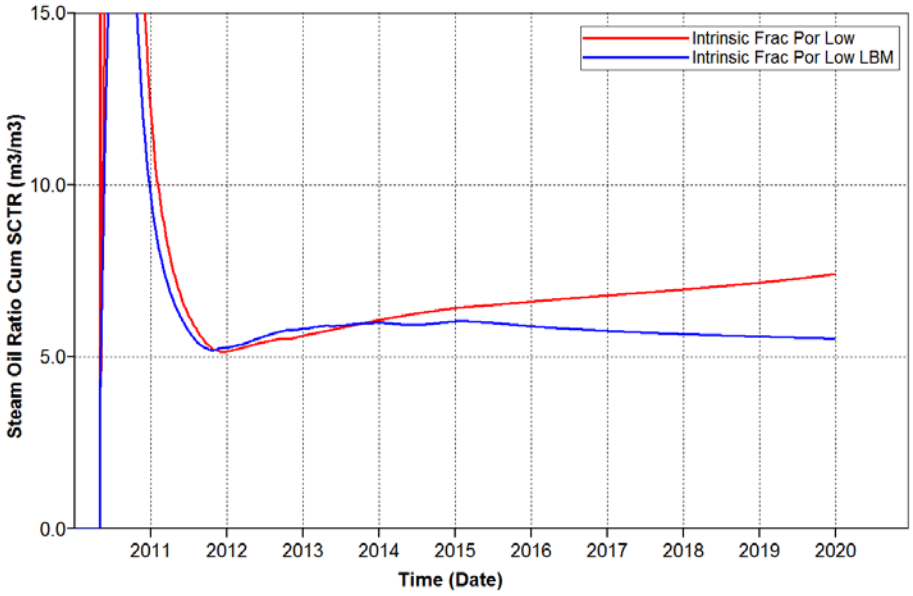

Figure 4-13 Comparison of cumulative steam-to-oil ratio between fixed linear model and LBM model when intrinsic fracture porosity is at a low level

The comparison suggests that an application of the fixed linear model will overestimate cSOR for SAGD processing. The bias can reach 35.73%, which demonstrates the necessity for changing fracture relative permeability curves at different fracture characteristics. In other words, it is important to apply a fracture relative permeability correlation in naturally fractured SAGD dynamic models.

Temperature distribution and oil viscosity distribution are analyzed in Figure 4-14 where intrinsic fracture porosity is 0.718.

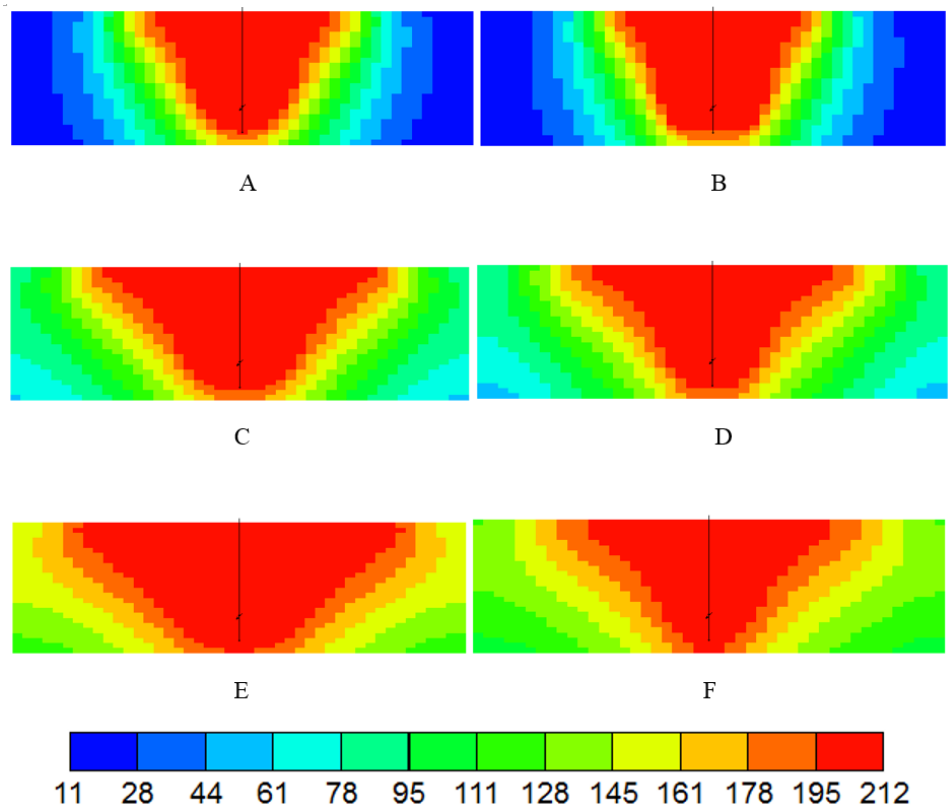

Figure 4-14 Temperature distribution comparison between two types of relative permeability (J layer: 3) (A: fixed linear model at the end of two years' production; B: LBM model at the end of two years' production; C: fixed linear model at the end of six years' production; D: LBM model at the end of two years' production; E: fixed linear model at the end of ten years' production; F: LBM model at the end of ten years' production)

Figure 4-14 shows temperature distribution of a matrix system at different years of SAGD operation. The distribution of temperature in the fracture system is the same as in the matrix. The temperature distribution pattern represents the shape and volume of each steam chamber. For the early stages of the SAGD process, the shape and volume of a steam chamber between the two models are similar, which results in the same cumulative oil production and cumulative water injection. At the middle stage of operation, a difference occurs. The volume of the steam chamber in the LBM model begins to be smaller than in the fixed linear model. This is the time

when bifurcation of cumulative oil production appears. At the end of our SAGD forecasting model, the difference in temperature distribution between the two models can be clearly observed. The large difference of cumulative oil production, water injection and cSOR has a good agreement with the comparison of the two models in this picture. In addition, steam sweep is easier in the top of the reservoir compared with the bottom of the reservoir. The radius of the heated zone at the bottom of reservoir is almost unchanged at the whole range of SAGD operation in both the fixed linear model and the LBM model. In contrast, the radius of the heated zone at the top of the reservoir enlarged significantly from the early stage to the end stage of operation. This phenomenon is in accordance with the physical theory that the density of steam is less than the density of oil and moves upward to the top of the reservoir continuously.

The volume of the steam chamber determines the volume of oil heated by steam that will affect cumulative oil production during the SAGD process. At the same time, the steam chamber which is described by temperature will determine oil viscosity distribution which depends on temperature. Figure 4-15 shows oil viscosity distribution between two types of relative permeability models in the early, middle and late stages of SAGD operation. The oil viscosity plot matched temperature distribution figures well. Where oil viscosity is low, temperature is high. For every stage of operation, oil viscosity distribution corresponds to temperature distribution. In Figure 4-15 F, oil viscosity in the corner is still very high which illustrates that steam sweep efficiency in the LBM model is less than in the fixed linear model.

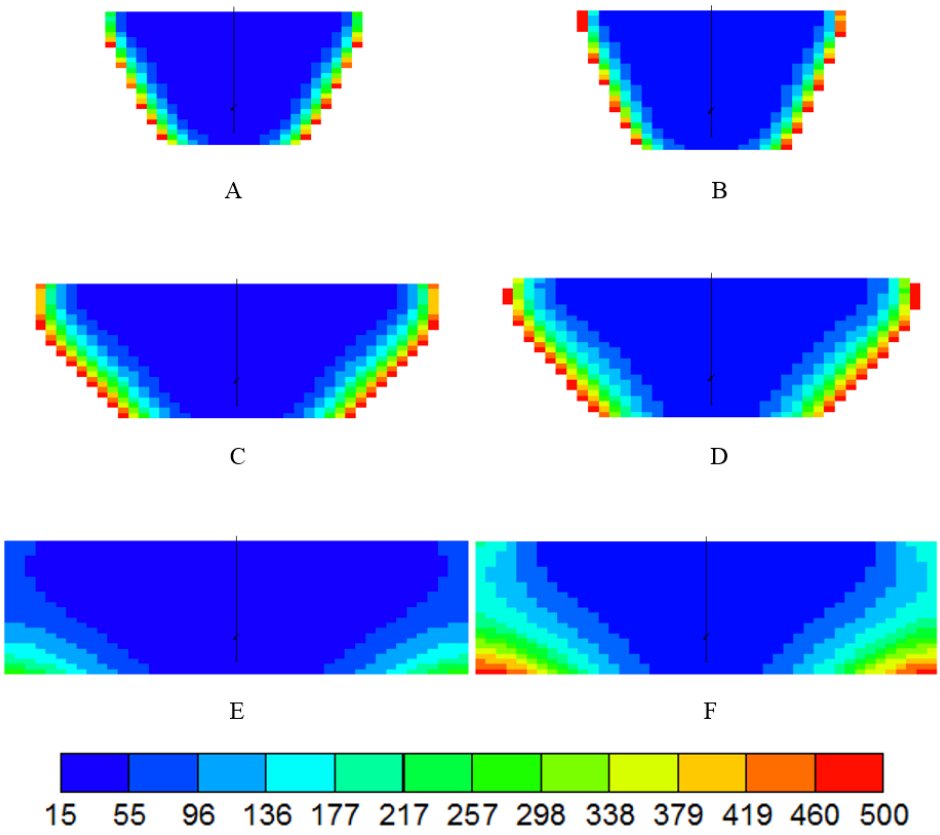

Figure 4-15 Oil viscosity distribution comparison between two types of relative permeability (J layer: 3) (A: fixed linear model at the end of two years' production; B: LBM model at the end of two years' production; C: fixed linear model at the end of six years' production; D: LBM model at the end of two years' production; E: fixed linear model at the end of ten years' production; F: LBM model at the end of ten years' production)

4.4 Influence of Fracture Relative Permeability Correlation Application in SAGD Performance in Different Reservoir Conditions

In the last section, the necessity of applying a relative permeability correlation, calculated from the LBM model in Chapter 3, has been demonstrated. Reservoir properties such as permeability, thickness, porosity, oil saturation, and rock thermal conductivity will influence the efficiency of the SAGD. Nguyen et al. did a sensitivity study of the effects on SAGD performance in 2012 and concluded that porosity, thickness and oil saturation ranked as most sensitive reservoir

parameters on SAGD performance. In this section, the study will investigate the impact of a relative permeability correlation application on SAGD performance with different reservoir parameters. In detail, the study investigates reservoir thickness, matrix porosity and oil saturation. Each parameter is divided into high, medium and low levels. Comparison of SAGD performance between the fixed linear model and the LBM model will be completed using these three reservoir conditions. Table 4-4 displays detailed values for three levels of those three reservoir parameters.

Table 4-4 Reservoir parameters for three levels

Level / Parameter	High	Medium	Low
Thickness (m)	34	26	18
Porosity	0.36	0.27	0.18
Saturation	0.84	0.75	0.65

4.4.1 Impact of Relative Permeability Correlation Application in Reservoirs with Different Thickness

Thickness is ranked as the most sensitive reservoir parameter in the SAGD operation process. Generally, a thin reservoir is not suitable for SAGD production, as a steam chamber will reach overburden in a short time, with a great deal of heat loss. For a general sandstone reservoir, it is common knowledge that the reservoir should not be less than 15m if SAGD operation is required. The low level of thickness is set as 18m in our study, while the high level of thickness is set as 34m in our study.

4.4.1.1 High level of intrinsic fracture porosity: impact of relative permeability correlation application for all levels of thickness

Cumulative oil production is analysed in Figure 4-16. The starting points of cumulative oil production curves are different. The thicker the reservoir, the later the oil production begins. Thick reservoirs require more heating time in order to reach the point of oil mobility. In the cumulative oil production plot, there is a point where the oil production rate changed, which implied the time when well communication was built. The point of this occurrence is dependent upon thickness levels. This point occurred in the first year of operation in the thin reservoir. In the medium thickness reservoir, it appeared in the second year of operation, while in the thick reservoir, it occurred at the end of the third year of production. Although the starting point occurred latest in the thick reservoir, the increasing rate of this curve is larger than in the other two groups of curves. Comparing the linear model and the LBM model for fracture relative permeability in each reservoir, there is not much difference in cumulative oil production. The model which uses the linear fracture relative permeability will over-estimate cumulative oil production at the end of 10 years of operation.

Cumulative water injection is illustrated in Figure 4-17. The SAGD models which implemented the LBM nonlinear fracture relative permeability shows that the cumulative water injection volume is influenced positively by the thickness of the reservoir. In contrast, the model which implemented the linear relative permeability has not been affected by reservoir thickness. The difference in the volume of water injected increased with a decrease in reservoir thickness. The difference is 4% in a thick reservoir, 43.38% in a medium thick reservoir and 77.46% in a thin

reservoir. An application of a nonlinear fracture relative permeability in the SAGD model is required in order to obtain accurate water injection forecasting.

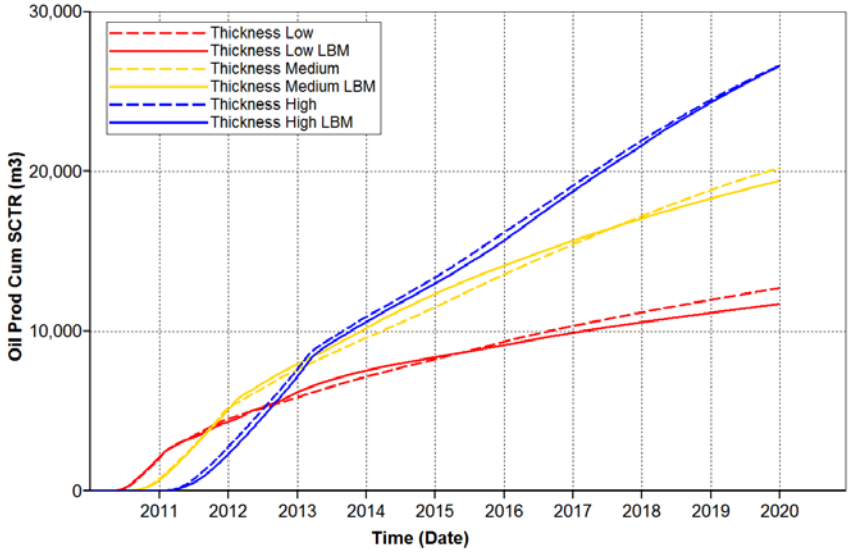

Figure 4-16 Cumulative oil production for all levels of reservoir thickness when intrinsic fracture porosity is at a high level

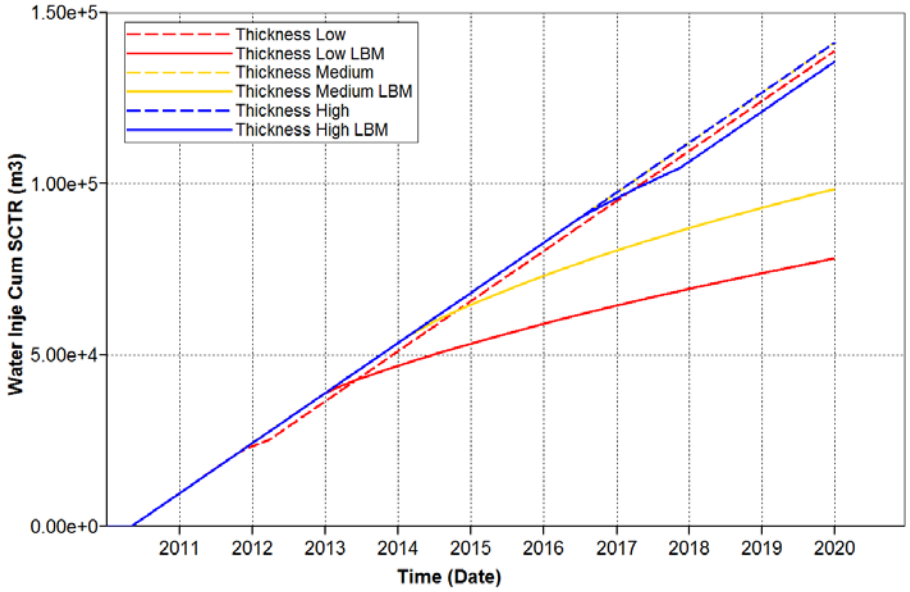

Figure 4-17 Cumulative water injection for all levels of reservoir thickness when intrinsic fracture porosity is at a high level

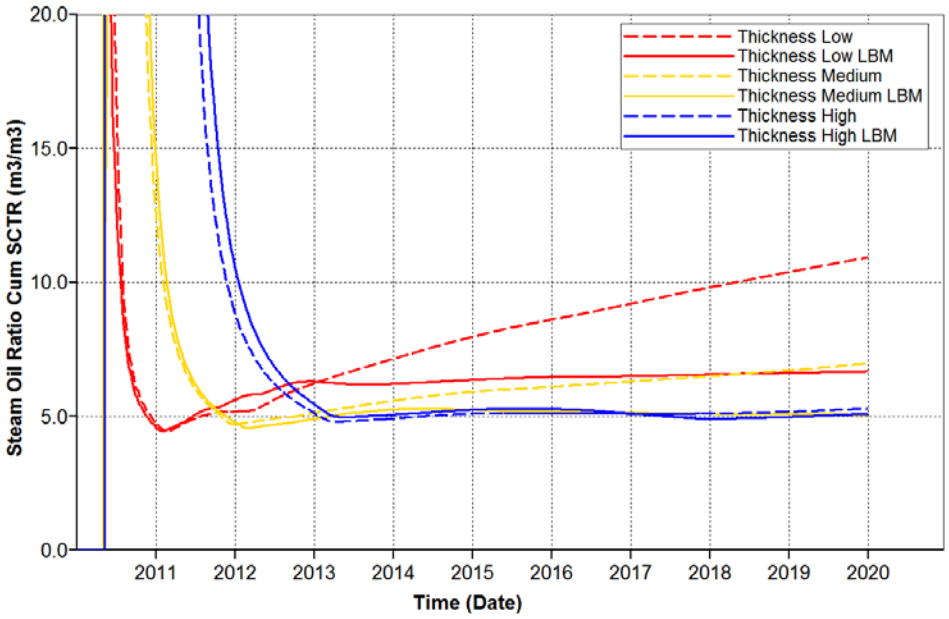

Figure 4-18 Cumulative SOR for all levels of reservoir thickness when intrinsic fracture porosity is at a high level

Figure 4-18 shows cSOR for six simulation runs at different reservoir conditions and different fracture relative permeability curves. The difference of cSOR between the two types of relative permeability curves is small enough that it can be ignored when the reservoir is thick. For this thick reservoir, cSOR is as low as 5.3 m^3/m^3 which makes SAGD an economical method. Cumulative SOR increased with reservoir thickness reduction. At the same time, the difference of cSOR between the two types of fracture relative permeability curves increased with reservoir thickness reduction. When the reservoir is thin, the difference can be as high as 63.6%, which makes an application of a nonlinear fracture relative permeability necessary. When the reservoir is thick, the difference is just 4.5%.

In conclusion, the necessity of using nonlinear relative permeability curves becomes more important with a reduction in reservoir thickness. For all ranges of reservoir thickness, the linear

fracture relative permeability will over-estimate cSOR in the reservoir which has a high level of intrinsic porosity.

4.4.1.2 Medium level of intrinsic fracture porosity: impact of relative permeability correlation application for all levels of thickness

When the intrinsic fracture porosity decreases from a high level to a medium level, cumulative oil production is not influenced. The difference between the two types of fracture relative permeability is small. The plot and conclusion are similar to those in the reservoir with a high level intrinsic fracture porosity.

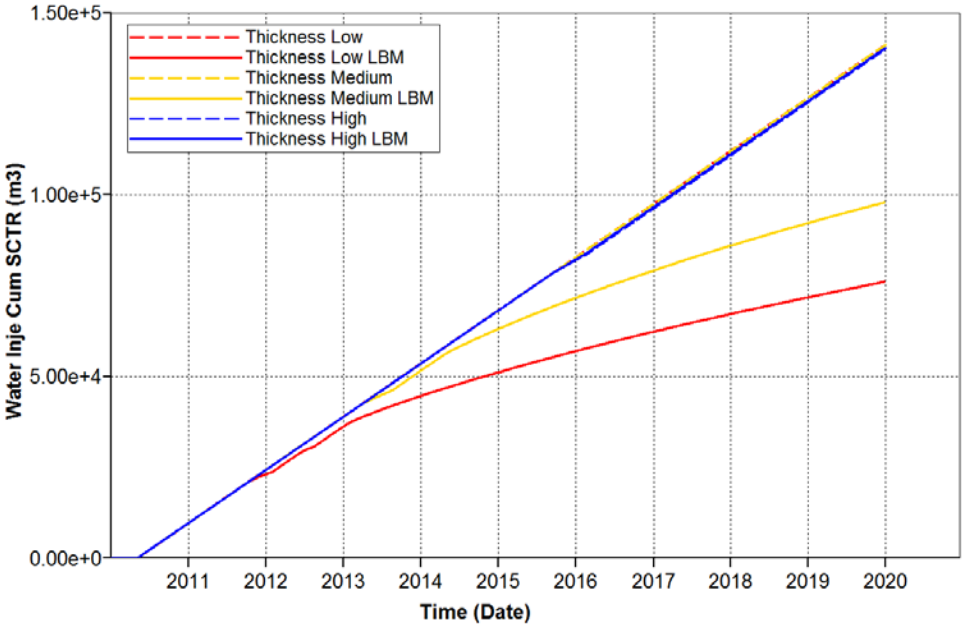

Figure 4-19 Cumulative water injection for all levels of reservoir thickness when intrinsic fracture porosity is at a medium level

Cumulative water injection is a little different, as shown in Figure 4-19. In a thick reservoir, a water injection volume will not be influenced by the shape of fracture relative permeability (linear or nonlinear). The flow rate of water injection is constant during the entire SAGD

process. In contrast, the difference in a reservoir with a medium thickness can be as high as 44.16%, and for a thin reservoir, the difference can even reach 85.5%. The volume of water injection will further influence calculations of a steam-to-oil ratio, and the accuracy of water injection predicting is important. Simulation runs for a thin and medium thickness reservoir need to input nonlinear fracture relative permeability in the model in order to obtain more accurate results.

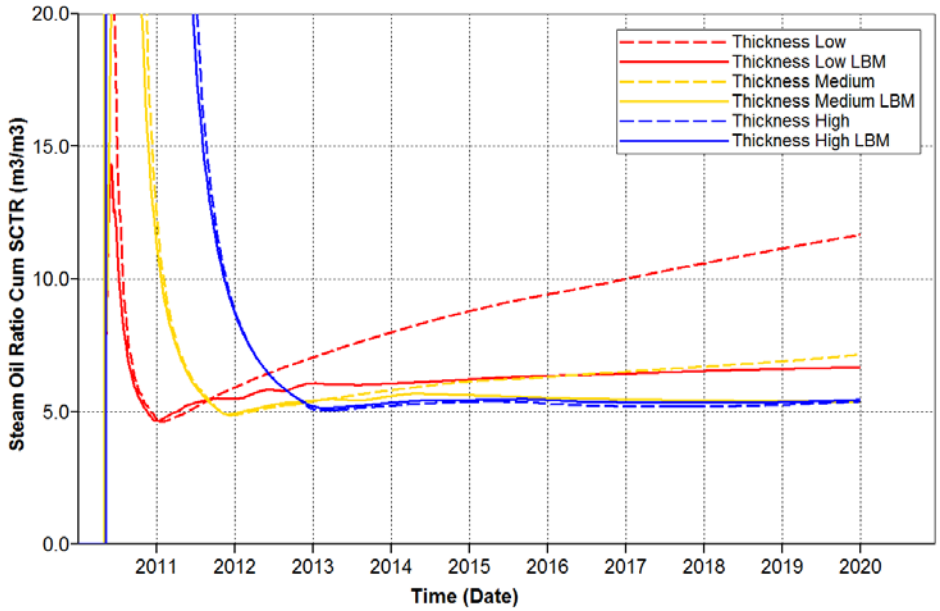

Figure 4-20 Cumulative SOR for all levels of reservoir thickness when intrinsic fracture porosity is at a medium level

The pattern of cumulative SOR at a medium level of intrinsic fracture porosity is similar to that at a high level of intrinsic fracture porosity (Figure 4-20). The thick reservoir is most suitable for the SAGD process. When the thickness is at a high or medium level, cSOR will not be affected. Cumulative SOR is higher in a thin reservoir. Simulation models with linear fracture relative

permeability will over-estimate results of cSOR in reservoirs with thin and medium levels of thickness.

4.4.1.3 Low level of intrinsic fracture porosity: impact of relative permeability correlation application for all levels of thickness

The trend of cumulative oil production in reservoirs with a low level of intrinsic fracture porosity is similar to those in reservoirs with medium and high levels of intrinsic fracture porosity. Comparing all cumulative oil production curves at all levels of intrinsic fracture porosity and reservoir thicknesses, we can conclude that the thicker the reservoir, the later the time when well communication is built.

Cumulative water injection patterns are displayed in Figure 4-21. A dynamic simulation model with linear fracture relative permeability has the same results as the two reservoirs with high and medium intrinsic fracture porosity. The nonlinear LBM model shows different water injection predictions from the last two comparisons. When intrinsic porosity is low, the biggest difference appeared in the reservoir with a medium thickness level, at 10 years of operation. However, if the prediction was for less than nine years, the conclusion is not changed: the thinner the reservoir, the larger the difference between the linear relative permeability model and the nonlinear relative permeability model. It is important to input nonlinear relative permeability in the fracture system to reduce uncertainty in the reservoir model.

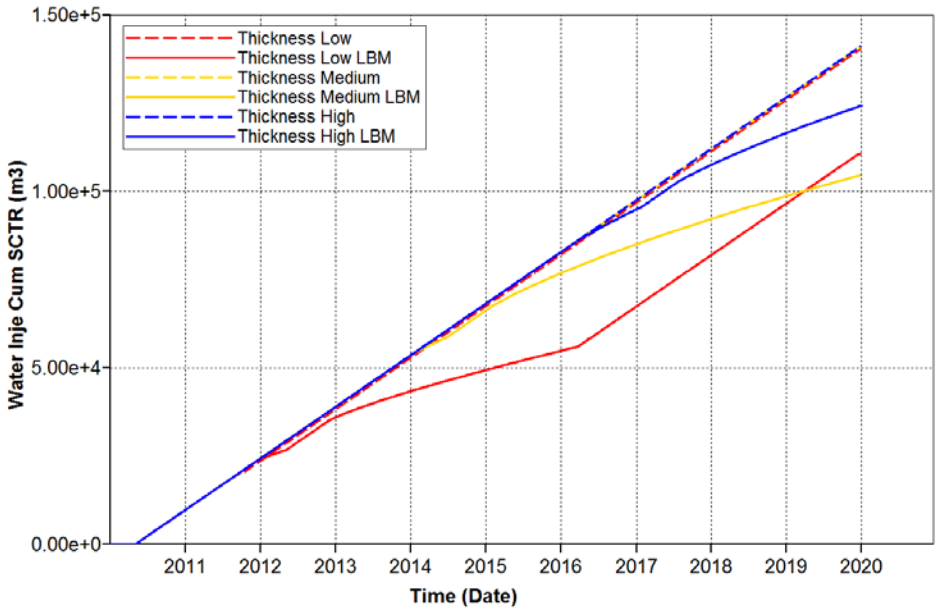

Figure 4-21 Cumulative water injection for all levels of reservoir thickness when intrinsic fracture porosity is at a low level

The pattern of cumulative SOR is similar to a case which has the medium level of intrinsic fracture porosity and will not be analyzed here again. Thickness ranked as the most sensitive parameter in SAGD processing, and cumulative oil production is determined by a steam chamber to some extent. Figure 4-22 displays a temperature distribution at the end of 10 years production at low, medium and high levels of reservoir thickness. From this figure, steam extends broadly better in thick reservoirs than in thin reservoirs. Thick reservoirs have more cumulative oil production and less cSOR. The volume of the steam chamber is bigger in the model with linear fracture relative permeability because the area of two-phase flow in nonlinear relative permeability curves is smaller. The temperature in the bottom of the reservoir increases with an increase in reservoir thickness.

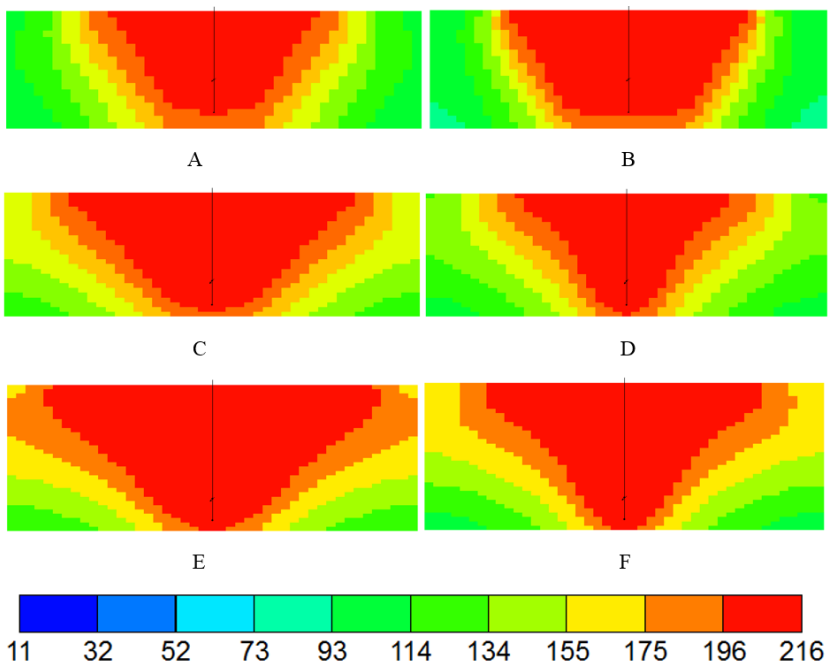

Figure 4-22 Temperature distribution comparison between two types of relative permeability and three levels of reservoir thickness (J layer: 3) (A: fixed linear model at low level reservoir thickness; B: LBM model at low level reservoir thickness; C: fixed linear model at medium level reservoir thickness; D: LBM model at medium level reservoir thickness; E: fixed linear model at high level reservoir thickness; F: LBM model at high level reservoir thickness)

4.4.1.4 Conclusion

Comparing cumulative oil production, water injection and cSOR in different reservoir thicknesses and intrinsic fracture porosity levels, the following conclusions can be drawn:

(1) An application of SAGD is more suitable in thick reservoirs. The influence of fracture relative permeability on prediction of cumulative oil production is small in thick reservoirs with any level of intrinsic fracture porosity. The difference is large in the reservoir with a medium level of thickness, especially with a high level of intrinsic fracture porosity.

(2) Cumulative water injection is sensitive to different types of fracture relative permeability curves. The thinner the reservoir, the more necessary it is to use nonlinear fracture relative permeability in the model.

(3) Cumulative SOR is also very sensitive to different fracture relative permeability models. Linear fracture relative permeability will over-estimate cSOR at all intrinsic fracture levels. The need to use nonlinear fracture relative permeability curves is less in thicker reservoirs. With cumulative water injection prediction, the thinner the reservoir, the more necessary it is to apply nonlinear fracture relative permeability in the model.

(4) The differences between two fracture relative permeability types in SAGD performance in different reservoirs are summarized in Table 4-5 below:

Table 4-5 difference between two types of fracture relative permeability in reservoirs with different thickness levels

Thickness \ Intrinsic fracture porosity		Low	Medium	High
Oil prod cum	Low	1.21%	6.03%	8.47%
	Medium	0.81%	8.34%	2.39%
	High	2.80%	0.86%	0.18%
Water injection cum	Low	26.89%	85.47%	77.46%
	Medium	35.05%	44.16%	43.38%
	High	13.64%	0.25%	4.10%
cSOR	Low	25.37%	74.92%	63.61%
	Medium	33.78%	33.06%	35.61%
	High	16.95%	1.10%	4.52%

4.4.2 Impact of Relative Permeability Correlation Application in Reservoirs with Different Porosity Levels

4.4.2.1 High level of intrinsic fracture porosity: impact of relative permeability correlation application

The number of grid blocks and all operation settings are not changed from the base case. Matrix porosity changed from a low level to a high level. For each level of matrix porosity, 12 simulation cases run. There are six cases for the fixed linear models, and intrinsic fracture porosity ranges from 1 to 0.497. Another 6 cases for the LBM model are analyzed, with intrinsic fracture porosity ranging from 1 to 0.497.

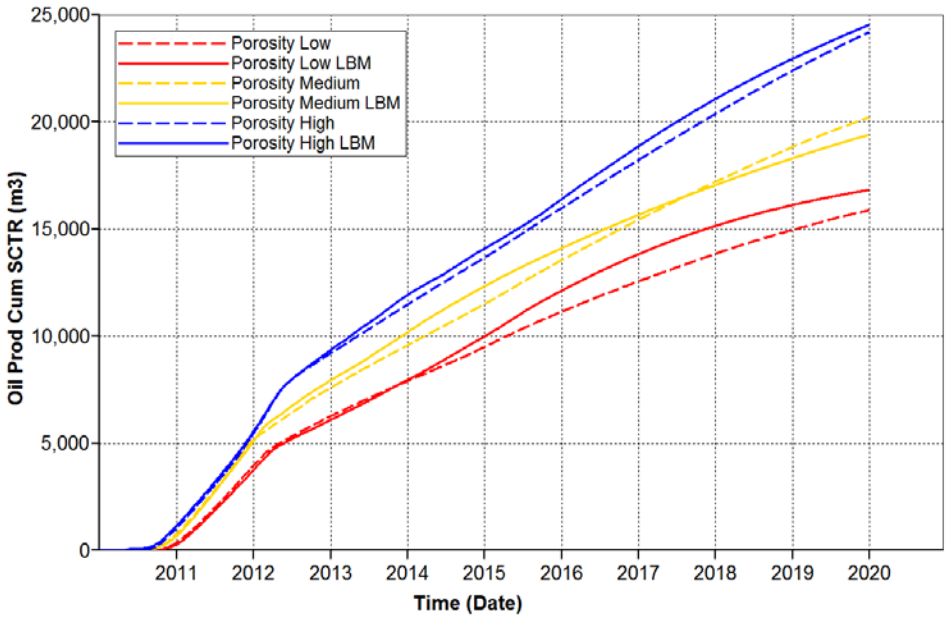

Figure 4-23 Cumulative oil production for all levels of matrix porosity when intrinsic fracture porosity is at a high level

Figure 4-23 displays cumulative oil production for all levels of matrix porosity when intrinsic fracture porosity is at a high level. The higher the matrix porosity, the higher the cumulative oil production for both the fixed linear model and the LBM model. This is because the higher the

matrix porosity the higher the original oil in place. For models which applied linear relative permeability, the trend and slope of cumulative oil production curves are almost the same, which means that the difference of matrix porosity will not influence the oil production rate. Cumulative oil production in the LBM model is higher than in the linear model in low level and high level matrix porosities. But when the matrix porosity is at a medium level, predicted cumulative oil production is lower in the LBM model than in the linear model. At the 10^{th} year of operation, the difference of predicted cumulative oil production between the linear model and the LBM model is 1.4%, 2.4% and 5.6%, correspond to matrix porosity of high, medium and low, respectively. Thus, the smaller the matrix porosity, the larger the difference between the two relative permeability models. The fixed linear model will under-estimate cumulative oil production when matrix porosity is high and low. In contrast, when matrix porosity is at a medium level, the fixed linear model will over-estimate cumulative oil production. However, the difference of forecasted cumulative oil production is small when the intrinsic fracture porosity is high at all ranges of matrix porosity.

In figure 4-24, cumulative water injection versus operation time is displayed for different matrix porosities. Simulation results demonstrate that the volume of a water injection rate will not be influenced by matrix porosity if a fixed linear model is applied in the SAGD simulation. In contrast, cumulative water injection is different for different matrices in the LBM model at a high level of intrinsic fracture porosity. Cumulative water injection will be over-estimated if the dynamic model uses a fixed linear model instead of the LBM model. Reservoirs which have a matrix porosity at a medium level will be influenced the most, while reservoirs which have a low level of matrix porosity will be affected the least. The difference between the two relative

permeability models is 30.2% at a high level of matrix porosity, 43.38% at a medium level of matrix porosity, and 28.3% at a low level of matrix porosity. Even the minimum difference between the two types of fracture relative permeability curves is higher than 25%, and the necessity of using the nonlinear relative permeability curves calculated from the LBM model is clear.

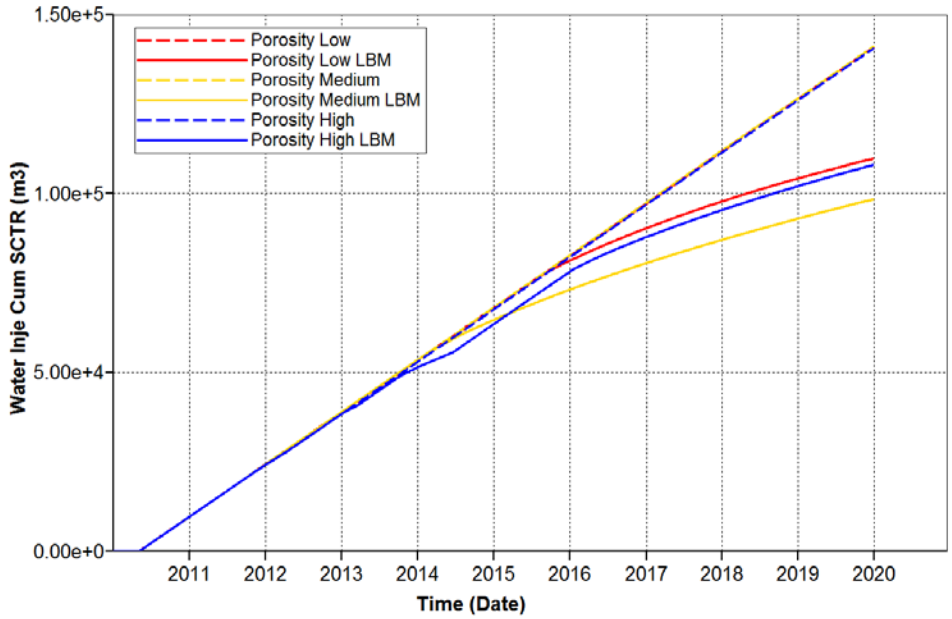

Figure 4-24 Cumulative water injection for all levels of matrix porosity when intrinsic fracture porosity is at a high level

Figure 4-25 demonstrates that no matter if linear fracture relative permeability or nonlinear fracture relative permeability calculated from the LBM model is applied in the SAGD simulation model, reservoirs which have a high level of matrix porosity are more suitable for SAGD production because the cSOR is low. In our SAGD model, when matrix porosity is at a high level (0.36), the cSOR can be as low as 4.41 m^3/m^3, which will be a more profitable SAGD operation. Additionally, the figure shows that the SAGD model which has applied a linear

relative permeability model will over-estimate cSOR no matter what the matrix porosity is. The difference of cSOR between the two types of relative permeability is 32.0%, 35.6% and 36%, corresponding to high, medium and low levels of matrix porosity, respectively. Thus, the lower the matrix porosity, the more important it is to implement nonlinear fracture relative permeability curves in order to reduce uncertainties and increase accuracy of forecasting results.

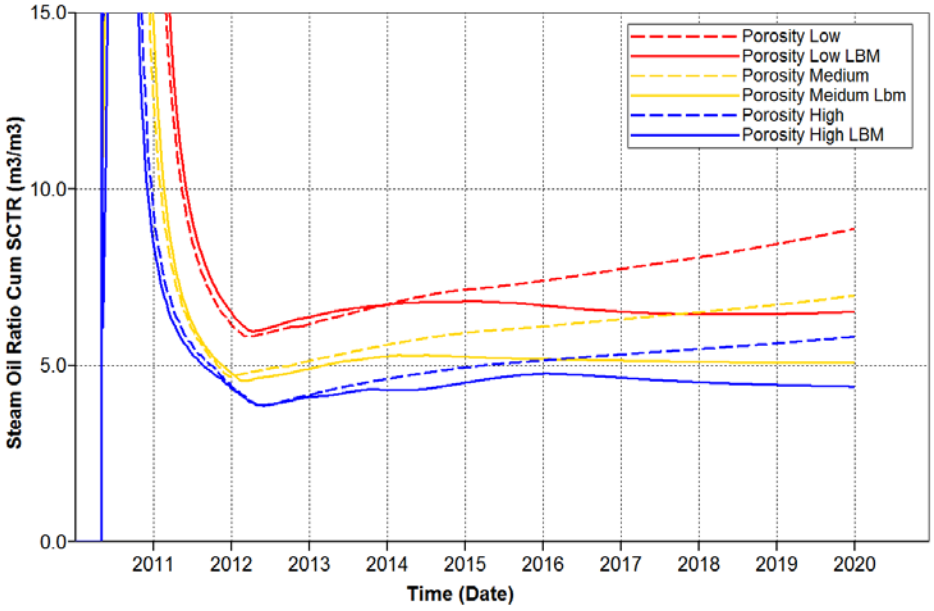

Figure 4-25 Cumulative SOR for all levels of matrix porosity when intrinsic fracture porosity is at a high level

4.4.2.2 Medium level of intrinsic fracture porosity: impact of relative permeability correlation application

The impact of nonlinear fracture relative permeability should not only be studied in a situation of high intrinsic fracture porosity. Intrinsic fracture at medium and low levels should also be analyzed. Cumulative oil production, water injection and cumulative SOR will be analyzed in this section.

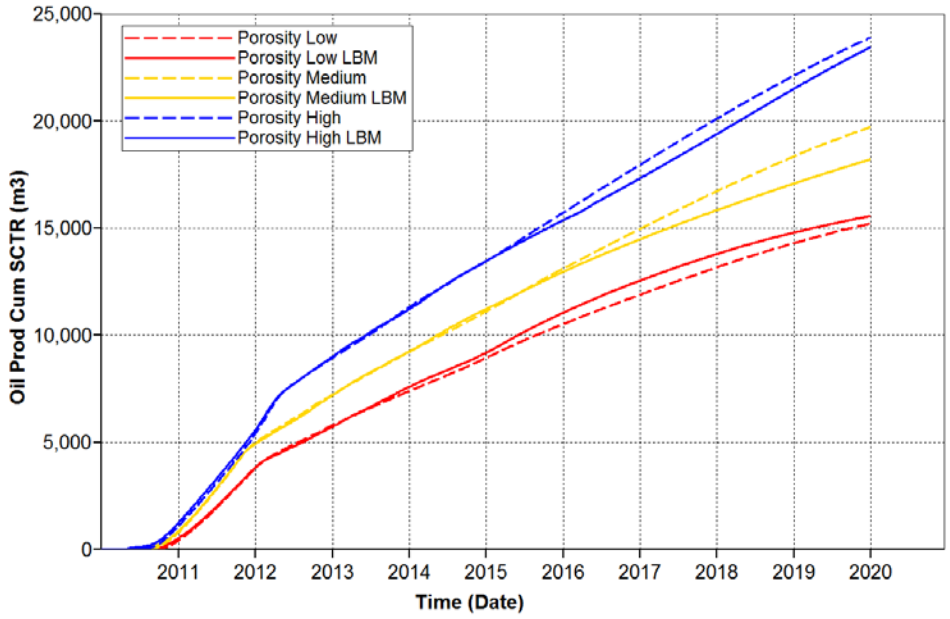

Figure 4-26 Cumulative oil production for all levels of matrix porosity when intrinsic fracture porosity is at a medium level

Figure 4-26 shows the impact of a nonlinear relative permeability application in low, medium and high levels of matrix porosity reservoirs. The figure shows that the higher the porosity of matrix, the higher cumulative oil production will be, which corresponds to a high level of intrinsic fracture porosity. An application of linear fracture relative permeability will over-estimate cumulative oil production in reservoirs which have high or medium matrix porosity. However, it will under-estimate cumulative oil production in the low matrix porosity reservoir. Similarly, the difference of cumulative oil production between the two types of fracture porosity is small at all ranges of matrix porosity. For reservoirs which have high and medium levels of matrix porosity, the difference appeared after five years of operation. Thus, if the forecasting of cumulative oil production is only for five years, it is not necessary to apply nonlinear fracture relative permeability calculated from the LBM model.

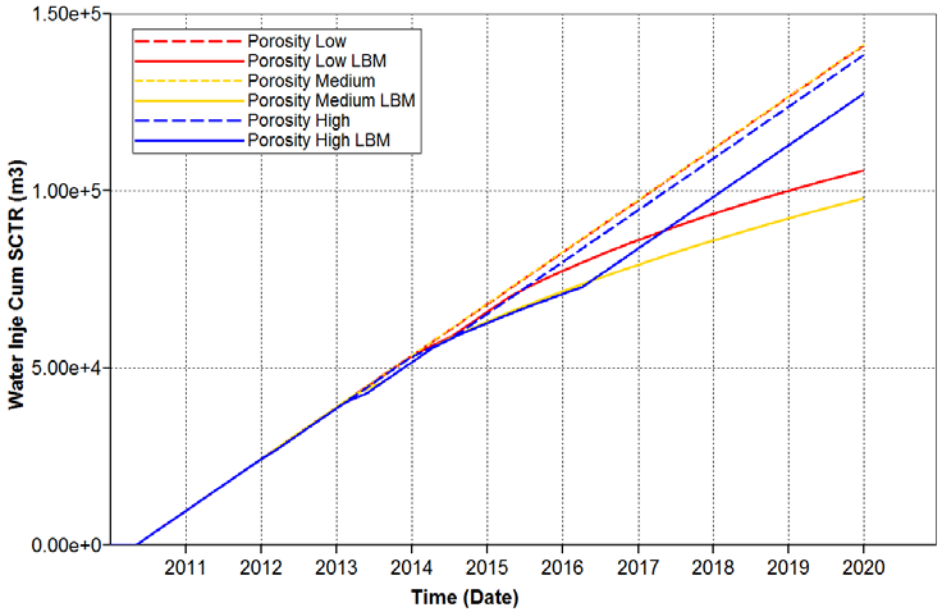

Figure 4-27 Cumulative water injection for all levels of matrix porosity when intrinsic fracture porosity is at a medium level

Cumulative water injection is analyzed in Figure 4-27. Compared to results at a high level of intrinsic fracture porosity, the matrix porosity will affect a water injection volume, even for the linear fracture relative permeability model. The ability of water injection is lower in the high porosity reservoir, according to forecasting results from the model which applied linear fracture relative permeability. In contrast, simulation results are different in the model which applied the nonlinear relative permeability model, in that high porosity reservoirs have the highest ability of injecting water. The lowest water injection ability appeared in the reservoir which has medium level of porosity. The biggest difference between the two relative permeability models occurred at a medium level of matrix porosity. Linear fracture relative permeability will over-estimate cumulative water injection, where the smallest difference can reach 8.5% and the largest difference can reach 44.15%. As a result, it is necessary to apply nonlinear relative permeability

in the SAGD simulation model, especially for reservoirs which have large porosity and small porosity.

Comparison of a cumulative steam-to-oil ratio is similar to the example which has a high level of intrinsic fracture porosity. The difference of cSOR between the linear relative permeability model and the nonlinear relative permeability model is 6.46% for a higher level of matrix porosity, 33.06% for a medium level and 36.54% for a low level of matrix porosity. The lower the matrix porosity, the bigger the difference of simulation results in cSOR at 10 years of operation. In addition, with low matrix porosity, cSOR is larger than 10 m^3/m^3 in the linear model, while it is 6.7 m^3/m^3 in the nonlinear model. This large difference in simulation results may lead to a different operation strategy. Thus, it is necessary to implement nonlinear fracture relative permeability in the dynamic model, especially for reservoirs which have low matrix porosity. The difference between the two types of relative permeability in cumulative oil production, water injection and cSOR prediction are not larger than 10% in reservoirs which have large matrix porosity. It can be concluded that the necessity of using nonlinear fracture relative permeability is weak for this type of reservoirs.

4.4.2.3 Low level intrinsic fracture porosity: impact of relative permeability correlation application

Figure 4-28 shows cumulative oil production for all levels of matrix porosity when intrinsic fracture porosity is low. In this figure, there is not much difference between the LBM fracture relative permeability model and the linear model, which agrees with the conclusion in both high and medium levels of intrinsic fracture porosity. The deviation in low intrinsic fracture porosity

is less than in the other two levels. Cumulative oil production forecasting when intrinsic fracture porosity is low is accurate in the model with linear fracture relative permeability. Comparing three cumulative oil production plots, the point which represents well communication built time occurred at the same time for all cases, which implies that the time of well communication will not be influenced by matrix porosity and fracture relative permeability types.

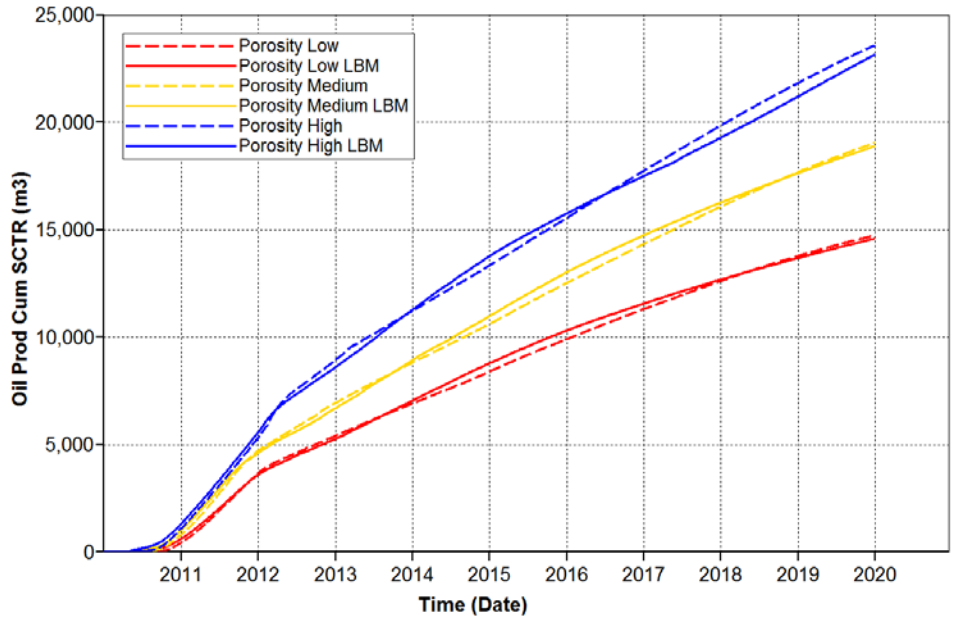

Figure 4-28 Cumulative oil production for all levels of matrix porosity when intrinsic fracture porosity is at a low level

Cumulative water injection is described in Figure 4-29. The pattern in this figure is similar to that in Figure 4-27 but there are some differences. First, the matrix porosity will not influence a water injection volume in an SAGD forecasting model where linear fracture relative permeability is implemented. The steam injection rate is constant during the entire SAGD operation. There are differences in the model with nonlinear fracture relative permeability. Steam injection rates are constant in the first four years of processing, and then the flow rate decreases in reservoirs which

have low and medium porosity. It is worthwhile to note that there is no difference between low porosity reservoirs and medium porosity reservoirs in the water injection rate and volume. In high porosity reservoirs, the water injection rate is a constant in the first four years of operation, and then decreases for approximately three years. In the last stage of operation, the rate of water injection recovers to its original injection rate. The difference of water injection rates between the linear relative permeability model and the nonlinear LBM model is smallest in the reservoir which has the highest matrix porosity. However, even for the smallest difference, the value can reach 13.8%. The difference can be as high as 35% in low and medium porosity reservoirs. Considering the large difference between the linear and nonlinear fracture relative permeability models at all levels of reservoir porosity, it is necessary to use nonlinear fracture relative permeability in the reservoir which has a low level of intrinsic fracture porosity for water injection forecasting.

Comparison of cSOR between the two relative permeability types in three levels of reservoir porosity, when intrinsic fracture porosity is at a low level, is similar to reservoirs with high and medium levels of intrinsic fracture porosity. These differences are 11.4%, 33.8% and 34.1% and correspond to high, medium and low levels of reservoir porosity, respectively. cSOR in reservoirs which have high and medium models is less than 6 m^3/m^3 in the model with nonlinear relative permeability, which is considered economic in a SAGD process. For reservoirs which have low reservoir porosity, cSOR is 9.58 m^3/m^3 in the linear fracture relative permeability implementation model and SAGD should not be used. For the model which has nonlinear fracture relative permeability cSOR is 7.14 m^3/m^3. While this is suitable for using a SAGD operation process, SAGD may not be the most suitable method. It is necessary to implement

nonlinear relative permeability in the SAGD dynamic model to forecast cSOR, especially for the reservoir which has a low level of matrix porosity.

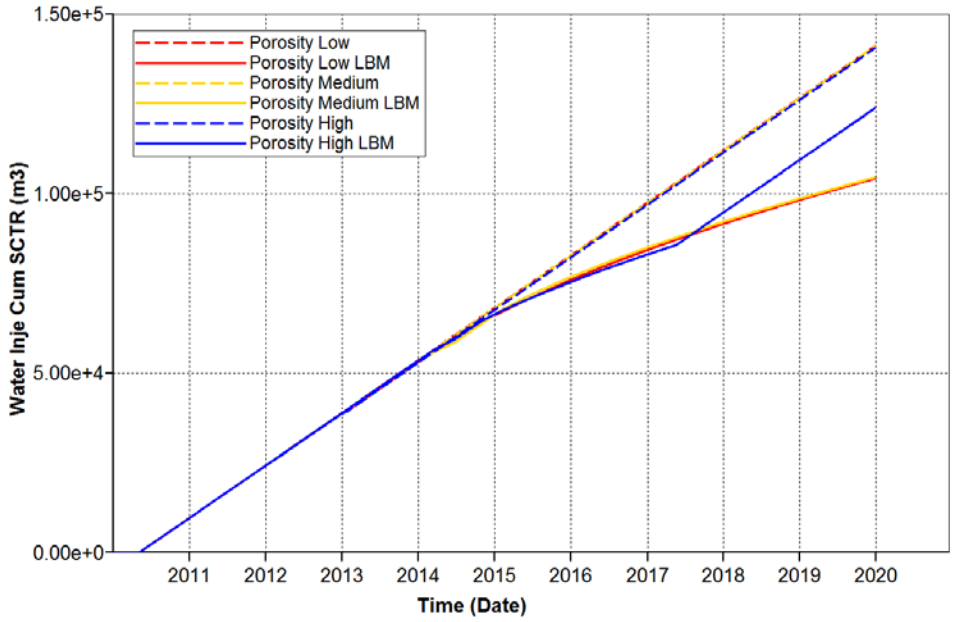

Figure 4-29 Cumulative water injection for all levels of matrix porosity when intrinsic fracture porosity is at a low level

4.4.2.4 Conclusion

Through an analysis of cumulative oil production, water injection and cSOR at all levels of reservoir matrix porosity and intrinsic fracture porosity, the following conclusions can be made:

(1) The difference between a fixed linear relative permeability model and a nonlinear relative permeability model, calculated from the LBM model, is small in predicting cumulative oil production for reservoirs with all levels of matrix porosity and intrinsic fracture porosity.

(2) The difference of SAGD performance between the two types of fracture relative permeability models is large when predicting water injection ability, especially for the reservoir with a medium level of matrix porosity.

(3) The difference in predicting cSOR at ten years of operation between the two models is large. For all intrinsic fracture porosities, the lower the matrix porosity, the higher the cSOR.

(4) A summary of differences between the two fracture relative permeability models in SAGD performance is listed in Table 4-6,

Table 4-6 difference between two types of fracture relative permeability in reservoirs with different matrix porosities

Intrinsic fracture porosity / Matrix porosity		Low	Medium	High
Oil prod cum	Low	0.96%	2.30%	5.64%
	Medium	0.81%	8.34%	2.39%
	High	1.65%	1.93%	1.40%
Water injection cum	Low	35.41%	33.40%	28.34%
	Medium	35.05%	44.16%	43.38%
	High	13.84%	8.52%	30.15%
cSOR	Low	34.13%	36.54%	36.00%
	Medium	33.78%	33.06%	35.61%
	High	11.39%	6.46%	31.99%

4.4.3 Impact of Relative Permeability Correlation Application in Reservoirs with Different Oil Saturation Levels

To estimate original oil in place (OOIP), initial oil saturation is an important parameter. Oil saturation ranked as third in the sensitivity study, and NPV increased with oil saturation linearly (Nguyen et al., 2012). After analyzing the impact of nonlinear relative permeability in reservoirs with different thicknesses and porosities, oil saturation was selected as the last parameter to be investigated. Comparing SAGD performance between a fixed linear X-type fracture relative permeability and a nonlinear LBM relative permeability, its influence can be investigated.

4.4.3.1 High level intrinsic fracture porosity: impact of relative permeability correlation application

Cumulative oil production comparison between two types of relative permeability and initial oil saturation is shown in Figure 4-30. Cumulative oil production increased with initial oil saturation. The start point of cumulative oil production curves occurred late, as oil saturation decreased, which implies that reservoirs with low level oil saturation need more heating time in order to reach critical oil mobility. The point which indicates well communication of those curves also occurred late, as oil saturation decreased.

Comparing two types of fracture relative permeability simulation results of cumulative oil production, feature points which are previously mentioned will not be influenced by fracture relative permeability types. Differences begin to appear after the time when communication of two wells is built. Reservoirs which have medium and low levels of initial oil saturation will be over-estimated in the model with linear relative permeability input. The difference of cumulative oil production between these two fracture relative permeability curves are 4.28%, 2.39% and 0.84%, corresponding to low, medium and high initial oil saturation, respectively. The lower the initial oil saturation, the bigger the difference between the two types of relative permeability curves, and the more important it is to apply nonlinear fracture relative permeability calculated from the LBM model. The difference in cumulative oil production prediction in reservoirs which have a high level of initial oil saturation is so small that it can be ignored.

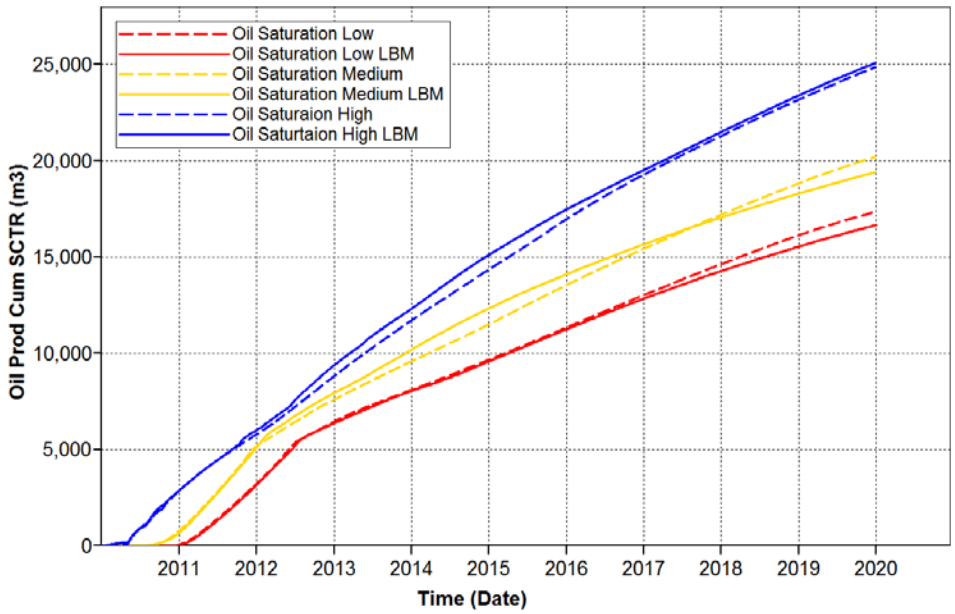

Figure 4-30 Cumulative oil production for all levels of initial oil saturation when intrinsic fracture porosity is at a high level

Figure 4-31 displays cumulative water injection in reservoirs with different initial oil saturation. Simulation models with linear fracture relative permeability show that initial oil saturation will not influence cumulative water injection, which contrasts with the results simulated from the model with nonlinear fracture relative permeability implemented. Water injection is not affected by initial oil saturation in the first three years of production. In the first five years of production, a variation in a water injection volume for all levels of initial oil saturation is not prominent. From five to seven years of production, the higher the initial oil saturation, the lower the water injection volume. After seven years of operation, the water injection rate increased sharply in reservoirs with a high level of oil saturation. Simulation models with linear fracture relative permeability will over-estimate cumulative water injection in reservoirs at all levels of initial oil

saturation. The differences are 9.76%, 43.38% and 38.38% in reservoirs with high, medium and low levels of initial oil saturation, respectively.

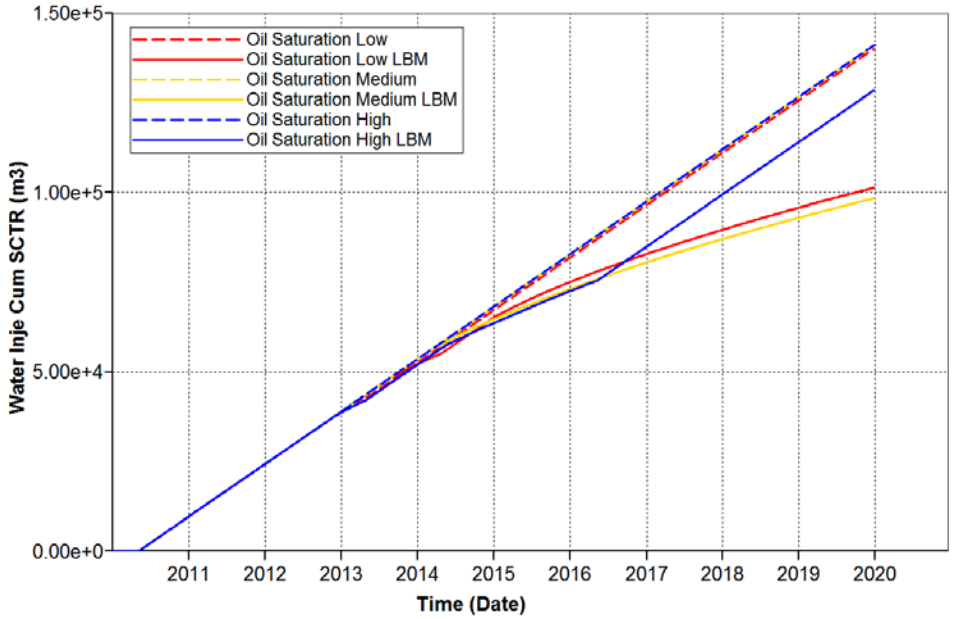

Figure 4-31 Cumulative water injection for all levels of initial oil saturation when intrinsic fracture porosity is at a high level

Comparison of cumulative SOR at three levels of initial oil saturation is illustrated in Figure 4-32. After the preheating period, a large volume of steam was injected into the reservoir, and on opening the injector, oil production is typically not high, which leads to a large SOR. As more of the reservoir is heated, oil mobility increases and an oil production rate increases, which leads to cSOR decreasing, below 10 m^3/m^3. This will not occur in the reservoir with a high level of oil saturation, as shown in Figure 4-32.

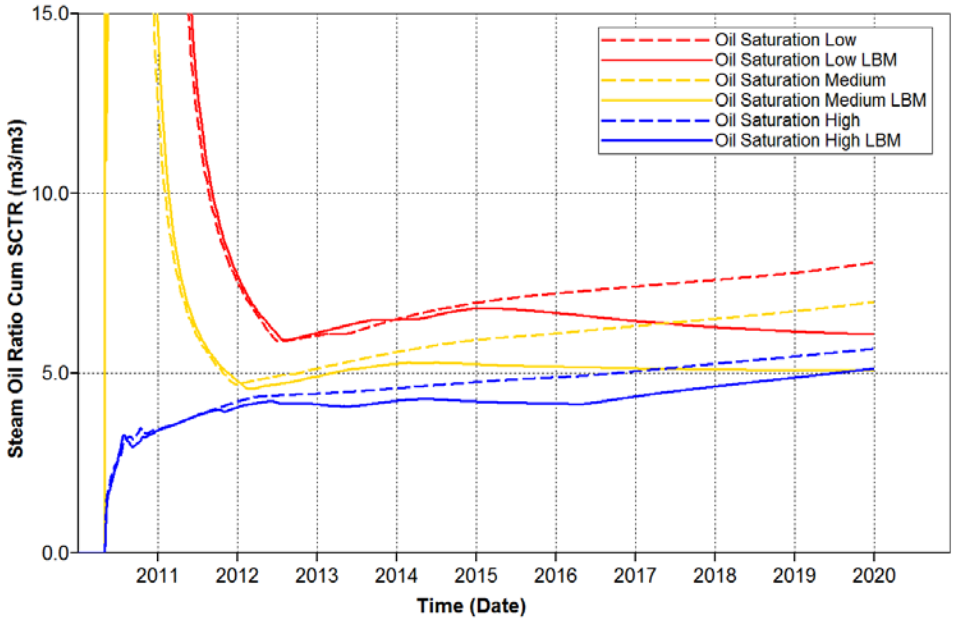

Figure 4-32 Cumulative SOR for all levels of initial oil saturation when intrinsic fracture porosity is at a high level

There is a period where cSOR increases sharply; however, the value is not very high and cSOR will stay around 5 m^3/m^3. The reason for this is that oil saturation is high in the fractures and flows out more easily than oil located in the matrix. At the early stage of operation, an oil production volume is high in reservoirs with high initial oil saturation, which leads to low cumulative SOR. Initial oil saturation influences the feature point at which the oil production rate increases. The higher the initial oil saturation of the reservoir, the earlier the feature point of curves occurred, which means that initial oil saturation will promote oil production to enter a high rate stage earlier. Comparing the two types of fracture relative permeability curves at the same initial oil saturation, linear fracture relative permeability will over-estimate cSOR. The differences in cSOR are 10.7%, 35.6% and 32.7% in a reservoir with low, medium and high levels of initial oil saturation, respectively. As the differences in all initial oil saturation levels

are larger than 10%, it is necessary to apply nonlinear relative permeability in an SAGD simulation model, especially to predict cSOR.

4.4.3.2 Medium level intrinsic fracture porosity: impact of relative permeability correlation application

Figure 4-33 describes cumulative oil production in reservoirs with medium intrinsic fracture porosity. Compared to Figure 4-30, which has a high level of intrinsic fracture porosity, cumulative oil production decreased for all three levels of initial oil saturation. The pattern of the two curves which describe the model with linear and nonlinear fracture relative permeability is almost the same in three levels of initial oil saturation. In the reservoir with high and medium level initial oil saturation, there is no difference between linear fracture relative permeability and nonlinear fracture relative permeability in oil cumulative production before five and half years of production. At that point, the model with linear fracture relative permeability begins to over-estimate cumulative oil production. In the reservoir which has a low level of initial oil saturation, things are more complex. In the first three years of production, there is no difference in cumulative oil production between the two types of fracture relative permeability. In the middle stage of operation, cumulative oil production prediction in the model with nonlinear fracture relative permeability will be higher. After six and half years of operation, the model with linear fracture relative permeability begins to over-estimate cumulative oil production. The differences in oil production between the two relative permeability models are all less than 10%.

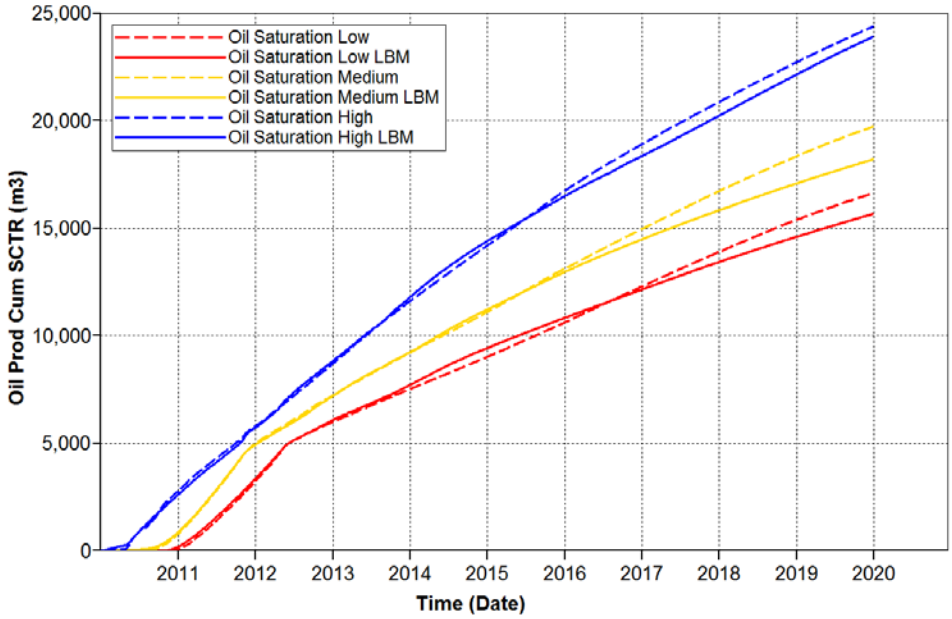

Figure 4-33 Cumulative oil production for all levels of initial oil saturation when intrinsic fracture porosity is at a medium level

A water injection plot for three levels of initial oil saturation and two types of fracture relative permeability is similar to Figure 4-31. The same conclusion of a fracture relative permeability impact on water injection is reached when a reservoir has a medium or high level of intrinsic fracture porosity.

Comparisons of cSOR between the two models of fracture relative permeability in three levels of initial oil saturation with a medium level of intrinsic fracture porosity are similar to those for the reservoir which has a high level of intrinsic fracture porosity (Figure 4-32). However, cSOR in the reservoir with a medium level of intrinsic fracture porosity is higher than in the reservoir with a high level of intrinsic fracture porosity, at all levels of initial oil saturation. Differences between the two kinds of fracture relative permeability at three levels of initial oil saturation are almost the same (10.5%, 33.1% and 34.7%) compared with Figure 4-32, which has a high level

of intrinsic fracture porosity. Thus, intrinsic fracture porosity will not influence differences in cSOR prediction between linear and nonlinear fracture relative permeability. It is still necessary to use nonlinear fracture relative permeability in the SAGD simulation model in a reservoir with medium intrinsic fracture porosity for all levels of initial oil saturation.

4.4.3.3 Low level intrinsic fracture porosity: impact of relative permeability correlation application

In the last two sections, a fracture relative permeability effect on cumulative oil production with high and medium levels of intrinsic fracture porosity were investigated. The same conclusion was reached that the maximum difference occurred in the reservoir with a medium level of initial oil saturation, which is in contrast to the phenomena in the reservoir with a low level of intrinsic fracture porosity.

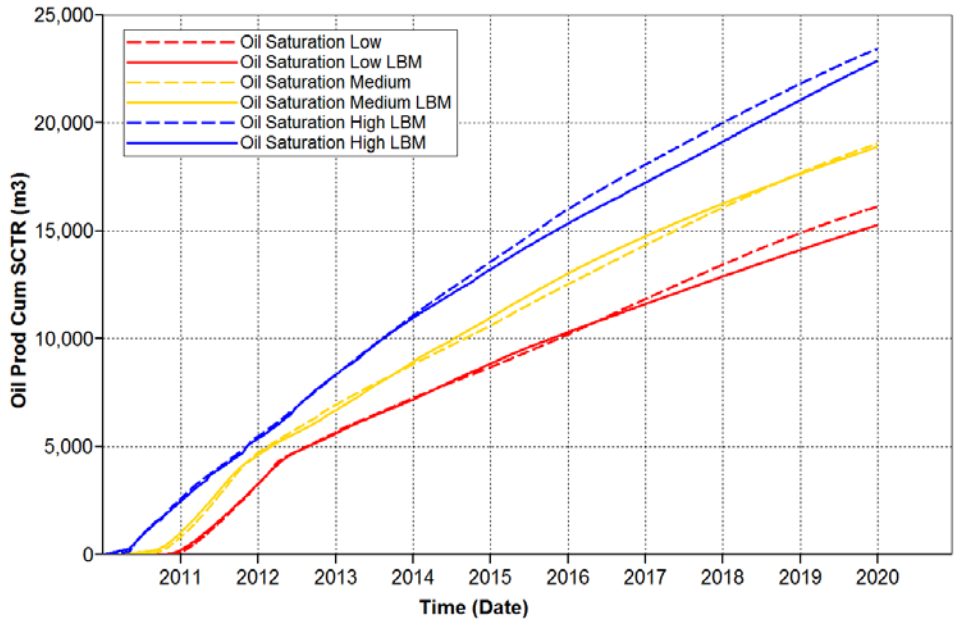

Figure 4-34 Cumulative oil production for all levels of initial oil saturation when intrinsic fracture porosity is at a low level

Figure 4-34 demonstrates that at the end of 10 years of operation, the smallest difference of cumulative oil production between the linear and nonlinear fracture relative permeability models occurred in the reservoir with a medium level of initial oil saturation. In the reservoir with high and low levels of initial oil saturation, there is little difference in cumulative oil production prediction in the early stage of operation. Then the simulation model with linear fracture relative permeability will over-estimate cumulative oil production, while in the reservoir with a medium level of initial oil saturation, the simulation model which inputs linear fracture relative permeability will under-estimate cumulative oil production in the middle stage of operation, and then it will over-estimate cumulative oil production, according to the trend of curves.

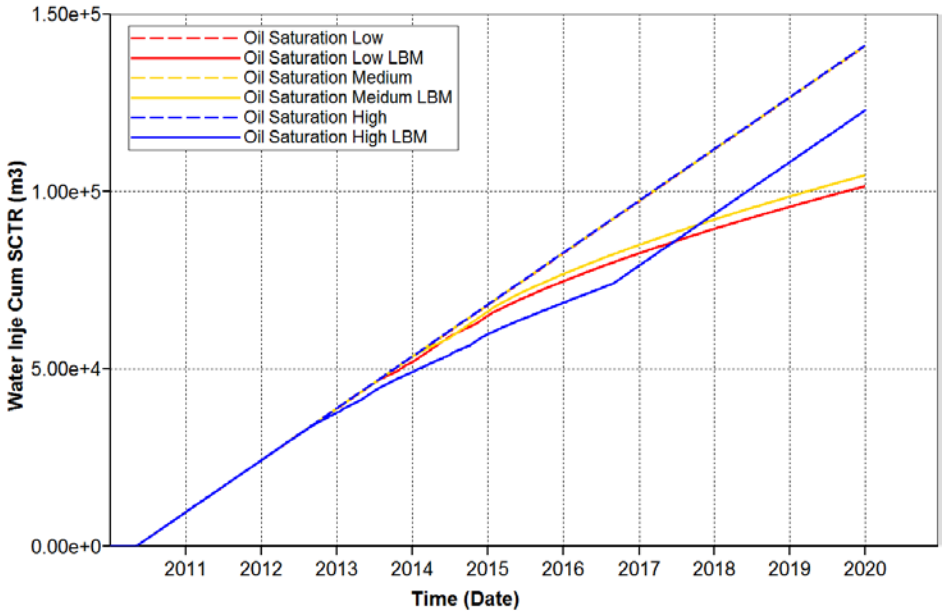

Figure 4-35 Cumulative water injection for all levels of initial oil saturation when intrinsic fracture porosity is at a low level

Patterns of cumulative water injection in the reservoir with a low level of intrinsic fracture porosity are similar to Figure 4-31 but there are some differences. In the first 2.5 years of production, oil saturation levels and fracture relative permeability types have no influence on

cumulative water injection. In the reservoir with a high level of initial oil saturation, the water injection rate decreased after 2.5 years of production, and then recovered to the original water injection rate in 6.5 years of production. For the reservoir with low and medium levels of oil saturation, after 3.5 or 4 years of production, the water injection rate reduced. Overall, the linear fracture relative permeability implementation model will over-estimate a water injection volume, and the lower the initial oil saturation, the bigger the derivation of cumulative water injection in SAGD operation forecasting.

Comparison of cSOR at all three levels of initial oil saturation shows that the minimum deviation of the linear fracture relative permeability model in cSOR is 12.1% in the reservoir with a high level of initial oil saturation. The derivation in medium and low levels of initial oil saturation reservoirs can be as high as 33.7%. It is necessary to input nonlinear fracture relative permeability into the model in order to have a more accurate estimate of cSOR, even in the reservoir with a high level of initial oil saturation.

4.4.3.4 Conclusions

(1) Differences of cumulative oil production prediction at all three levels between the linear and nonlinear fracture relative permeability models, in intrinsic fracture porosity and initial oil saturation are less than 10%, which is small.

(2) The prediction of cumulative water injection in reservoirs with a high initial oil saturation and in all ranges of intrinsic fracture porosity is a little more than 10%, while in the reservoir with medium and low levels of initial oil saturation, this derivation can be higher than 35.15% and reach 44.15%, which demonstrates the necessity of applying

nonlinear relative permeability in the model. Those results also demonstrate that nonlinear fracture relative permeability has a deeper effect on reservoirs without high initial oil saturation.

(3) Differences of cumulative SOR prediction are similar to those in cumulative water injection in that the deviation is a little more than 10% in the reservoir with a high initial oil saturation, in all ranges of intrinsic fracture porosity. In the reservoir with medium and low levels of initial oil saturation, this derivation is higher than 30% but less than 40%. These results demonstrate that a nonlinear fracture relative permeability application is necessary in cSOR prediction, especially in reservoirs with medium and high levels of initial oil saturation.

(4) A summary of differences between the fixed linear model and the LBM model for three levels of initial oil saturation and intrinsic fracture porosity is shown below:

Table 4-7 difference between two types of fracture relative permeability in reservoir with different initial oil saturation

Initial oil saturation \ Intrinsic fracture porosity		Low	Medium	High
Oil prod cum	Low	5.58%	6.11%	4.28%
	Medium	0.82%	8.34%	2.39%
	High	2.43%	1.97%	0.84%
Water injection cum	Low	38.96%	42.59%	38.38%
	Medium	35.05%	44.15%	43.38%
	High	14.87%	12.76%	9.75%
cSOR	Low	31.62%	34.38%	32.70%
	Medium	33.78%	33.06%	35.61%
	High	12.10%	10.58%	10.73%

Chapter Five: CONCLUSIONS AND RECOMMENDATIONS

5.1 Conclusions

In this study, a 2D LBM model is successfully developed to generate fracture relative permeabilities. It is shown that fracture relative permeabilities present nonlinear relationships with saturation, rather than the commonly used X-shape curves. Lubricating phenomena was observed when a viscosity ratio is much larger than 1. Irreducible water saturation and residual oil saturation are correlated linearly to intrinsic fracture porosity. They decrease linearly with an increase in intrinsic fracture porosity. It is also found that the coefficient of irreducible water saturation is larger than that of residual oil saturation. This demonstrates that intrinsic fracture porosity has a deeper impact on the water phase as compared to the oil phase. Initial oil relative permeability $k_{ro}(S_{wir})$ and final water relative permeability $k_{rw}(S_{or})$ also have a linear relationship with intrinsic fracture porosity. They increase as the intrinsic fracture porosity increases. The coefficient of oil relative permeability is larger than that of water relative permeability. The average changing rate of water relative permeability is linear with intrinsic fracture porosity, whereas the relationship between an oil relative permeability changing rate and intrinsic fracture porosity is nonlinear.

Fracture relative permeabilities, calculated from 3D LBM models (including gravity consideration), also demonstrate linear relationships between fracture relative permeability feature points and intrinsic fracture porosity. Correlation equations are provided in Chapter 3 for conditions with and without gravity consideration. By comparing relative permeability curves that do and do not consider gravity at the same intrinsic fracture porosity, it is found that the two phase flow area in the case which considers gravity is larger than the other. Irreducible water

saturation and residual oil saturation decreased with the help of gravity. The curvatures of oil and water relative permeability curves, however, are almost the same between the two conditions. Through a correlation analysis of results from the 3D model without gravity consideration, the coefficients of irreducible water saturation and residual oil saturation are close to each other. This means that the effects of intrinsic fracture porosity on the irreducible water saturation and residual oil saturation are in the same degree. The coefficient of the final water relative permeability is larger than the oil relative permeability coefficient indicating that intrinsic fracture porosity has a much deeper influence on the water relative permeability. In the 3D model which considers a gravity impact, the coefficient of irreducible water saturation is smaller than that of residual oil saturation, indicating that the intrinsic fracture has a deeper effect on residual oil saturation with the help of gravity. Its influence on the initial oil relative permeability and initial water relative permeability agrees with the conclusions from the 3D model without gravity.

A SAGD performance analysis indicates that cumulative oil production, water injection, and SOR are indeed different between simulation models implemented with fixed linear relative permeability and nonlinear fracture relative permeability as calculated from the 3D LBM model. The difference of cumulative oil production prediction is small; however, the difference becomes large in the prediction of cumulative steam injection and cumulative SOR. In terms of prediction of cumulative steam injection in SAGD operation, the biggest difference occurred in the reservoir with a thin level of thickness, medium level of porosity and medium level of initial oil saturation. In the forecasting of a cumulative steam-to-oil ratio, the biggest difference occurred in the reservoir with a low level of thickness, low level of porosity and medium level of initial oil

saturation. As a result, it is important to point out that implementing nonlinear fracture relative permeability in naturally fractured reservoirs has significant influences on the simulation results during the SAGD process. Therefore, in order to reduce the uncertainty of naturally fractured reservoir modeling and to promote the accuracy of forecasting from numerical simulation, during a SAGD process it is necessary and more practical to apply nonlinear fracture relative permeability curves and their correlation with intrinsic fracture porosity into naturally fractured reservoir simulations, especially for reservoirs with a thin level of thickness and medium level of matrix porosity and initial oil saturation.

5.2 Recommendations

Two recommendations for future work are:

(1) The effect of wettability of surface rock should be added into the models. This would allow the fracture relative permeability of the models, coupled with intrinsic fracture porosity, gravity and wettability, to be calculated. As a result, its effect on the SAGD performance due to different wettability can be studied.

(2) Typical thermal recovery methods include the SAGD process as well as the cyclic steam stimulation (CSS) and steam flooding processes. In addition, thermally assisted gas/oil gravity drainage (TAGOGD) is also widely used in carbonate reservoir operations. The effect of nonlinear fracture relative permeability implementation needs to be studied in those different thermal recovery methods in naturally fractured reservoirs.

References

Abdel-Halim, T., & Subramanian, M. (2002). *U.S. Patent No. 6,357,526*. Washington, DC: U.S. Patent and Trademark Office.

Aharonov, E., & Rothman, D. H. (1993). Non-Newtonian flow (through porous media): a lattice-Boltzmann method. *Geophysical Research Letters*, *20*(8), 679-682.

Akhondzadeh, H., & Fattahi, A. (2015). Impact of well configuration on performance of steam-based gravity drainage processes in naturally fractured reservoirs. *Journal of Petroleum Exploration and Production Technology*, *5*(1), 13-25.

Akin, S. (2001). Estimation of fracture relative permeabilities from unsteady state corefloods. *Journal of Petroleum Science and Engineering*, *30*(1), 1-14.

Ali, F., Hamed, A., Nawi, D. M., Hussin, Y. M., & Soheil, N. (2012). Impact of reservoir heterogeneity on Steam Assisted Gravity Drainage in heavy oil fractured reservoirs. *Energy Exploration & Exploitation*, *30*(4), 553-566.

Al-Ahmadi, H. A., & Wattenbarger, R. A. (2011, January). Triple-porosity models: one further step towards capturing fractured reservoirs heterogeneity. In *SPE/DGS Saudi Arabia Section Technical Symposium and Exhibition*. Society of Petroleum Engineers.

Benioug, M., Golfier, F., Tinet, A. J., Buès, M. A., & Oltéan, C. (2015). Numerical Efficiency Assessment of IB–LB Method for 3D Pore-Scale Modeling of Flow and Transport. *Transport in Porous Media*, *109*(1), 1-23.

Benzi, R., & Succi, S. (1990). Two-dimensional turbulence with the lattice Boltzmann equation. *Journal of Physics A: Mathematical and General*, *23*(1), L1.

Bhatnagar, P. L., Gross, E. P., & Krook, M. (1954). A model for collision processes in gases. I. Small amplitude processes in charged and neutral one-component systems. *Physical review*, *94*(3), 511.

Boerrigter, P., Maas, J. G., & de Vries, A. (1989, January). A fractured reservoir simulator capable of modeling block-block interaction. In *SPE Annual Technical Conference and Exhibition*. Society of Petroleum Engineers.

Canbolat, S., Serhat, A., & Kovscek, A. R. (2002, January). A study of steam-assisted gravity drainage performance in the presence of noncondensable gases. In *SPE/DOE Improved Oil Recovery Symposium*. Society of Petroleum Engineers.

Chen, S., Wang, Z., Shan, X., & Doolen, G. D. (1992). Lattice Boltzmann computational fluid dynamics in three dimensions. *Journal of Statistical Physics*, *68*(3), 379-400.

Chen, C. Y., Horne, R. N., & Fourar, M. (2004). Experimental study of liquid gas flow structure effects on relative permeabilities in a fracture. *Water Resources Research, 40(8).*

Chen, C. Y., & Horne, R. N. (2006). Two phase flow in rough walled fractures: Experiments and a flow structure model. *Water resources research*, *42*(3).

Chen, C.-Y., Li, K., & Horne, R. N. (2007, October 1). Experimental Study of Phase Transformation Effects on Relative Permeabilities in Fractures. Society of Petroleum Engineers. doi:10.2118/90233-PA.

Chen, Z. (2007). Reservoir Simulation: Mathematical Techniques in Oil Recovery. CBMS-NSF Regional Conference Series in Applied Mathematics, Vol. 77, SIAM, Philadelphia.

Chen, Z., Huan, G. and Ma, Y. (2006). Computational Methods for Multiphase Flows in Porous Media. Computational Science and Engineering Series, Vol. 2, SIAM, Philadelphia.

Chima, A., Chavez Iriarte, E. A., Carrillo, C., & Himelda, Z. (2010, January). An Equation to predict two-phase relative permeability curves in fractures. In *SPE Latin American and Caribbean petroleum engineering conference*. Society of Petroleum Engineers.

Chima, A., & Geiger, S. (2012, January). An Analytical Equation to Predict Gas/Water Relative Permeability Curves in Fractures. In *SPE Latin America and Caribbean Petroleum Engineering Conference*. Society of Petroleum Engineers.

Dana, E., & Skoczylas, F. (2002). Experimental study of two-phase flow in three sandstones. I. Measuring relative permeabilities during two-phase steady-state experiments. *International journal of multiphase flow*, *28*(11), 1719-1736.

Das, S. K. (2007, January). Application of thermal processes in heavy oil carbonate reservoirs. In *SPE Middle East Oil and Gas Show and Conference*. Society of Petroleum Engineers.

D'humières, D., & Lallemand, P. (1986). Lattice gas automata for fluid mechanics. *Physica A: Statistical Mechanics and its Applications*, *140*(1-2), 326-335.

Dou, Z., & Zhou, Z. F. (2013). Numerical study of non-uniqueness of the factors influencing relative permeability in heterogeneous porous media by lattice Boltzmann method. *International Journal of Heat and Fluid Flow*, *42*, 23-32.

Edmunds, N., & Chhina, H. (2001). Economic optimum operating pressure for SAGD projects in Alberta. *Journal of Canadian Petroleum Technology*, *40*(12).

Fatemi, S. M. (2009). Simulation study of steam assisted gravity drainage (SAGD) in fractured systems. *Oil & Gas Science and Technology-Revue de l'IFP*, *64*(4), 477-487.

Ferréol, B., & Rothman, D. H. (1995). Lattice-Boltzmann simulations of flow through Fontainebleau sandstone. *Transport in Porous Media*, *20*(1), 3-20.

Fourar, M., Bories, S., Lenormand, R., & Persoff, P. (1993). Two phase flow in smooth and rough fractures: Measurement and correlation by porous medium and pipe flow models. *Water Resources Research*, *29*(11), 3699-3708.

Frisch, U., Hasslacher, B., & Pomeau, Y. (1986). Lattice-gas automata for the Navier-Stokes equation. *Physical review letters*, *56*(14), 1505.

Ghassemi, A., & Pak, A. (2011). Numerical study of factors influencing relative permeabilities of two immiscible fluids flowing through porous media using lattice Boltzmann method. *Journal of Petroleum Science and Engineering*, *77*(1), 135-145.

Gunstensen, A. K., Rothman, D. H., Zaleski, S., & Zanetti, G. (1991). Lattice Boltzmann model of immiscible fluids. *Physical Review A*, *43*(8), 4320.

Hatiboglu, C. U., & Babadagli, T. (2008). Pore-scale studies of spontaneous imbibition into oil-saturated porous media. *Physical Review E*, *77*(6), 066311.

He, X., Luo, L. S., & Dembo, M. (1996). Some progress in lattice Boltzmann method. Part I. Nonuniform mesh grids. *Journal of Computational Physics*, *129*(2), 357-363.

Hecht, M., & Harting, J. (2010). Implementation of on-site velocity boundary conditions for D3Q19 lattice Boltzmann simulations. *Journal of Statistical Mechanics: Theory and Experiment*, *2010*(01), P01018.

Higuera, F. J., Succi, S., & Benzi, R. (1989). Lattice gas dynamics with enhanced collisions. *EPL (Europhysics Letters)*, *9*(4), 345.

Honarpour, M. M., Koederitz, F., & Herbert, A. (1986). Relative permeability of petroleum reservoirs.

Honarpour, M., & Mahmood, S. M. (1988). Relative-permeability measurements: An overview. *Journal of petroleum technology*, *40*(08), 963-966.

Hosseininejad Mohebati, M., Yang, D., & MacDonald, J. (2014). Thermal Recovery of Bitumen from the Grosmont Carbonate Formation-Part 1: The Saleski Pilot. *Journal of Canadian Petroleum Technology*, *53*(04), 200-211.

Hou, S., Shan, X., Zou, Q., Doolen, G. D., & Soll, W. E. (1997). Evaluation of two lattice Boltzmann models for multiphase flows. *Journal of Computational Physics*, *138*(2), 695-713.

Imani, G., Maerefat, M., & Hooman, K. (2012). Lattice Boltzmann simulation of conjugate heat transfer from multiple heated obstacles mounted in a walled parallel plate channel. *Numerical Heat Transfer, Part A: Applications*, *62*(10), 798-821.

Inamuro, T., Konishi, N., & Ogino, F. (2000). A Galilean invariant model of the lattice Boltzmann method for multiphase fluid flows using free-energy approach. *Computer physics communications*, *129*(1-3), 32-45.

Khaleeq, A. (2014). *Impact of Initial Water Saturation on SAGD Performance* (Doctoral dissertation, University of Calgary).

Kiasari, H. H., Sola, B. S., & Naderifar, A. (2010). Investigation on the effect of the reservoir variables and operational parameters on SAGD performance. *Brazilian journal of petroleum and gas*, *4*(2).

Landry, C. J. (2013). *Pore-scale imaging and lattice Boltzmann modeling of single-and multi-phase flow in fractured and mixed-wet permeable media* (Doctoral dissertation, The Pennsylvania State University).

Latva-Kokko, M., & Rothman, D. H. (2005). Diffusion properties of gradient-based lattice Boltzmann models of immiscible fluids. *Physical Review E*, *71*(5), 056702.

Llaguno, P. E., Moreno, F., Garcia, R., Mendez, Z., & Escobar, E. (2002, January). A reservoir screening methodology for SAGD applications. In *Canadian International Petroleum Conference*. Petroleum Society of Canada.

Mahabadian, M. A., Ghayyem, M. A., & Jamialahmadi, M. (2015). Multicomponent Multiphase Lattice-Boltzmann Modeling of Fingering during Immiscible Displacement. *Energy Sources, Part A: Recovery, Utilization, and Environmental Effects*, *37*(6), 642-648.

Maini, B., Coskuner, G., & Jha, K. (1990). A Comparison of Steady-State and Unsteady-State Relative Permeabilities Of Viscocities Oil and Water In Ottawa Sand. *Journal of canadian petroleum technology*, *29*(02).

Martys, N. S., & Chen, H. (1996). Simulation of multicomponent fluids in complex three-dimensional geometries by the lattice Boltzmann method. *Physical review E*, *53*(1), 743.

McNamara, G. R., & Zanetti, G. (1988). Use of the Boltzmann equation to simulate lattice-gas automata. *Physical review letters*, *61*(20), 2332.

Mendoza, C. A. (1993). *Capillary pressure and relative transmissivity relationships describing two-phase flow through rough-walled fractures in geologic materials*. University of Waterloo.

Modaresghazani, J. (2015). *Experimental and Simulation Study of Relative Permeabilities in Heavy Oil/Water/Gas Systems* (Doctoral dissertation, University of Calgary).

Mohammadzadeh, O., & Chatzis, I. (2009, January). Pore-level investigation of heavy oil recovery using steam assisted gravity drainage (SAGD). In *International Petroleum Technology Conference*. International Petroleum Technology Conference.

Montgomery, D. C., Peck, E. A., & Vining, G. G. (2015). *Introduction to linear regression analysis*. John Wiley & Sons.

Morgan, J. T., & Gordon, D. T. (1970). Influence of pore geometry on water-oil relative permeability. *Journal of Petroleum Technology*, *22*(10), 1-199.

Mukherjee, N. J., Gittins, S. D., & Edmunds, N. R. (1994, March). Impact and Mitigation of Certain Geological and Process Factors in the Application of AOSTRA's UTF. In *The Canadian SPE/CIM/CANMET International Conference on Recent Advances in Horizontal Well Applications, 11th Annual Heavy Oil Sands Technical Symposium, Calgary, Mar. 2, 1994, paper 94* (Vol. 51).

Murphy, J. R., & Thomson, N. R. (1993). Two phase flow in a variable aperture fracture. *Water Resources Research*, *29*(10), 3453-3476.

Nguyen, H. X., Wisup, B., Tran, X., Ta, D. Q., & Nguyen, H. D. (2012, January). Effects of reservoir parameters and operational design on the prediction of SAGD performance in Athabasca Oilsands. In *SPE Europec/EAGE Annual Conference*. Society of Petroleum Engineers.

Nowamooz, A., Radilla, G., & Fourar, M. (2009). Non Darcian two phase flow in a transparent replica of a rough-walled rock fracture. *Water resources research, 45(7)*.

Odeh, A. S. (1959). Effect of viscosity ratio on relative permeability. *Trans. AIME, 216*, 346-353.

Pan, X. (1999). Immiscible two-phase flow in a fracture.

Parmar, G., Zhao, L., & Graham, J. (2009). Start-up of SAGD wells: history match, wellbore design and operation. *Journal of Canadian Petroleum Technology*, *48*(01), 42-48.

Persoff, P., & Pruess, K. (1995). Two phase flow visualization and relative permeability measurement in natural rough walled rock fractures. *Water Resources Research*, *31*(5), 1175-1186.

Pyrak-Nolte, L. J., Helgeson, D., Haley, G. M., & Morris, J. W. (1992, January). Immiscible fluid flow in a fracture. In *The 33th US Symposium on Rock Mechanics (USRMS)*. American Rock Mechanics Association.

Qi, J., & Yuan, J. Y. (2013). History Matching Grosmont C Carbonate Thermal Production Performance. *Paper SPE, 165560*.

Ramstad, T., Øren, P. E., & Bakke, S. (2010). Simulation of two-phase flow in reservoir rocks using a lattice Boltzmann method. *SPE Journal*, *15*(04), 917-927.

Rossen, W. R., & Kumar, A. T. (1992, January). Single-and two-phase flow in natural fractures. In *SPE Annual Technical Conference and Exhibition*. Society of Petroleum Engineers.

Rothman, D. H., & Keller, J. M. (1988). Immiscible cellular-automaton fluids. *Journal of Statistical Physics*, *52*(3), 1119-1127.

Saboorian-Jooybari, H. (2016). Analytical Estimation of Water-Oil Relative Permeabilities through Fractures. *Oil & Gas Science and Technology–Revue d'IFP Energies nouvelles*, *71*(3), 31.

Saraf, D. N., & Fatt, I. (1967). Three-phase relative permeability measurement using a nuclear magnetic resonance technique for estimating fluid saturation. *Society of Petroleum Engineers Journal*, *7*(03), 235-242.

Sasaki, K., Ono, S., Sugai, Y., Ebinuma, T., Narita, H., & Yamaguchi, T. (2009). Gas production system from methane hydrate layers by hot water injection using dual horizontal wells. *Journal of Canadian Petroleum Technology*, *48*(10), 21-26.

Schembre, J. M., & Kovscek, A. R. (2003). A technique for measuring two-phase relative permeability in porous media via X-ray CT measurements. *Journal of Petroleum Science and Engineering*, *39*(1), 159-174.

Shad, S. A. E. E. D., & Gates, I. D. (2010). Multiphase flow in fractures: co-current and counter-current flow in a fracture. *Journal of Canadian Petroleum Technology*, *49*(02), 48-55.

Shan, X., & Chen, H. (1993). Lattice Boltzmann model for simulating flows with multiple phases and components. *Physical Review E*, *47*(3), 1815.

Shin, H., & Polikar, M. (2007). Review of reservoir parameters to optimize SAGD and Fast-SAGD operating conditions. *Journal of Canadian Petroleum Technology*, *46*(01).

Singhal, A. K., Ito, Y., & Kasraie, M. (1998, January). Screening and design criteria for steam assisted gravity drainage (SAGD) projects. In *SPE International Conference on Horizontal Well Technology*. Society of Petroleum Engineers.

Song, Q. (2015). *Steam Injection Strategies for Bitumen Recovery from an Element of the Grosmont Carbonate Reservoir* (Doctoral dissertation, University of Calgary).

Sola, B. S., & Rashidi, F. (2006, January). Application of the SAGD to an Iranian carbonate heavy oil reservoir. In *SPE Western Regional/AAPG Pacific Section/GSA Cordilleran Section Joint Meeting*. Society of Petroleum Engineers.

Sola, B. S., Rashidi, F., & Babadagli, T. (2007). Temperature effects on the heavy oil/water relative permeabilities of carbonate rocks. *Journal of petroleum science and engineering*, *59*(1), 27-42.

Succi, S., Benzi, R., & Higuera, F. (1991). The lattice Boltzmann equation: A new tool for computational fluid-dynamics. *Physica D: Nonlinear Phenomena*, *47*(1-2), 219-230.

Succi, S., d'Humieres, D., Qian, Y. H., & Orszag, S. A. (1993). On the small-scale dynamical behavior of lattice BGK and lattice Boltzmann schemes. *Journal of scientific computing*, *8*(3), 219-230.

Succi, S. (1997). Lattice Boltzmann equation: Failure or success? *Physica A: Statistical Mechanics and its Applications*, *240*(1-2), 221-228.

Sun, D., Zhu, M., Pan, S., & Raabe, D. (2009). Lattice Boltzmann modeling of dendritic growth in a forced melt convection. *Acta Materialia*, *57*(6), 1755-1767.

Swift, M. R., Osborn, W. R., & Yeomans, J. M. (1995). Lattice Boltzmann simulation of nonideal fluids. *Physical Review Letters*, *75*(5), 830.

Tsang, Y. W. (1989). On two-phase relative permeability and capillary pressure of rough-walled rock fractures. *Lawrence Berkeley National Laboratory*.

Tölke, J. (2002). Lattice Boltzmann simulations of binary fluid flow through porous media. *Philosophical Transactions of the Royal Society of London A: Mathematical, Physical and Engineering Sciences*, *360*(1792), 535-545.

Vanegas, J. W., Cunha, L. B., & Alhanati, F. J. (2005, January). Impact of operational parameters and Reservoir variables during the start-up phase of a SAGD process. In *SPE International Thermal Operations and Heavy Oil Symposium*. Society of Petroleum Engineers.

Vincent, K. D., MacKinnon, C. J., & Palmgren, C. T. S. (2004, January). Developing SAGD operating strategy using a coupled wellbore thermal reservoir simulator. In *SPE International*

Thermal Operations and Heavy Oil Symposium and Western Regional Meeting. Society of Petroleum Engineers.

Vinegar, H. J., & Wellington, S. L. (1987). *U.S. Patent No. 4,663,711*. Washington, DC: U.S. Patent and Trademark Office.

Wolf-Gladrow, D. A. (2000). Lattice-gas cellular automata and lattice Boltzmann models-Introduction. *LATTICE-GAS CELLULAR AUTOMATA AND LATTICE BOLTZMANN MODELS*, *1725*, 1-13.

Wong, R. K., Pan, X., & Maini, B. B. (2008). Correlation between pressure gradient and phase saturation for oil-water flow in smooth and rough walled parallel plate models. *Water resources research, 44(2)*.

Wyllie, M. R. J., & Spangler, M. B. (1952). Application of electrical resistivity measurements to problem of fluid flow in porous media. *AAPG Bulletin*, *36*(2), 359-403.

Yan, Y. Y., & Zu, Y. Q. (2007). A lattice Boltzmann method for incompressible two-phase flows on partial wetting surface with large density ratio. *Journal of Computational Physics*, *227*(1), 763-775.

Yang, D., Hosseininejad Mohebati, M., Brand, S., & Bennett, C. (2014). Thermal recovery of bitumen from the Grosmont Carbonate Formation—Part 2: Pilot interpretation and development strategy. *Journal of Canadian Petroleum Technology*, *53*(04), 212-223.

Yiotis, A. G., Psihogios, J., Kainourgiakis, M. E., Papaioannou, A., & Stubos, A. K. (2007). A lattice Boltzmann study of viscous coupling effects in immiscible two-phase flow in porous media. *Colloids and Surfaces A: Physicochemical and Engineering Aspects*, *300*(1), 35-49.

Yuan, J. Y., & Nugent, D. (2013). Subcool, fluid productivity, and liquid level above a SAGD producer. *Journal of Canadian Petroleum Technology*, *52*(05), 360-367.

APPENDIX A: REGRESSION ANALYSIS

Table A-1 Regression analysis: residual oil saturation versus intrinsic fracture porosity

Analysis of variance

Source	DF	Adj SS	Adj MS	F-Value	P-Value
Regression	1	0.013743	0.013743	80.72	0.001
Fracture porosity	1	0.013743	0.013743	80.72	0.001
Error	4	0.001084	0.000271		
Total	5	0.014827			

Model summary

S	R-sq	R-sq (adj)	R-sq (pred)
0.0164601	95.69%	94.86%	93.60%

Coefficients

Term	Coef	SE Coef	T-Value	P-Value	VIF
Constant	0.2514	0.0259	9.70	0.002	
Fracture porosity	-0.2741	0.0385	-10.12	0.001	1.00

Regression Equation

$S_{or} = 0.2514 - 0.2741 \times \emptyset_f$

Table A-2 Regression analysis: $K_{rw}(S_{or})$ versus intrinsic fracture porosity

Analysis of variance

Source	DF	Adj SS	Adj MS	F-Value	P-Value
Regression	1	0.061689	0.061689	192.36	0.000
Fracture porosity	1	0.061689	0.061689	192.36	0.000
Error	4	0.001283	0.000321		
Total	5	0.062971			

Model summary

S	R-sq	R-sq (adj)	R-sq (pred)
0.0179078	97.96%	97.45%	96.03%

Coefficients

Term	Coef	SE Coef	T-Value	P-Value	VIF
Constant	0.3678	0.0282	13.05	0.000	
Fracture porosity	0.5807	0.0419	13.87	0.000	1.00

Regression equation

$k_{rw}(S_{or}) = 0.3678 + 0.5807 \times \emptyset_f$

Table A-3 Regression analysis: $K_{ro}(S_{wir})$ versus intrinsic fracture porosity

Analysis of variance

Source	DF	Adj SS	Adj MS	F-Value	P-Value
Regression	1	0.085309	0.085309	80.28	0.001
Fracture porosity	1	0.085309	0.085309	80.28	0.001
Error	4	0.004251	0.001063		
Total	5	0.089559			

Model summary

S	R-sq	R-sq (adj)	R-sq (pred)
0.0325985	95.25%	94.07%	89.79%

Coefficients

Term	Coef	SE Coef	T-Value	P-Value	VIF
Constant	0.3527	0.0513	6.87	0.002	
Fracture porosity	0.6829	0.0762	8.96	0.001	1.00

Regression equation

$k_{ro}(S_{wir}) = 0.3527 + 0.6829 \times \emptyset_f$